This Document Contains Missing Page/s That Are Unavailable In The Original Document
PAGE 72, TABLE 3.8

USNRDL-TR-700
OCD Subtask No. 3212A
20 November 1963

RADIOLOGICAL RECOVERY OF LAND TARGET COMPONENTS - COMPLEX III

by
W.L. Owen
J.D. Sartor*

*Presently at Stanford Research Institute

U.S. NAVAL RADIOLOGICAL DEFENSE LABORATORY
SAN FRANCISCO 24, CALIFORNIA

12ND. P7463

TECHNICAL DEVELOPMENTS BRANCH
R.R. Soule, Head

CHEMICAL TECHNOLOGY DIVISION
L.H. Gevantman, Head

ADMINISTRATIVE INFORMATION

This work is part of a project sponsored by the Office of Civil Defense. The studies reported are part of Program B-3, Problem 2, most recently described in this Laboratory's USNRDL Technical Program Summary for Fiscal Years 1963, 1964 and 1965 dated 1 November 1962.

AVAILABILITY OF COPIES

Requests for additional copies by agencies or activities of the Department of Defense, their contractors and AEC activities or contractors certified to DDC (formerly ASTIA), should be directed to the Defense Documentation Center for Scientific and Technical Information, Cameron Station, Alexandria, Virginia.

All other persons and organizations should direct requests for this report to the U.S. Department of Commerce, Office of Technical Services, Washington 25, D.C.

This report has been reviewed in the Office of Civil Defense, Department of Defense, and approved for publication.

Eugene P. Cooper
Scientific Director

E.B. Roth, CAPT USN
Commanding Officer and Director

ABSTRACT

The radiological recovery of essential facilities within a fallout area is a complex task. It involves the scheduling, application and control of a variety of tools and skills for recovery. Execution of a recovery operation must be swift and efficient to avoid the over-exposure of work crews to the radiation hazard. Thus, safe and effective performance will depend upon the advance formulation of a detailed radiological recovery plan.

A special recovery planning procedure has been under development for several years. In its present form the procedural concept has proved quite feasible, as demonstrated by the results of the Complex II experiment. However, a number of critical planning variables and related factors have required closer inspection and measurement. For this reason the Complex III experiment was instituted.

Some of the pertinent experimental results, leading to a more refined recovery planning procedure, are as follows:

1. Contribution factor calculations were confirmed by the experimentally determined values; so much so, in fact, that the resulting improved method of calculation is recommended for recovery planning purposes.

2. Reclamation coefficients (used in estimating recovery dose) appeared to vary with surface-method combination and effort. Because of experimental differences, comparison of these coefficients with their counterparts derived from Complex II results indicated no more than an approximate agreement.

3. Final effectiveness in the reduction of the general radiation level by the combined action of weathering (by winds) and recovery was 97 %. Wind action accounted for approximately 1/3 of the total reduction.

4. Total recovery time (or effort) predictions were low by approximately 10 % because of the consistent trend in underestimating the times expected for individual reclamation jobs.

5. At least 1/5 of the total recovery time was devoted to support functions - those tasks not directly contributing to the dislodgement and removal of fallout material.

SUMMARY

Problem

Following a nuclear attack, it is the responsibility of the radiological defense system to reduce the hazardous conditions created by the radioactive fallout. Aside from the employment of personnel shelters (during the emergency), an effective radiological defense relies upon the physical removal and/or suppression of the fallout material (following the emergency). This part of the defense effort is called radiological recovery.

The radiological recovery of essential facilities within a fallout area is an extensive and complicated task. Because of the variety of surface conditions encountered, a wide assortment of tools and skills for recovery are required. The effective reduction of fallout (or its effects) must be carried out quickly and efficiently to avoid overexposure of the recovery crews to the radiation hazard. Thus it is evident that a successful recovery operation will depend upon thorough advance planning. Furthermore, radiological considerations must govern the planning procedure.

A recovery planning procedure is currently available as a direct result of the Complex II fallout target recovery experiment. Although the procedure proved to be quite feasible, certain improvements were required to broaden its application. The Complex III experiment was performed to measure critical planning variables and related factors which would improve the current recovery planning procedure.

Findings

A test site containing approximately 3 acres was contaminated with a radioactively traced fallout simulant. The entire site (including building roofs, grounds, and streets) was then recovered using six different reclamation methods. Documentation of the required information was achieved through;

(1) A system of continuously recording remote gamma measuring devices.
(2) Monitoring of all reclamation tasks with portable radiacs.
(3) On site meteorological measurements.
(4) Time and motion studies.

As a result, the fallout reduction effects of wind erosion and recovery effort were determined. The list of reclamation coefficients (needed to compute reclamation crew dosage) was extended, and the behavior of these coefficients as a function of method and effort was studied. The method for predicting the radiation contributions of various target components to a common location of interest was made more reliable. Correction factors were found for adjusting recovery time and effort estimates. Together, these findings will permit further refinement of the recovery planning procedure.

ACKNOWLEDGMENTS

This land Target Complex experiment was of such magnitude that it could not have been fulfilled without the whole-hearted assistance and cooperation of several organizations and their personnel:

Los Alamos Scientific Laboratory, Los Alamos, N. M.
Air Force Special Weapons Center, Kirtland Air Force Base, N. M.
Commanding Officer, Camp Parks, Pleasanton, Calif.

Particularly outstanding was the performance of the personnel from the Mobile Construction Battalion Center, Port Hueneme, California.

Of the members of the Naval Radiological Defense Laboratory who participated, the authors are especially appreciative to those whose individual contributions were indispensable in the planning, execution, and reporting of the experiment:

Mr. H. Lee	Planning, Recovery Operations and Shielding Measurements
Mr. D. E. Clark, Jr.	Synthetic Fallout Dispersal and Recovery Operations
Mr. W. B. Lane	Synthetic Fallout Production
Mr. P. A. Covey	Instrumentation
Mr. H. R. Rinnert	Shielding Measurements
Mr. J. Corn	Data Reduction (Author of Appendix G)
Mr. R. Johnson	Data Reduction

CONTENTS

FIGURES

GLOSSARY OF RADIOLOGICAL DEFENSE TERMS*

Emergency phase. The first phase of the radiological defense system. During this period of peak radiological hazard the controlling countermeasure consists of adequate shelter.

Operational recovery phase. The second phase of the radiological defense system that immediately follows the emergency phase. Recovery of essential facilities is accomplished to permit resumption of the basic mission.

Radiological Recovery. That part of the overall recuperative effort concerned with reducing the radiation hazards to a level that permits the resumption of an installation's essential functions. Recovery embraces whatever countermeasures are necessary.

Countermeasure. Any of several methods or principles used in reducing fallout radiation effects. Three types of countermeasures applicable during the recovery phase are reclamation, shielding and scheduled control of personnel.

Reclamation. The reduction of radiation intensity by removing fallout material or burying it in place. Firehosing and plowing are examples of available procedures.

Effectiveness. The measure of the fallout-removal capability of a countermeasure or an entire recovery operation. It is usually expressed in terms of the fraction remaining (F) or the percent removed [100(1-F)] with respect to either the decay-corrected radiation level or the amount (mass) of fallout material initially present.

Standard radiation intensity. The observed radiac dose rate 3 feet above a uniformly contaminated open area produced by the total deposited fallout corrected for decay to 1 hour after detonation.

Specific activity. A measure of the radioactivity per unit mass ($\mu c/g$) of fallout simulant. For real fallout, specific activity is given in fissions/g.

*Generally used in radiological defense.

Residual Number (RN). A measure of countermeasure effectiveness. It is the fraction of the potential dose from the unaltered radiation field that would be received after application of the countermeasure. The more effective the countermeasure, the smaller the residual number and, hence, the smaller the dose.

CHAPTER 1

INTRODUCTION

The threat of a high radiation field created by radioactive fallout after a nuclear attack has prompted the development of a radiological defense system. This system is predicated upon the combined concept of shelter protection during the emergency phase* and the physical reduction of fallout (or its effects) during the operational recovery phase. The actual task of fallout reduction is called the radiological recovery. Developing the means for planning its timely and efficient execution is the prime concern of this report.

1.1 BACKGROUND

Radiological recovery of essential facilities within a fallout pattern is a large and complicated process. Due to the variety of surface conditions that will be encountered, a wide assortment of tools and recovery skills will be involved. In areas of high fallout concentration, tons of accumulated fallout must be removed. For this reason considerable numbers of heavy equipment, with operators, will be required. In addition, optimum recovery of a given built-up target complex may require the coordinated application of sweeping, flushing, burial and soil-removal reclamation methods.

Obviously an operation of such magnitude must be preceded by an intensive planning stage. A random recovery program could achieve the desired reduction of the fallout hazard, but the recovery effort might be greater than necessary. Also, this could mean needless and perhaps dangerous overexposure of recovery teams to the radioactive field. Conventional planning, as practiced in non-radiological situations, will minimize the waste of time, manpower and supplies. However, efficient recovery planning techniques must include radiological considerations to obtain an acceptable balance between the gains in fallout reduction and the cost in dose to personnel.

In 1959 and 1960 a series of three "Target Complex" experiments were conducted at Camp Parks to reconcile the operational requirements of

*See glossary for definition of underlined terms.

radiological recovery with those of dosage control. Each experiment involved the full scale recovery of an artificially contaminated built-up complex including buildings, streets and grounds. The first test, Complex I,[1] demonstrated the feasibility of a full scale radiological recovery effort. Of greater significance, however, was the verification in principle of Lee's[2] approach to recovery planning. The second test, Complex II,[1] crystalized these principles into an improved recovery planning procedure. The worth of this procedure for planning to a safe dose limit was established by the experimental evidence.

A third test, Complex III, was performed to measure critical planning variables and related factors leading to a more refined recovery planning procedure. During this experiment tighter control was maintained over the various reclamation methods than was previously possible. Technical improvements in the radiation detection systems improved the accuracy of the data and broadened its coverage.

1.2 OBJECTIVES

Complex III had the following objectives:

a. To obtain a more precise measure of those factors pertinent to effective planning (shielding factors, contribution factors, and dose reduction factors).

b. To determine the overall cost and performance of a target complex recovery operation (in terms of reclamation effectiveness, effort, rate and dose.)

c. To measure the removal effectiveness by weathering and evaluate its contribution to the total recovery of the target complex.

d. To observe the effect of heavier mass loading upon the performance and results of radiological recovery.

1.3 REPORT PLAN

In meeting the above objectives, the Complex III test results may appear to be unrelated. However, the results all contribute toward the improvement in the radiological recovery planning procedure. In order to conserve space and because it is described in the Complex I and II report, the recovery planning procedure has been omitted from the Complex III report. Instead, sufficient theory associated with the planning procedure has been included where necessary to permit an understanding of the findings.

Chapter 2 presents the radiological conditions simulated and the experimental details necessary to conduct an experiment of this size. The properties of the fallout simulant, including a description for its production and dispersal techniques are described.

Chapter 3 - Results and Discussion - covers four main topics. In the first section, Time and Motion Studies, an analysis is made of those factors found to affect manpower requirements and reclamation method efficiency - two important aspects of recovery planning.

The second section is entitled Dose Rate Reduction. Curves of dose rate versus time demonstrate the reduction in the radiation fields (at different locations within the complex) due to the migration and removal of the fallout simulant by wind action and recovery effort. Comparisons of the reduction effectiveness of these two processes are made as a function of surface type. This information is valuable in improving future dose predictions and also in selecting effective reclamation methods.

The third section, Recovery Dose, presents the concept for computing expected dose to recovery personnel. Derivations of dose reduction factors are given together with tables of the actual factors for a number of reclamation method to surface combinations. This ability to estimate gamma dose to recovery crews is a critical requirement in the planning procedure.

The subject of Radiation Contributions is treated in the fourth and last section of Chapter 3. An improved system for calculating contribution factors is given. These factors are compared with measured contributions to demonstrate the validity and accuracy of the system. The capability for obtaining reliable contribution factors is extremely important, since it forms the basis for all estimates of such planning values as the target shielding factor, dose reduction factors and recovery effectiveness values.

CHAPTER 2

EXPERIMENTAL DETAILS

2.1 RADIOLOGICAL CONDITIONS

Complex III simulated the recovery of a target complex subjected to the idealized radiological conditions listed in Table 2.1. The conditions* shown were based on calculations made by Miller[3] in his development of a fallout model for land surface detonations.

Simulated fallout (radiotraced silica particles) was deposited on the non-vertical surfaces of the target complex. The total area thus covered contained just over 3 acres of building roofs, streets, lawns, walks and fields. The average amount of material deposited on each square foot was governed by the chosen standard intensity. Table 2.1 indicates that for the 1-MT weapon yield and distance involved, a fallout deposit of 90 g/ft^2 would give an H+1 hr intensity of 2700 r/hr, at 3 ft above the surface. If the wind were 15 mph and essentially unidirectional at all altitudes through which the particles fall, this standard intensity (and mass loading) would be found at a distance of 33 miles downwind from the point of detonation. The experimental conditions for Complex I and II are also given in Table 2.1 for comparison.

The selection of the silica grain sizes used in the fallout simulant was based on the assumed weapon yield, wind velocity, and the distance from the explosion. The largest particles arriving would be about 350 μ (0.0137 in.) in diameter, and the smallest about 150 μ (0.0059 in.). The first ones would arrive at about 1.5 hr after the detonation and the last at about 2-3/4 hr, with the most rapid rate of deposition between 2 to 2-1/4 hr. As the particles accumulate on the area, the gamma radiation rate would increase gradually with time until it reached a maximum level of 780 r/hr at about 2-1/4 hr after detonation, and from then on would decrease due to radioactive decay. The dose rate build-up and decay predicted from Miller's model are shown in Fig. 2.1.

*See Appendix A for a derivation of these conditions from criteria established in Ref. 3.

Table 2.1

Assumed Radiological Conditions for a Land-Surface Burst

	Complex III	Complex I	Complex II
Weapon yield (KT)	1000	1000	100
Distance downwind (miles)	33	40	13
Standard intensity (r/hr)	2700	2000	1000
Fallout arrival time (hr after burst)	1.5	1.75	0.7
Fallout cessation time (hr after burst)	2.75	3.25	1.1
Maximum particle size (microns)	350	320	500
Minimum particle size (microns)	150	150	275
Nominal mass loading (g/ft^2)	90	50	30

The experiments were done in a temperate climate, and the data collected is restricted to these conditions. Other climatic conditions, such as freezing temperatures, snow, or large amounts of rain would greatly alter recovery in terms of expected reclamation effectiveness and effort expended.

2.2 TEST SITE CONDITIONS

The target complex site utilized for Complex I and II again served as the test site for Complex III. Figure B.1 (Appendix B) shows the location of the target complex in relation to other facilities used at Camp Parks in this experiment. Figure B.2 shows the layout of the target complex area and the location of the fixed remote area monitoring system (RAMS). Descriptions of the various components are given in Table 2.2.

The size and configuration of the target complex area were the same as for Complex II. However, additional sidewalks were constructed behind buildings 572 and 573, additional lawns were planed around building 573 and the Volleyball Court was taken out and made part of the East Land area. Figures 2.2 and 2.3 show the various components of the complex.

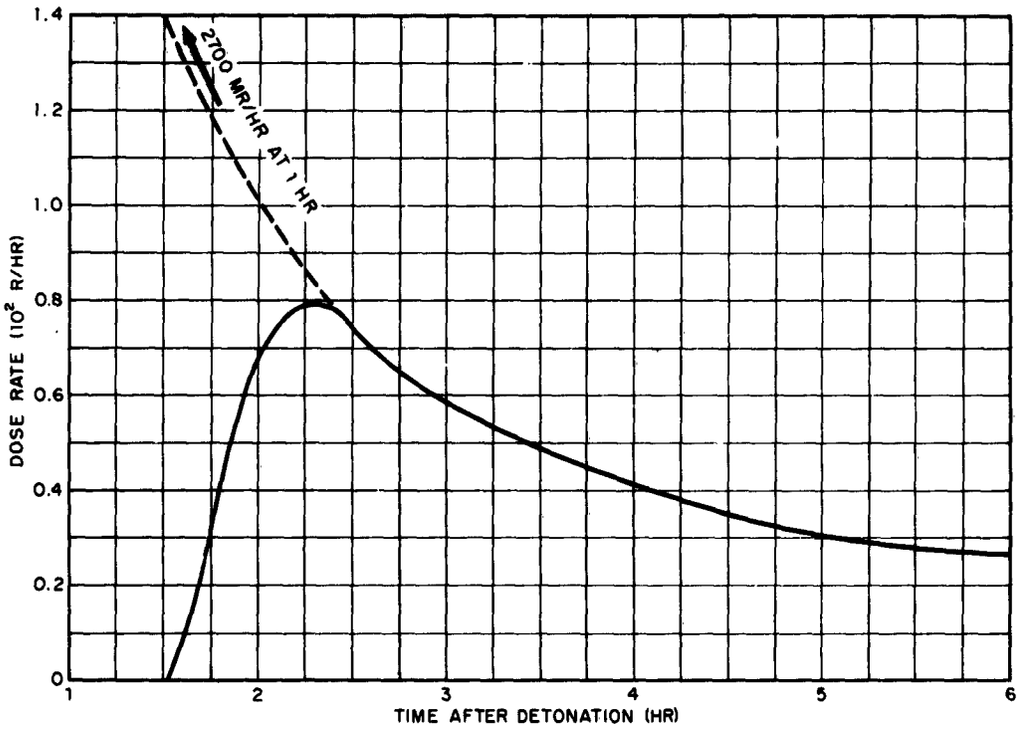

Fig. 2.1 Dose Rate Build-up and Decay - 33 Miles From a 1 MT Burst at 3 Feet Above the Ground

TABLE 2.2

Target Complex Components

Component	Size (ft^2)	Description
Bldg. 570	2,700	Tar and gravel roof; single story, light wooden frame supply building.
Bldg. 571	2,700	Tar and gravel roof; single story, light wooden frame supply building.
Bldg. 572	2,700	Tar and gravel roof; single story, light wooden frame supply building.
Bldg. 573	5,830	Tar and gravel roof; two story, wooden frame BOQ quarters.
10th St	14,185	Asphaltic concrete street. 32 ft wide; concrete curbs on both sides.
Hamilton Ave.	13,230	Asphaltic concrete street. 32 ft wide; concrete curbs on both sides.
Plaza	29,820	Large asphalt paved area. New 2 in. topping of asphalt paving.
Parking Strips	7,525	Various asphalt paved parking strips and loading areas near buildings.
Terrace	21,330	Large cultivated sloping land area behind bldgs 572 and 573.
East Field	16,940	Land area east of complex. Cultivated and harrowed.
Lawns	13,550	Lawns planted around buildings. New sod not deeply rooted.
Planter Beds	2,130	2-3 ft wide planting areas between sidewalks and buildings.
Sidewalks	8,720	Portland cement and asphaltic concrete sidewalks around buildings.
	141,360	

Fig. 2.2 View of Target Complex Looking West

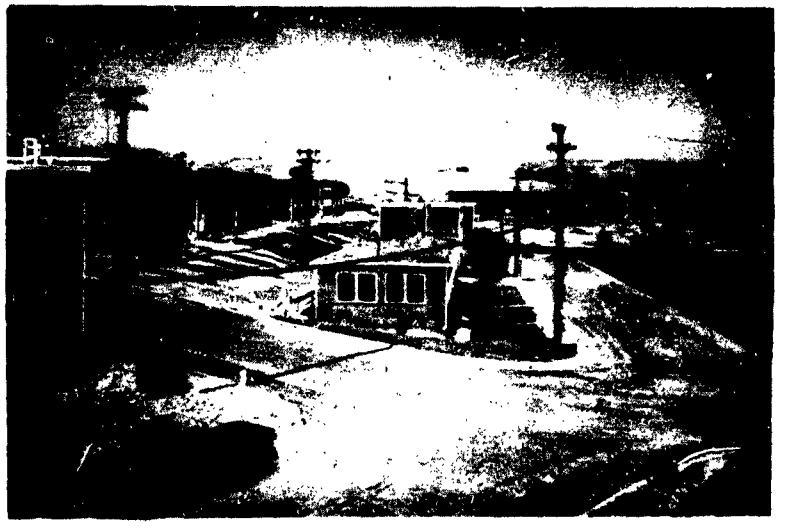

Fig. 2.3 View of Target Complex Looking East

2.3 OPERATIONAL SCOPE

The experiment consisted of four distinct phases, namely; pre-planning and preparation, simulant production, dispersal of simulant, weathering and recovery. Starting with the pre-planning and the preparation of facilities to the final stages of recovery the experiment extended over a three month period. Included in this period was the training of enlisted personnel* in the techniques of radiological recovery.

2.4 FALLOUT MATERIAL

A dry fallout simulant, consisting of sized sand particles tagged with a radioactive tracer, simulated fallout resulting from the radiological conditions hypothesized in Section 2.1. For the test application, it was unnecessary to duplicate or simulate all of the properties of real fallout. However, the measurement and control of four critical fallout properties were required:

a. Mass per unit area as related to standard intensity.
b. Size distribution.
c. Particle density.
d. Insolubility of tracer.

The radiotracer provided a means of

a. Verifying the initial mass levels of fallout.
b. Following the effects of weathering on the dose rate.
c. Determining the final levels of contamination.
d. Measuring actual gamma dosage to recovery crews.

The specific activity used had no special significance, but was sufficiently high to yield easily measurable radiation rates after the effects of weathering, recovery and decay.

It should be pointed out here that no attempt was made to create r/hr radiation fields experimentally. Although particle sizes and mass loadings were achieved, radiation levels were held to 100 mr/hr or less for obvious reasons of safety. It is interesting and important to note that Ba^{140}-La^{140} (the isotope used as the tracer) contribute about 65 % of the gamma dose from gross fission products at about the same time after fission that is postulated in this experiment. It follows that all findings related to gamma ray properties (e.g., dosage and attenuation) closely approximate those from real fallout.

*From the Construction Battalion Center, Port Hueneme, Calif.

The preparation and use of fallout simulant consisted of the following phases: (1) hot-cell processing of the isotope; (2) sieving the bulk carrier material (sand); (3) tagging the sand with the radiotracer; (4) dispersing the resultant fallout simulant; and (5) conducting radioactive analyses of samples taken from this same material. A resume of these phases follows.

2.4.1 Isotope Procurement and Processing

The radioisotope Ba^{140}-La^{140} was used as the tracer in the fallout simulant. The required quantities of the radiobarium-140 were obtained from the Los Alamos Scientific Laboratory and transported via air to the test site in an uranium shipping container. One thousand curies of Ba^{140} (with ~ 1200 curies of La^{140} daughter) were received as nitrate salts combined with inactive barium nitrate carrier. The radioisotopes were further processed in a hot cell.

When the parent-daughter mixture of Ba^{140}-La^{140} reaches equilibrium, over 90 % of the potential gamma radiation exposure is contributed by the daughter La^{140}. To avoid this potential exposure during the production of the fallout simulant, the La^{140} was chemically separated from the Ba^{140} within the confines of the hot-cell. Thus the radioisotope solution prepared for the tagging of the sand contained only Ba^{140} (representing less than 10 % of the potential gamma dose rate). However, prior to dispersal and the start of the experiment, the fallout simulant material was stored for ten days to permit the La^{140} to reach equilibrium with the Ba^{140} and thereby avoid ambiguity in the radiation measurements.

2.4.2 Bulk Carrier Material

Commercial Monterey sand* was obtained for use as the bulk carrier material. To provide the particle size range conforming with the assumed fallout conditions, it was necessary to further sieve the material. The 150 to 350 μ bulk carrier was separated from the #60 Del Monte sand by a single pass through a NoVo** screening machine equipped with a -48 mesh screen (297 μ openings). The original particle size distribution of the commercial sand and the selected particle size is given in Table 2.3.

---

* Obtained from Del Monte Properties Co., Sand Department, 600 Market St., San Francisco, Calif.

**NoVo Division, Industrial Enterprises Inc., 9705 Cottage Grove Ave., Chicago 28, Ill.

TABLE 2.3

Sand Sieve Analysis

Tyler Standard Sieve No.	Mesh Opening (μ)	#60 Sand (as received)		Sieved Bulk Carrier (Avg. of six samples)	
		% Retained on Screen	Cumulative % Less Than Stated Size	% Retained on Screen	Cumulative % Less Than Stated Size
35	420	8.2	91.8	0	100.0
42	350			1.6	98.4
48	297	48.4	43.4	11.7	86.7
60	250	21.3	22.1		
80	177	19.9	2.2	81.6	5.1
100	149	1.3	0.9	3.3	1.8
150	105	0.9	0		
200	74			1.7	0.1
		100.0		100.0	

2.4.3 Production of Fallout Simulant

The tagging of the bulk carrier material with the radiobarium-140 was accomplished in modified 14-ft^3 concrete mixers. First a 500-lb batch of the sieved sand was placed into a mixer. The prepared radiobarium solution was then pumped from the hot cell to a nozzle mounted in the rotating mixer and sprayed onto the sand particles. To obtain the specific activity necessary for adequate instrument response to gamma radiation, approximately 50 curies of Ba^{140} were sprayed onto each 500-lb batch of sand. A solution of water glass (sodium silicate) was then sprayed onto the tagged particles to coat the sand particles with an average thickness of a few microns. The batch was dried in the mixer by forced draft hot air.

After drying, the tagged sand was transferred into stainless steel pans, placed into a gas fired refractory lined furnace, and fired for 1 hour at 1000°C to fuse the silicate coating and thereby seal in the radionuclides. After cooling, each 500-lb batch of tagged sand was transferred to a holding hopper and stored for the ten day aging period as explained in Section 2.4.1. Laboratory leaching experiments in water on samples of the tagged sand indicated less than 0.5 % leaching.

After the aging period, each 500-lb batch of tagged sand was blended in a transit mix truck with 3500 lb of inert sand having the same particle size distribution. This 7-to-1 dilution produced the required specific activity (approximately 9 μc/g at start of dispersal).

2.4.4 Radioactivity Analysis

A sample from each 500-lb batch of fallout simulant was analyzed to determine the specific activity of the dispersed material. The material collected in the sampling pans was also counted to determine final specific activity and the uniformity of blending the tagged with the untagged particles. Table 2.4 lists the data obtained from these analyses. It can be seen that the specific activity was sensibly constant throughout the production and dispersal phases.

Decay measurements taken on an aliquot of the radiobarium solution verified the Ba^{140} rate of decay over the period of the experiment. Decay correction factors for all gamma measurements were therefore based on a 12.8 day half life.

TABLE 2.4

Specific Activity* of Fallout Simulant

Hopper No.	Low Geometry Scintillation Counter (c/m/g)	Low Geometry Scintillation Counter (μc/g)	4π Ion Chamber (10^{-9} ma/g)	4π Ion Chamber (μc/g)
		Prior to Dispersal		
9	1660	8.52	436	8.63
7	1900	9.75	494	9.78
6	1850	9.50	472	9.34
5	1830	9.39	464	9.19
4	1700	8.72	461	9.13
3	1660	8.52	424	8.39
2	1800	9.24	455	9.01
1	1640	8.42	432	8.55
	Average	9.01		9.00

Target Components	Location of Pan Samples	No. of Samples	Low Geometry Scintillation Counter (c/m/g)	Low Geometry Scintillation Counter (μc/g)	Mass Loading (g/ft^2)	Unit Activity ($\mu c/ft^2$)
			After Dispersal			
Roofs	Bldg 570	6	1750	8.97	92.5	828.0
	571	6	1670	8.56	103.2	883.0
	572	6	1700	8.72	95.9	836.0
	573	10	1660	8.51	96.7	823.0
Grounds	Lawn 570	9	1870	9.59	96.0	921.0
	Lawn 571	4	1890	9.69	81.0	785.0
	Park'g stripe 571	12	1730	8.87	93.0	825.0
	Lawn 572	6	1830	9.38	76.4	717.0
	Park'g stripe 572	2	1740	8.92	67.0	597.0
	Lawn 573	6	2060	10.56	99.0	1046.0
	Walk 573	17	1760	9.02	56.0	505.0
Fields	East Field	16	1890	9.68	84.0	814.0
	Terrace	12	1811	9.29	97.0	902.0
Pavements	10th St	24	1700	8.72	111.0	967.0
	N. Hamilton	12	1600	8.20	98.0	803.0
	S. Hamilton	12	1590	8.15	105.0	855.0
	N. Plaza	12	1670	8.56	103.0	882.0
	C. Plaza	12	1800	9.23	79.0	729.0
	S. Plaza	12	1640	8.40	108.0	907.0
			Weighted Averages	9.00	95.0	854.0

*All specific activities decayed to a common time of 0001 hr on D+0 days.

2.5 DISPERSAL OF FALLOUT SIMULANT

The synthetic fallout was dispersed on the large paved and unpaved areas by means of a Burch Hydron Spreader. The spreader was mounted on the rear of a 2-1/2 yd^3 dump truck and was fed from a hopper which had a capacity of 3000 lb. Raising the truck bed delivered the sand to the spreader, and a positive displacement feed roll dispersed the fallout simulant in an 8-ft wide path.

Hand-pulled garden spreaders were used to disperse the fallout simulant on all roofs, lawns, sidewalks, and other areas where the dump truck could not be used. The spreaders had a hopper capacity of 200 lb of sand and a spreading width of 23 in. Each spreader was calibrated to disperse the desired amount of material for a given hopper slot setting and forward speed. Several spreaders usually were operated in tandem, paced by one spreader equipped with a tachometer.

Representative samples of the simulant were collected in shallow pans placed just prior to the dispersal of a given area. From the weight of each sample and the area of the pans (1.22 ft^2) the average amount and concentration of material was determined. A total of 31,800 lb of fallout simulant were dispersed. Table 2.5 gives the amount and concentration of synthetic fallout material dispersed on each component surface as determined by means of the sampling pans.

An average mass loading of 95 g/ft^2 was dispersed over the entire complex area. This resulted in an average unit activity of 0.85 mc/ft^2 which created initial radiation levels of 100 mr/hr at a height of 3 ft.

2.6 INSTRUMENTATION

The measurements required to fulfill the objectives specified in Section 1.2 were obtained with the following types of instruments:

a. Laboratory gamma radiation counters.
b. Fixed remote area monitoring system.
c. Portable radiacs.
d. Meteorological instruments.
e. Topographical survey instruments.

A brief description and usage of each type of instrument follows:

2.6.1 Laboratory Gamma Radiation Counters

The specific activities shown in Table 2.4 were measured with the two types of counters described below. The first instrument counted

TABLE 2.5

Amount and Concentration of Fallout Simulant Dispersed

Component and Location		Area (ft^2)	Amount (lb)	Average Mass Loading (g/ft^2)	
Roofs: Bldg.	570	2,700	550	92.5	
	571	2,700	613	103.2	
	572	2,700	570	95.9	
	573	5,830	1,240	96.7	
	Sub-totals	13,930	2,973	97	Wtd avg
Grnds* Bldg	570	8,319	1,760	96	
	571	9,202	1,800	85	
	572	7,258	1,180	74	
	573	7,909	1,270	73	
	Sub-totals	32,688	6,010	84	Wtd avg
Fields: East Field		16,180	2,990	84	
Terrace		21,330	4,560	97	
		37,510	7,550	92	Wtd avg
Pavements: 10th St		14,185	3,470	111	
Hamilton		13,230	2,970	102	
Plaza		29,820	8,880	100	
	Sub-totals	57,235	15,320	103	Wtd avg
	Grand Totals	141,361	31,800	95	Wtd avg

*Includes lawn, beds, walks and parking strips.

a layer of simulant spread over a sampling pan. The second instrument counted a mass sample (nominally 10 g) confined in a test tube.

(a) Low Geometry Scintillation Counter

This instrument employed a NaI crystal scintillation probe which could be inserted into a specially constructed cave assembly. The cave accommodated samples as large in area as 288 square inches. It consisted of a hollow cubodial lead and steel shield with outside dimensions of 20 x 24 x 26 inches. Inside dimensions were 16 x 18 x 24 inches. The detecting surface of a 2-in. long x 2-in. diameter sodium iodide crystal scintillation probe (Nuclear Chicago, Model 05-5) was placed approximately 21 in. above the center of the cave floor. A Nuclear Chicago Model-183B scaler was coupled to the probe unit.

(b) 4-pi Gamma Ionization Chamber

This instrument is an argon-filled (600 psig at 70°F) steel ionization chamber 11 in. in diameter x 14 in. high. It is shielded with 3 in. of lead and has a re-entrant sample thimble 1-3/4 in. I.D. x 12 in. deep. Current produced in the chamber by ionizing radiation was applied to suitable lead resisters. The resultant voltage drop drove a plate difference amplifier and was read out on a microammeter.

2.6.2 Remote Area Monitoring System (RAMS)*

The RAMS system was employed to obtain a continuous gamma dose rate history during the weathering phase of the experiment at 20 preselected fixed locations in the target complex. The system consisted of 20 remote ion chambers, two power supplies and control panels, and 20 station unit panels. An instrument trailer, located outside of the target complex area, contained the control panels and a 20-channel multipoint Brown recorder. The latter provided a continuous record of the gamma dose rate history. Appendix C lists the RAMS data taken during the experiment. All detectors were mounted three feet above paved and unpaved surface and floor. The temperature dependence of the RAMS system encountered during Complex I and II was eliminated in Complex III through an NRDL modification of the system.[4] Figure 2.4 shows a detector station on the Plaza and Fig. 2.5 shows one in bldg. 573. The locations of the 20 stations in the target complex are shown in Fig. B.2.

2.6.3 Portable Radiacs

Portable radiacs, AN/PDR-27C and the CP 3 IM (Cutie Pie) were used to obtain:

*Remote Area Monitoring System (RAMS) manufactured by Jordan Electronics, Alhambra, Calif.

Fig. 2.4 RAMS Station 4 on the Plaza

Fig. 2.5 RAMS Stations 9 and 10 Bldg 573

a. Gamma radiation measurements during the sequential contamination of the target complex.

b. Gamma dose-rate history of the recovery crews during the recovery of the target complex.

During the weathering phase, the portable radiacs were also used to obtain periodic gamma radiation measurements at each RAMS station to provide back-up data in the event of a RAMS station failure. Appendix D lists the portable radiac survey readings taken during the experiment.

2.6.4 Meteorological Measurements

Meteorological measurements during the experiment included:

a. Continuous wind speed and direction data at four locations in the complex area.

b. Continuous ambient air temperature data.

c. Precipitation measurements.

Wind measurements were made with the Bendix Friez AN/UMQ-3C wind-measuring set which included a wind direction-velocity transmitter and a wind direction-velocity recorder.

The ambient air temperature was continuously measured with a spring wound Taylor thermograph recorder. A plot of the air temperatures during the experiment is given in Fig. 2.6.

Precipitation measurements were obtained with a standard rain gage.

2.6.5 Topographical Survey

The target complex area, as indicated in Table 2.2 contained buildings, land areas, paved areas, sidewalks, etc., presenting surfaces of many geometries. To assist in the computation and analysis of dose rate contribution factors from the various surfaces, a complete topographical survey was made of the complex area. Figure B.3 presents the elevation readings at various locations in the complex area. Elevation profiles through several axes of the target complex area are shown in Figs. B.4 through B.6.

2.7 RECOVERY OPERATIONS

2.7.1 Extent of Recovery

Following dispersal, the fallout simulant was allowed to weather in place for 233 hours. On the morning of the ninth day the radiological

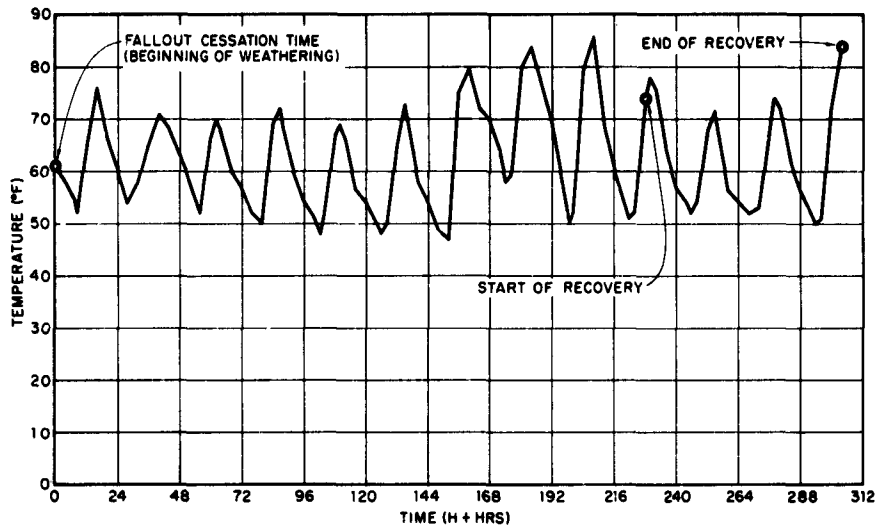

Fig. 2.6 Plot of Air Temperature During Weathering and Recovery Phase

recovery of the target complex commenced. This recovery operation was conducted in two stages. In the first stage, roofs, pavements and land areas were reclaimed by firehosing, sweeping and burial techniques. During the second stage lawns were reclaimed by soil removal methods, namely, scraping and shoveling. The recovery phase of the test schedule in Table 2.6 shows a detailed breakdown of both stages giving the various reclamation methods and their approximate working times. Four equipment operators and eight laborers were required over the four-day recovery phase.

2.7.2 Reclamation Techniques

From the standpoint of their basic function and availability, fallout reclamation methods are quite conventional. However, the manner in which they are adapted to the problem of displacing fallout is often quite specialized. For instance, the technique of removing fallout material by firehosing is in no way related tothat of putting out a fire. As an aid to prospective users, a description of the equipment, manpower and procedural requirements comprising the reclamation methods employed in the complex experiment follows.

Burial in place with motor grader. Ordinarily, burial of fallout in place is easily accomplished by plowing. The Terrace, situated behind buildings 572 and 573 (see Fig. 2.7) because of its shape and relatively steep cross slope, was not suited to this method. Therefore, a motor grader was used to reclaim this particular target component. A four-step procedure was devised to completely bury the fallout simulant.

(1) Simulant from the upper half of the Terrace was bladed into a windrow.
(2) A trench was cut alongside the windrow.
(3) The contaminated windrow was then pushed into the trench.
(4) Clean fill from the trench was replaced and compacted on top of the spoil.

This whole process was repeated on the lower half of the Terrace to complete the reclamation. One man, the grader operator, was required.

Mixing in place with rototiller. In order to get a comparison with plowing performance observed at the previous complex experiments, the land area along the east side of the complex (see Fig. 2.7) was rototilled. The rototiller which was pulled by a D-6 caterpillar tractor (see Fig. 2.8), was capable of making a swath approximately 4 ft wide. It mixed the simulant and soil to a depth of 8 to 10 in. The action of the rototiller was controlled entirely by the tractor operator.

TABLE 2.6

Test Schedule

Date	Day	Action	Surface or Location	Approx. Time In	Out
		Simulant Production Phase			
9/22/60		Contam., fix, fire and blend	Bldg. 131	0830	-
		sand for storage	Bldg. 170	-	1540
		Simulant Dispersal Phase			
10/5/60	D-3	Hand spreaders	Bldg. roofs	0910	1430
10/6/60	D-2	Hand spreaders and	Lawns,	0815	-
		truck spreader	planters and land areas	-	1630
10/7/60	D-1	Truck spreader	Pavements	0800	1600
		Weathering Phase (winds)			
10/8/60	D+0	Official start	Complex	0000	-
10/17/60	D+9	Official finish		-	0900
		Recovery Phase: Stage 1			
10/17/60	D+9	Power sweep (1st pass)	Pavements	0910	1058
		Motor grade	Terrace		
		Load and haul swpr. spoil	Waste area	1305	1345
		Rototill (start 1st pass)	East field	1350	1409
		Firehose roofs	570,571 & 572	1343	1612
10/18/60	D+10	Firehose roof	573	0838	1118
		Sweep walks	570,571,572	0838	0953
		Shovel beds	570, 571	1034	1126
		Shovel beds	572	1251	1310
		Rototill (1st pass)	East field	1253	1340
		Rototill (2nd pass)	East field	1357	1429
		Sweep walks	573	1328	1335
		Power sweep (2nd pass)	Pavements	1343	1441
		Shovel to assist rototill	East field	1415	1428
		Load sweeper spoil	Waste area	1450	1455
		Motorflush pavements	Streets	1453	1551
		Motorflush pavements	Plaza	1633	1644
		Firehose pavements	Driveways	1510	1624
10/19/60	D+11	Sweep walks	573	0838	0920
		Shovel beds	573	0938	1016
		Motor flush pavements	Plaza and Hamilton	0838	1000
		Recovery Phase: Stage 2			
10/19/60	D+11	Scrape lawns	572	1035	1127
		Shovel to assist scraping	572-lawns	1045	1124
		Shovel lawns	571	1047	1129
		Load and haul soil	572	1056	1139
		Scrape lawns	572,573 and east field	1237	1625
		Shovel lawns	570, 571	1240	1524
		Load and haul soil	571, 572, 573	1237	1521
		Shovel to assist loading	FS-2	1311	1318
		Shovel to assist scraping	573-lawns	1445	1615
		Motor grade lawn	571	1500	1511
		Load and haul soil	571, 573	1546	1614
		Shovel to assist loading	571-lawns	1615	1625
		Shovel to assist scraping	East lands	1616	1646
		Shovel to assist loading	573-lawns	1544	1639
10/20/60	D+12	Scrape lawn	570	0824	0932
		Shovel to assist scraping	570-lawns	0818	0858
		Loading and haul soil	Terrace	0824	0844
		Shovel to assist loading	10th St	0825	0925
		Load and haul soil	10th St	0844	0935
		Shovel to assist loading	Terrace	0839	0935
		Load and haul soil	570 lawns	0935	1251
		Shovel to assist loading	570 lawns	0909	1208
		Police with scraper	570-lawns and terrace	1045	1208
		Shovel to assist scraping	Terrace	1115	1139
		Load and haul	10th St	1215	1256
		Shovel to assist loading	10th St	1247	1256
		Load and haul soil	571-beds	1346	1508
		Shovel to assist loading	571-beds	1346	1508
		Recovery Completed			

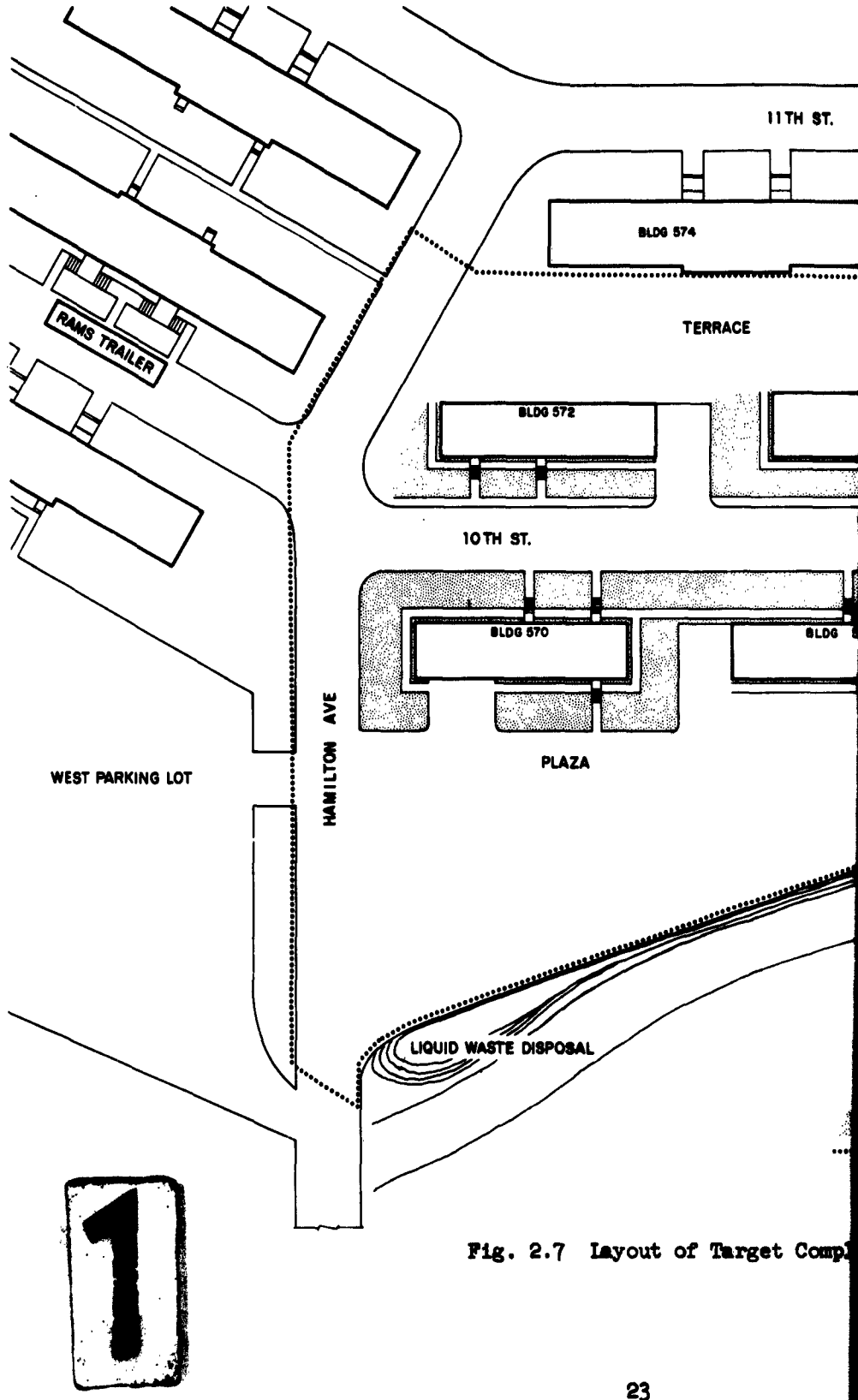

Fig. 2.7 Layout of Target Compl

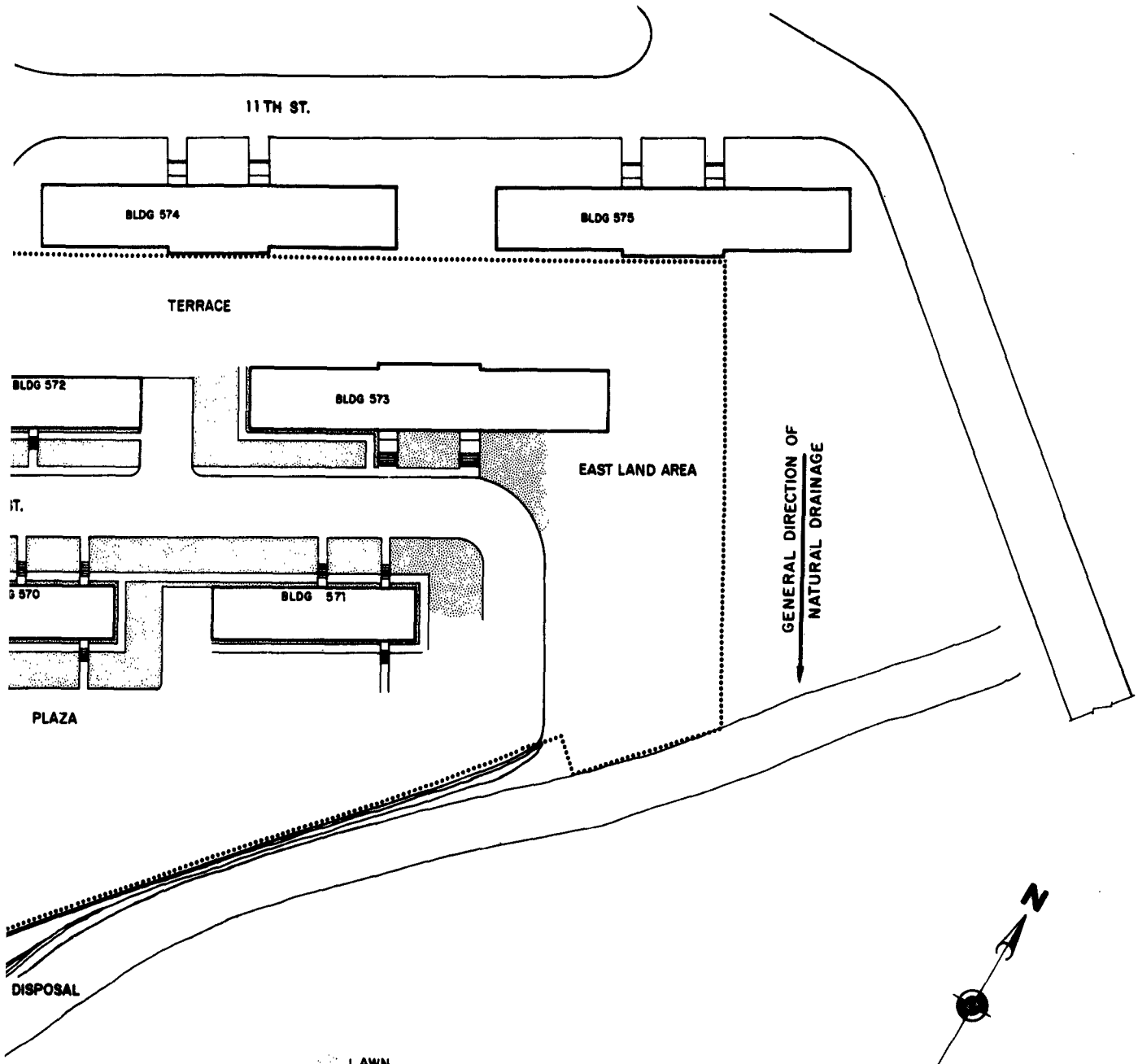

2.7 Layout of Target Complex

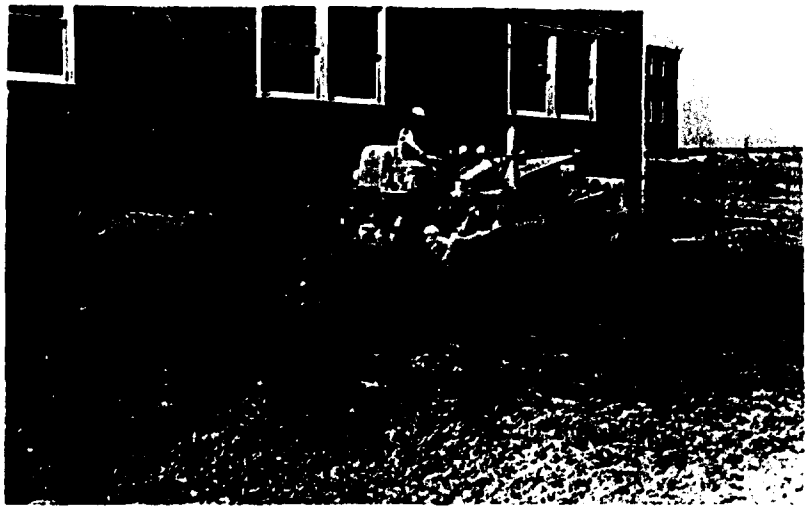

Fig. 2.8 Rototilling East Field Using a D-6 Caterpillar

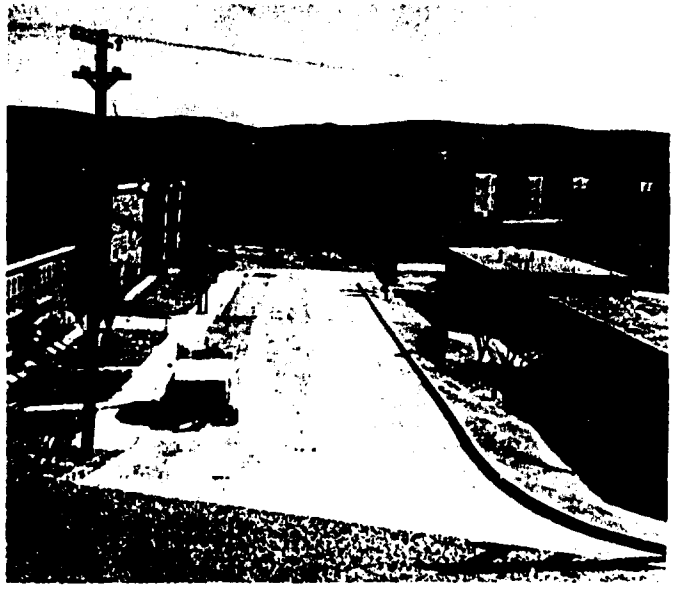

Fig. 2.9 Initial Reclamation of Hamilton With Wayne (Model 450) Sweeper

Collection and removal with street sweeper. All paved areas were swept twice by a Wayne (Model 450) street sweeper (see Fig. 2.9). Except for interruptions to empty the hopper, sweeping progressed along an orderly pattern. More than the normal number of trips were made to the temporary waste collection point (just beyond the complex) to prevent the buildup of gamma dose rates from the radioactive simulant in the hopper. Sweeper spoil was later trucked to a permanent disposal site. One man was required to operate the sweeper.

Dislodgement and transport with water streams. A team effort was required in firehosing the roofs and parking strips. The firehosing operation required two three-man hose teams and one pump tender for a total of seven men. Each hose team manned a 1-1/2 in. firehose delivering water through a straight tapered (suicide) nozzle having a 5/8-in. tip. A 500-gpm pump inserted in the system near a fire hydrant maintained a constant pressure at the nozzle of approximately 75 psi on roofs and 80 psi on paved areas. A 2-1/2 in. firehose served as a delivery line to the 1-1/2 in. firehoses at the area being decontaminated. Figure 2.10 depicts one hose team operating on bldg 573.

For a given roof one three-man hose team was adequate. Starting at one end, the water stream was directed so as to push the contaminant and loose gravel from the roof centerline to the eaves. The team worked diagonally across one corner, and successive strips about 4 ft wide were swept out by the water streams. Upon reaching the other end, the team reversed direction and firehosed the remaining half of the roof.

The procedure followed was dictated by the size of the roofs, i.e., the width of the roofs (26 to 34 ft) limited the direction of travel by the firehosing teams. For broader roof areas it would be advantageous to push the contaminant in a direction normal to the eaves, thereby reducing the distance of travel between centerline and eaves by 30 %.

Firehosing of parking strips was conducted in a straightforward manner. Taking advantage of the natural drainage, water streams were employed to push the simulant material onto the streets and the Plaza, where it could be later removed by other methods, i.e., sweeping and flushing.

Dislodgement and transport with street flushers. Following the second sweeping pass, the paved areas were given a final cleaning with a conventional street flusher (see Fig. 2.11). The flusher was equipped with a 2100-gal tank, a 500-gpm pump, and two forward and two side discharge nozzles.

Fig. 2.10 Firehosing Tar and Gravel Roof of Building 573

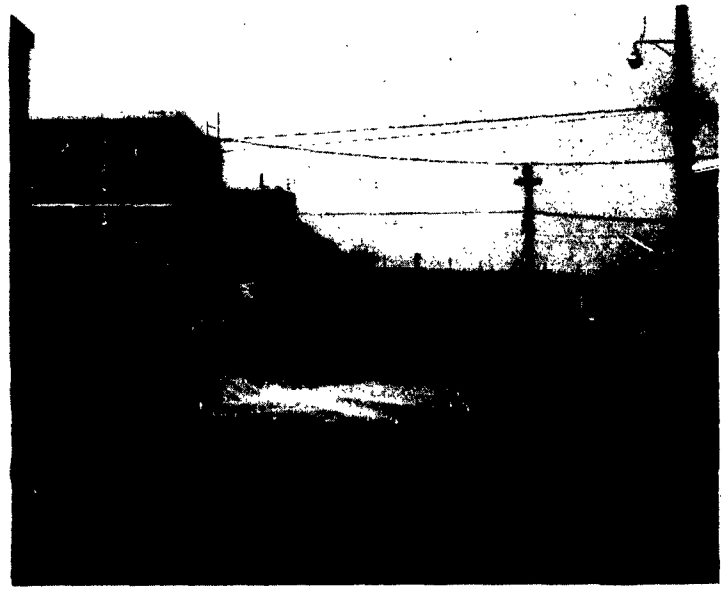

Fig. 2.11 Final Reclamation of 10th St With Conventional Street Flusher

Successful reclamation by street flushing depends upon the careful adjustment of the forward nozzle streams. These were matched to push the simulant clear of the flusher's path as a grader blade would. One side nozzle was set to augment this blade like thrust. By using three of the four nozzles in this manner the average flow rate was 150 gpm and the average pressure was 55 psi.

By taking advantage of the natural drainage of the complex (see Fig. 2.7), successive flusher passes moved the residual simulant material from the streets to the Plaza. This, together with the Plaza residual, was similarly flushed into the liquid waste sump. Although it is ideal to have someone else manipulate the nozzle valve levers, the driver performed the added tasks unassisted.

Surface removal by mechanized scraping. A rubber-tired tractor equipped with a hydraulically operated scraper (see Fig. 2.12) was used to reclaim the majority of the lawn areas. The material was scraped into the street for later removal to the disposal area. In addition to the tractor operator, one to four men were required to hand shovel contaminated strips of sod left along curbs, walks and foundations.

Miscellaneous manual tasks.

(1) Four men swept simulant from the walks into the flower beds with hand brooms.
(2) Four men spaded the flower beds thus burying the simulant.
(3) Four men shoveled out certain lawn areas not accessible to the scraper.

Loading and hauling spoil for disposal. As the spoil (a mixture of soil, sod and simulant) from the scraping and shoveling procedures accumulated on the paved areas, it was loaded into trucks and carried to the permanent waste disposal site. Equipment employed (see Fig. 2.13) was as follows:

(1) One 1-1/2 yd^3 payloader.
(2) One 3/4 yd^3 skiploader.
(3) Two 2-1/2 yd^3 dump trucks.

Besides the four drivers that operated the above rigs, one to six shovelmen assisted the loading and policed the work area.

For a more thorough coverage of reclamation method performance and a description of reclamation equipment, see the results of the

Stoneman test series reported in Refs. 5, 6 and 7. Two more NRDL reports on pertinent tests conducted at Camp Parks are presently in preparation.*

* D. E. Clark, W. C. Cobbin. Removal Effectiveness of Simulated Dry Fallout From Paved Areas by Motorized and Vacuumized Street Sweeper.

D. E. Clark, W. C. Cobbin. Removal Effectiveness of Simulated Dry Fallout From Paved Areas by Motorized Street Flusher.

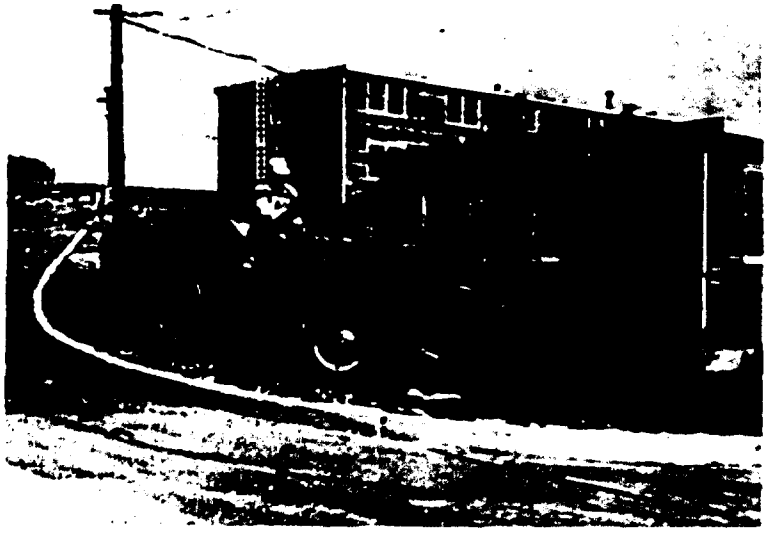

Fig. 2.12 Lawn Removal by Tractor Scraping

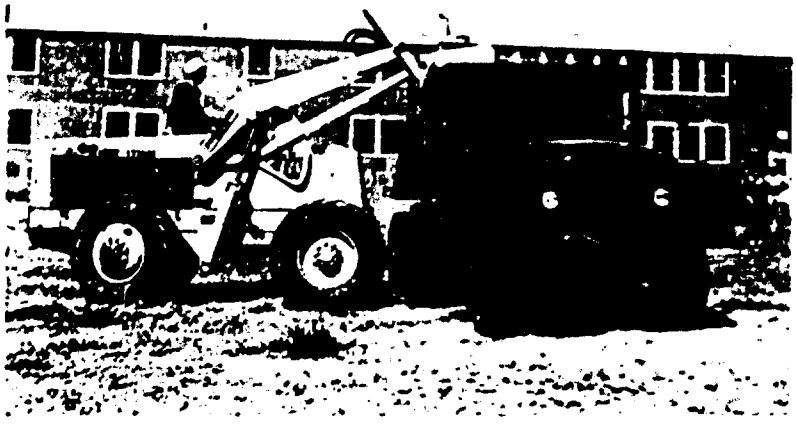

Fig. 2.13 Loading Spoil for Final Disposal

CHAPTER 3

RESULTS AND DISCUSSION

3.1 TIME AND MOTION STUDIES

Detailed time and motion data were obtained from Complex III by recording the pertinent actions of each operator or crew. The results are shown in Tables 3.1 and 3.2 in terms of time, rate, and effort for each recovery operation. The time and effort values have been split to show the amount spent in productive work and the amount needed for support. Their totals are given in the columns headed "operational".

Production time (or effort) is that portion of the operational time devoted to the actual dislodgement, collection and transport of fallout. Any other time (or effort) spent is classified as support. Since support functions add to the operational time without contributing directly to the productive effort, they should be held to an absolute minimum. Of the 122.8 man-hrs expended during the complex recovery, over 18 %, or 22.5 man-hrs, went for support.

Table 3.3 lists the four reclamation methods whose support functions accounted for 95 % of the total complex support effort. Support functions are shown in parentheses for each method. The first three columns contain the total times consumed by each method in productive, support and operational effort, respectively. Column 4 indicates the decimal fraction of the operational time required for the support function. Columns 5 and 6 show comparable values from the two previous complex experiments. The average of columns 4, 5 and 6 is given in column 7.

Except for trucking spoil, the support time-fractions of Complex III are in reasonable agreement with those of Complexes I and II. Apparently the support times have approached the minimum value, unless some drastic change is made in equipment design. In the case of trucking spoil, the total (operational) times spent for Complexes II and III were essentially the same (over eight hours). Because of the longer route used in Complex II, the hauling time was 50 % greater than for Complex III. Conversely, the stand around and loading time during Complex II was 70 % less than for Complex III. Thus, using a shorter route had no effect on the

TABLE 3.1

Effort for Pavement and Roof Reclamation

Recovery Operation	Surface Area (10^3 ft^2)	No. Men	Productive			Support		Operational	
			Time (hr)	Rate (10^3 ft^2/hr)	Effort (man-hr)	Time (hr)	Effort (man-hr)	Time (hr)	Effort (man-hr)
Motor Sweeping:									
Hamilton	13.28	1	0.23	57.4	0.23	0.06	0.06	0.29	0.29
10th St									
First Pass	14.18	1	0.41	34.5	0.41	0.06	0.06	0.47	0.47
Second Pass	14.18	1	0.45	31.4	0.45	0.06	0.06	0.50	0.50
Plaza									
First Pass	29.82	1	0.44	67.8	0.44	0.18	0.18	0.62	0.62
Second Pass	29.82	1	0.41	72.8	0.41	0.06	0.06	0.47	0.47
Motor Flushing:									
Hamilton	13.23	1	0.33	40.1	0.33	0.20	0.20	0.53	0.53
10th St	14.18	1	0.34	41.6	0.34	0.16	0.16	0.50	0.50
Plaza	29.82	1	1.01	29.6	1.01	0.54	0.54	1.55	1.55
Firehosing Pavements	2.15	2-3	1.08	2.0	2.54	0.06	0.12	1.14	3.06
Firehosing Roofs:									
Area set up	-	6		-		0.27	1.60	0.27	1.60
Bldg 570	2.70	3	1.18	2.29	3.55	0	0	1.18	3.55
Bldg 571	2.70	3	0.81	3.34	2.43	0.05	0.15	0.86	2.58
Bldg 572	2.70	3	1.07	2.53	3.20	0.05	0.15	1.12	3.35
Bldg 573	5.83	3	1.95	2.99	5.85	0.29	0.88	2.24	6.73
Area Roll up	-	6				0.28	1.70	0.28	1.70
Pump Tender		1				6.23	6.23	6.23	6.23
Sweeping Sidewalks	8.72	4	1.86	4.68	7.43	0	0	1.86	7.48
			Totals		29.02		12.15		41.17

Note: Approximately one hour was consumed by coffee breaks for entire recovery operation.
Breathing spells were taken on an individual basis when there was an opportunity to do so without affecting the rest of the recovery effort.
Another hour was lost due to minor equipment adjustments and repairs.

TABLE 3.2

Effort for Field and Lawn Reclamation

Recovery Operation	Surface Area (10^3 ft^2)	No. Men	Productive			Support		Totals	
			Time (hr)	Rate (10^3 ft^2/hr)	Effort (man-hr)	Time (hr)	Effort (man-hr)	Time (hr)	Effort (man-hr)
Grading:									
Terrace	21.33	1	1.48	14.40	1.48	0	0	1.48	1.48
Lawns	1.87	1	0.56	3.34	0.56	0	0	0.56	0.56
Rototilling:									
East Field									
First Pass	16.18	1	0.74	21.90	0.74	0.09	0.09	0.83	0.83
Second Pass	16.18	1	0.53	30.5	0.53	0.0	0.0	0.53	0.53
Tractor Scraping:									
Lawns	9.66	1-2	5.20	1.86	5.20	0.51	0.86	5.71	6.06
Terrace	0.45	1	0.42	1.07	0.42	0	0	0.42	0.42
East Field	0.76	1	0.22	3.44	0.22	0	0	0.22	0.22
Shovel Assist to Scraping:									
Lawns	-	1-4	5.64	-	6.09	0	0	5.64	6.09
Terrace	-	2	0.23	-	0.63	0	0	0.23	0.63
East Field	-	2-3	0.38	-	0.92	0	0	0.38	0.92
Shoveling lawns and yards	2.02	4	3.04	0.66	12.16	0	0	3.04	12.16
Spading Beds	2.13	4	1.62	1.31	6.48	0	0	1.62	6.48
Loading and Hauling Spoil:									
Payloader		1	9.27	-	9.27	0	0	9.27	9.27
Skiploader		1	0.63	-	0.63	0	0	0.63	0.63
Grader		1	0.47	-	0.47	0	0	0.47	0.47
Shovels		1-6	3.97	-	17.60	0	0	3.97	17.60
Truck #1	19 trips	1	4.25		4.25	5.00	5.00	9.25	9.25
Truck #2	19 trips	1	3.63		3.63	4.40	4.40	8.03	8.03
				Totals	71.28		10.35		81.63

TABLE 3.3

Fraction of Recovery Operating Times Required for Support Functions

Method (Support Function)	1	2	3	4	5	6	7
	Times in Hours			Support Time-Fraction			
	Prdctv	Suppt	Oprting ① + ②	Cmplx III ②/③	Cmplx II	Cmplx I	Avg
Motor Sweeping (Dumping Hopper)	1.94	0.41	2.35	0.17	0.19	0.25	0.22
Motor Flushing (Filling Tank)	1.68	0.90	2.58	0.35	-	0.32	0.33
Firehosing Roofs (Set-up, moves, rollup)	4.20	0.89	5.09	0.17	0.25	0.20	0.21
Trucking Spoil (Loading Time)	3.94	4.70	8.64	0.54	0.25	-	0.40

operational time. Obviously, an extra loader would have shortened both the support and operational times.

The productive reclamation rates shown in Tables 3.1 and 3.2 have been averaged for each method and listed in Table 3.4. Each observed entry is accompanied by the predicted rate. Results and experience from Complex I and Complex II form the basis for these predicted rates. Predicted and observed rates for motor sweeping, firehosing (roofs), grading, rototilling and spading (beds) agree fairly well. For the remaining methods, predicted rates were consistently higher than observed rates. Such optimistic predictions are the result of two types of errors. The first type, a planning error, stems from the lack of information needed to downgrade known test-rate values for the retarding effects of a full scale recovery effort. The second type, an operational error, is created by last minute changes in manpower assignments, changes in reclamation procedural-techniques, and unforeseen changes in the physical environment.

For instance, the rate discrepancies shown in Table 3.4 for motor flushing are of the first type. That is, the predicted rate was not sufficiently adjusted for turn-around losses. Time required to drive around the block or back up (to reposition the flusher for successive cleaning passes) was much greater than anticipated. As a result, observed rates were proportionately less than predicted, i.e., by 33 and 50 % for streets and plaza, respectively.

An error of the second type appears to be responsible for the extremely low rate observed for firehosing of parking strips and sweeping of walks. During Complex I this same procedure was performed ten times faster - at essentially the same rate predicted in Table 3.4 (20,000 ft^2/hr). It must be surmised that the firehosing crew was unusually deliberate in the performance of this particular reclamation process.

Run-off from the earlier firehosing of roofs created layers of mud and wet sand on much of the walk areas. Hand-sweeping of the walks, therefore, was augmented by considerable scraping with hand shovels - a slower method than sweeping. For this reason, the observed rate for hand sweeping was only 1/5 that predicted.

In the case of tractor-scraping lawns, the observed rate was about 1/2 the predicted value. It is possible than an equipment alteration was responsible for this loss in performance. A 55-gal drum containing water was lashed to the scraper blade in an attempt to improve the cutting action. Although successful in this respect, the added weight overloaded the hydraulic power unit. As a result the response between the blade and the controls for raising and lowering was very sluggish.

TABLE 3.4

Comparison of Predicted and Observed Reclamation Rates

Operation	Rates in 10^3 ft^2/hr Predicted	Observed	Rate Basis
Motor Sweeping:			per machine
1st pass	53.0	53.0	
2nd pass	53.0	51.0	
Motor Flushing:			per machine
Streets	60.0	41.0	
Plaza	60.0	29.6	
Firehosing Parking Strips	20.0	2.0	per nozzle
Firehosing Roofs	3.0	2.8	per nozzle
Sweeping Walks	6.0	1.2	per man
Grader-Burial	10.0	14.5	per machine
Rototilling	22.5	25.4	per machine
Tractor scraping	3.6	1.9	per machine
Shoveling lawns	0.28-0.46	0.16	per man
Spading beds	0.30	0.33	per man

This, in turn, increased the time consumed for all blade adjustments and thereby reduced the expected scraping rate.

The predicted rates for shoveling lawns were based on a six-man team (4 shovels and 2 wheelbarrows). However, only four men were eventually assigned to this task. Since one of the men had to periodically interrupt his shoveling to wheel spoil to the collection point, the shoveling rate suffered accordingly.

Table 3.5 compares predicted and observed values of time and effort for the individual reclamation methods used. These values are condensed from Tables 3.1 and 3.2. The same types of errors mentioned in connection with estimating rates also affect time and effort predictions. Although a number of the paired values do not match, the totals given at the bottom of Table 3.5 are quite close. The total predicted time of 17 hours is within 7 % of the observed* value. Total predicted effort is

*The 18.25 hours total observed time is an adjusted value. It equals the total, continuous, recovery-time of 25 hours less breaks and experimental delays.

TABLE 3.5

Comparison of Predicted and Observed Operational Time and Effort Values

Reclamation Method	Time (hrs) Prdctd	Time (hrs) Obsrvd	Effort (man-hrs) Prdct	Effort (man-hrs) Obsrvd	Percent of Total Observed Effort	No. of Men Prdctd	No. of Men Req'd
Motor sweeping	3.71	2.35	3.71	2.35	1.92	1	1
Motor flushing	2.95	2.58	5.98	2.58	2.02	2	1
Firehosing pavement	0.76	1.14	2.28	3.06	2.49	3	2-3
Firehosing roofs	3.84	5.09	19.92	19.51	15.90	3-6	3-6
(Pump tender)	4.25	6.23	4.25	6.23	5.08	1	1
Sweeping sidewalks	0.46	1.86	1.84	7.43	6.05	4	4
Grader scraping	2.00	2.04	2.00	2.04	1.66	1	1
Rototilling	0.70	1.36	0.70	1.36	1.11	1	1
Tractor scraping	3.26	6.34	3.26	6.70	5.46	1	1-2
(Shovel assist.)	3.26	6.24	3.26	7.64	6.22	1	1-4
Shoveling lawns	3.26	3.04	19.56	12.16	9.92	6	4
Spading beds	2.08	1.62	12.48	6.48	5.28	6	4
Loading spoil	7.50	9.27	12.00	27.97	22.80	1-2	4-11
Hauling spoil	8.00	9.25	16.00	17.28	14.08	2	2
Totals	17.00	18.25	107.1	122.8	100.0	3-12	2-12

within 13 % of the observed value. Thus, in the aggregate, the effect of individual prediction errors appear to be greatly compensated. However, the totals for time and effort still reflect the tendency for optimistic prediction. This bias is probably due to the first type (planning) error mentioned earlier. In this case, more complete time-and-motion data are required for planning corrections to existing information on the test-performance characteristics of reclamation methods.

The bar chart of Fig. 3.1 presents an overall picture of the recovery effort. Showing the overlapping and concurrent execution of the various reclamation procedures in this way demonstrates the value of time and motion requirements. It also illustrates the sequence of operations and emphasizes the extent and complexity of radiological recovery. Reclamation procedures shown below the dotted line in Fig. 3.1 comprise support tasks which were necessary to recovery but did not affect the established sequence.

3.2 DOSE RATE REDUCTION

The total reduction in the gamma dose rate at any location within the complex was due to the combined effects of weathering, reclamation and radioactive decay. These effects were recorded at all 20 RAMS stations. In addition portable radiacs were used to obtain comparable data at 3 ft above all building roofs. The results presented here show the resolution of the separate effects.

3.2.1 Target Dose Rate History

A series of curves depicting dose rate as a function of time was prepared for eight of the major target components. To place these dose rate histories in a more realistic framework, the experimental Ba^{140}-La^{140} mr/hr measurements were converted to r/hr fallout intensities. This was accomplished through use of appropriate fallout decay curves dictated by the radiological conditions described in Table 2.1.

The conversion may be expressed mathematically as

$$I_r = SI_x \, (i_r/i_c) \qquad (1)$$

where I_r = converted (r/hr) intensity after weathering or recovery at any time t_x
I_x = converted (r/hr) standard intensity decayed to the time t_x of interest - from fallout decay curve

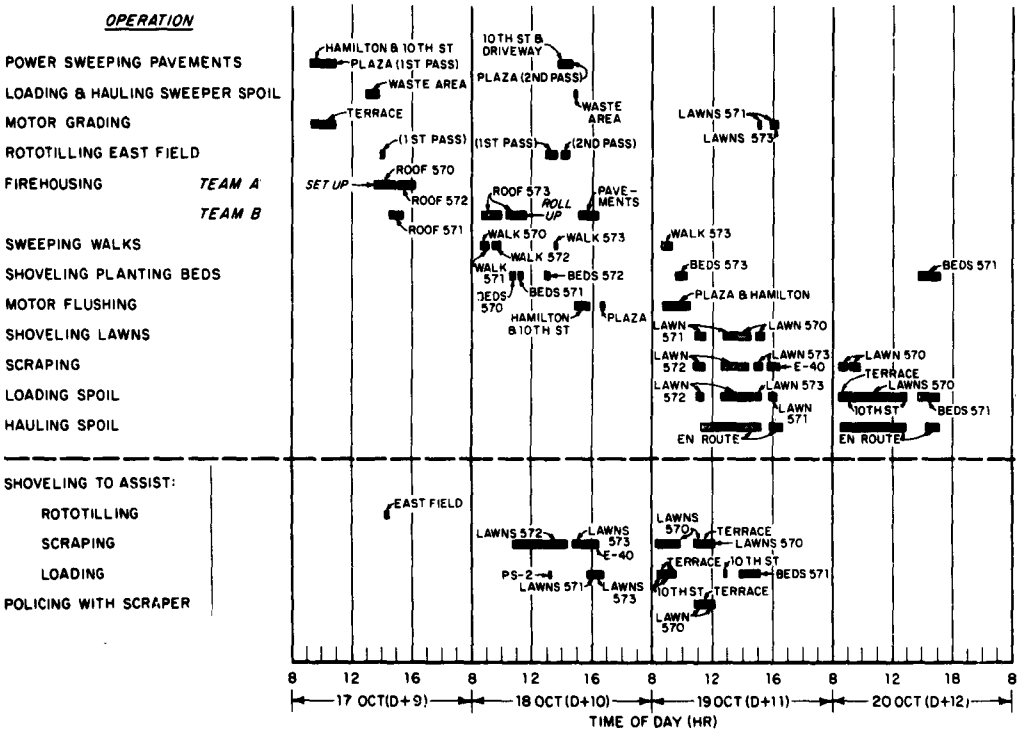

Fig. 3.1 The Recovery Effort

i_c = Ba-La decay-corrected (mr/hr) intensity measured at the end of dispersal at station of interest

i_r = Ba-La decay-corrected (mr/hr) intensity measured after weathering or recovery at time t_x

S = shielding reduction factor for entire complex reference station of interest.

Product SI_x = the shielded standard intensity decayed to time t_x.

Ratio i_r/i_c = the reduction in dose rate due to weathering and/or recovery.

In converting the measurements obtained with either the RAMS system or the radiacs, the intensity i_c in Eq. 1 was set equal to the ratio 105/S; where 105 mr/hr was the intensity measured at the end of dispersal at Station 19. (This is the station nearest to the center of the complex which was established as the reference location for the fallout conversion). That is 105/S mr/hr was taken to be directly proportional to the 670 r/hr value read off the theoretical fallout-model decay-curve at time of fallout cessation (2.75 hr). By using Eq. 1 in conjunction with this same decay-curve, all the i_r measurements were automatically converted to the desired fallout situation.

Figures 3.2 through 3.14 contain the resulting dose rate histories curves. The conversion procedure correctly positioned each curve with respect to the dose rate history at station 19. In constructing the curves, it was assumed that after the start of recovery no weathering occurred, and that after each day's recovery operations the dose rate curve followed the fallout decay curve.

3.2.2 Effects of Weathering* and Recovery

From the dose rate history and theoretical decay curves, it is possible to determine the percent reduction due to weathering, recovery, and weathering plus recovery. Some typical dose rate reductions are shown in Table 3.6. The stations indicated, in each case, represent the survey location nearest the center of each target component.

For either weathering or recovery the reduction in dose rate indicated in Table 3.6 for the various target components does not necessarily provide a true measure of the actual fallout removal effectiveness. The dose rate reduction for each target component has been influenced by the gamma radiation contributions from the remainder of the complex.

*The term weathering, as used throughout this report, refers only to the erosive action of the wind.

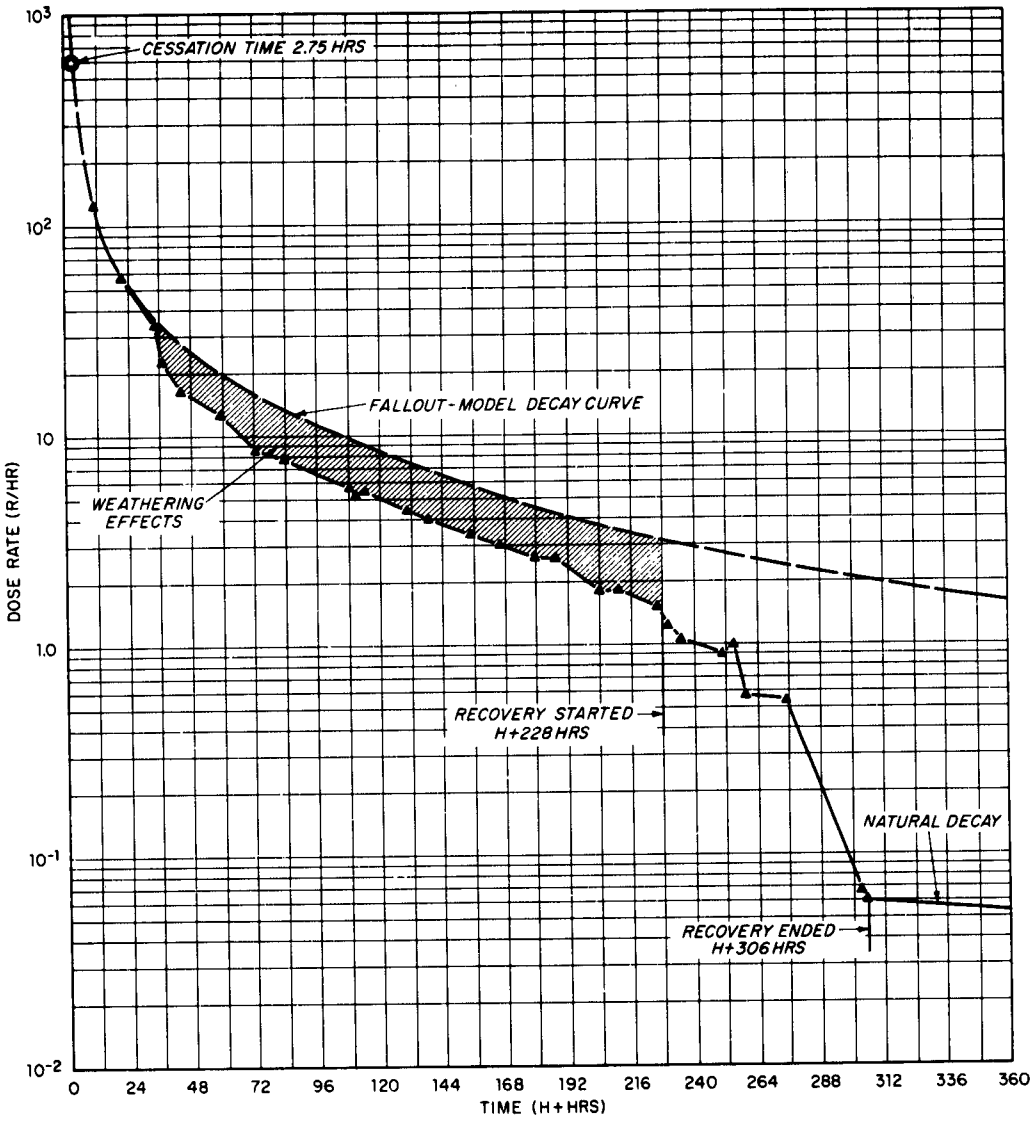

Fig. 3.2 Dose Rate History of Weathering and Recovery - 10th Street (Station 19)

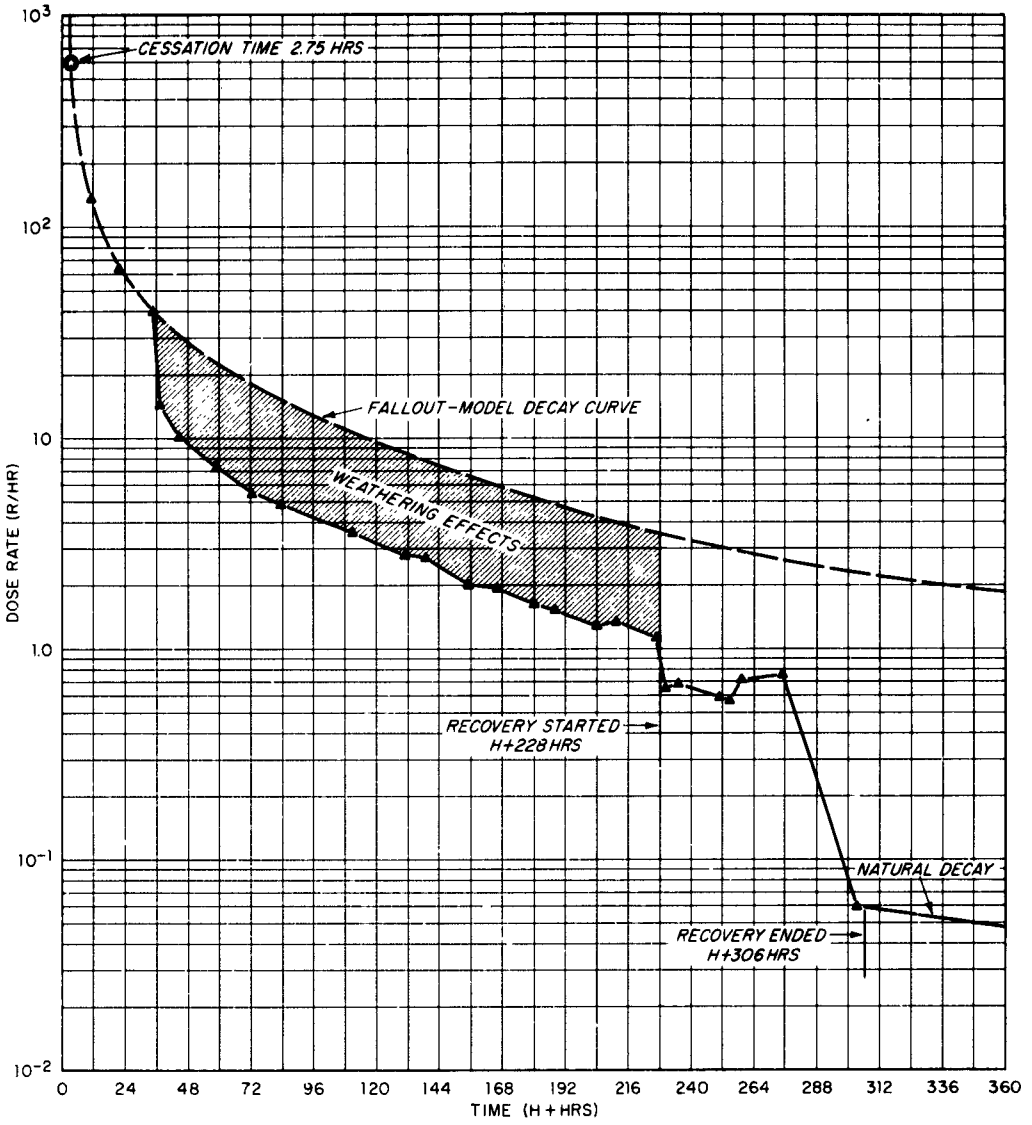

Fig. 3.3 Dose Rate History of Weathering and Recovery - Plaza (Station 4)

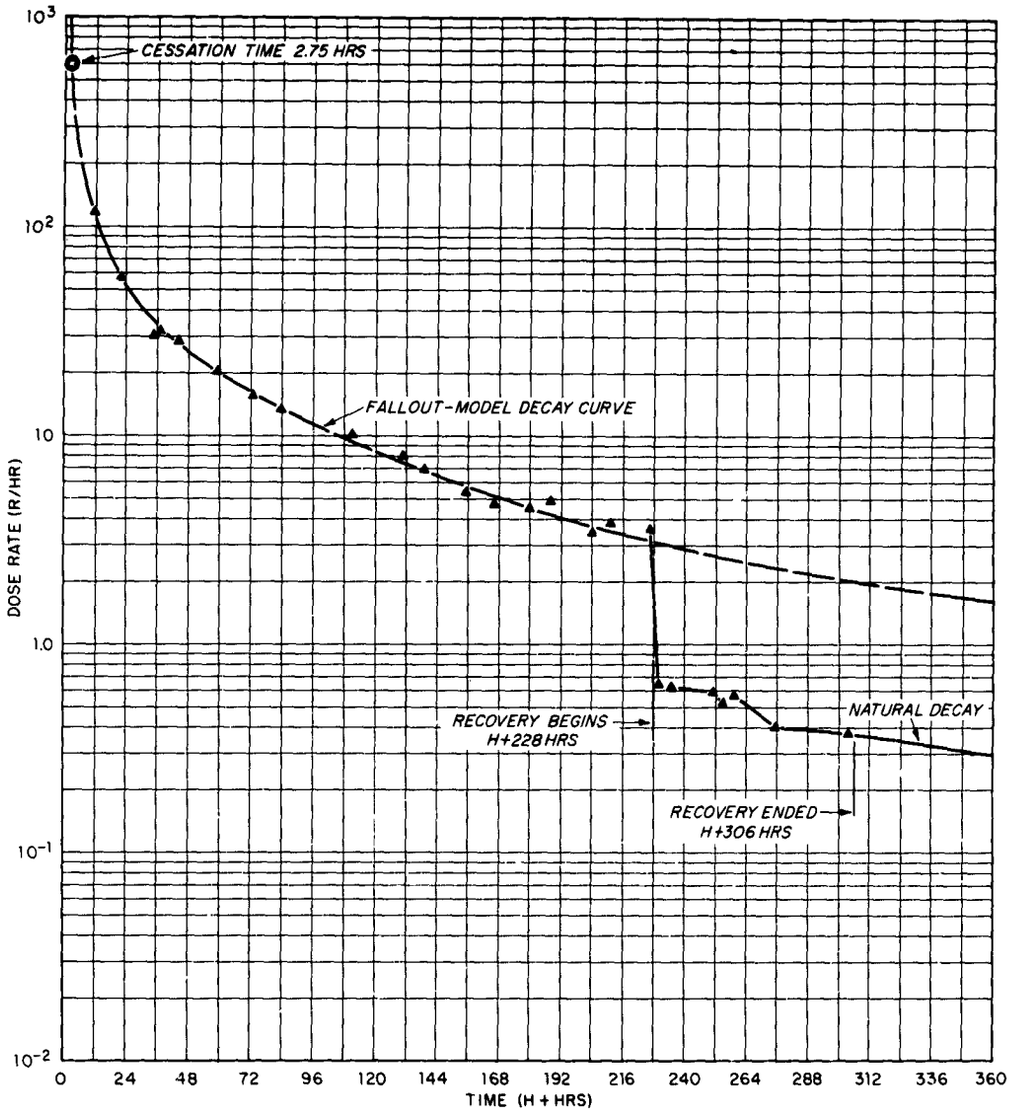

Fig. 3.4 Dose Rate History of Weathering and Recovery - Terrace (Station 2)

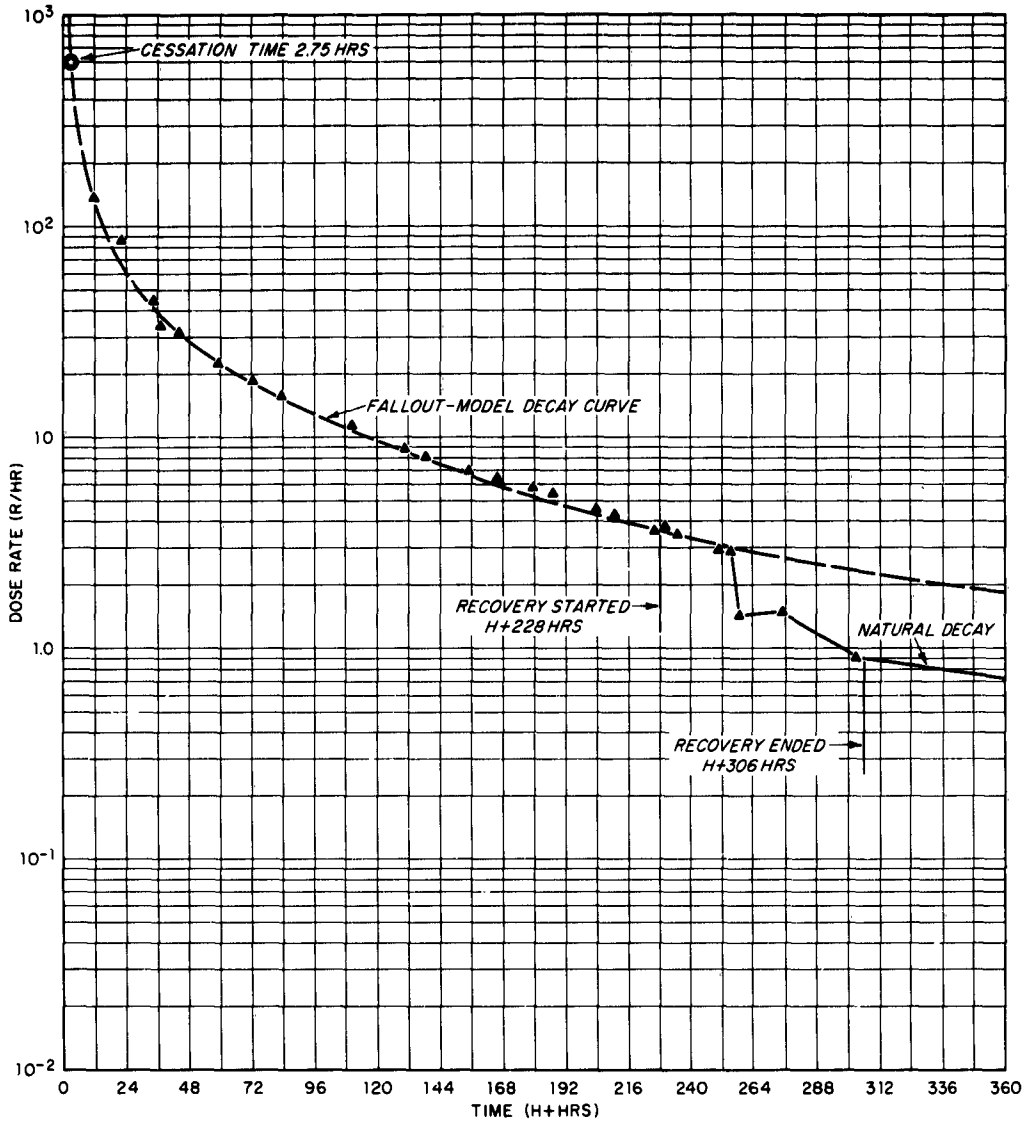

Fig. 3.5 Dose Rate History of Weathering and Recovery - East Field (Station 3)

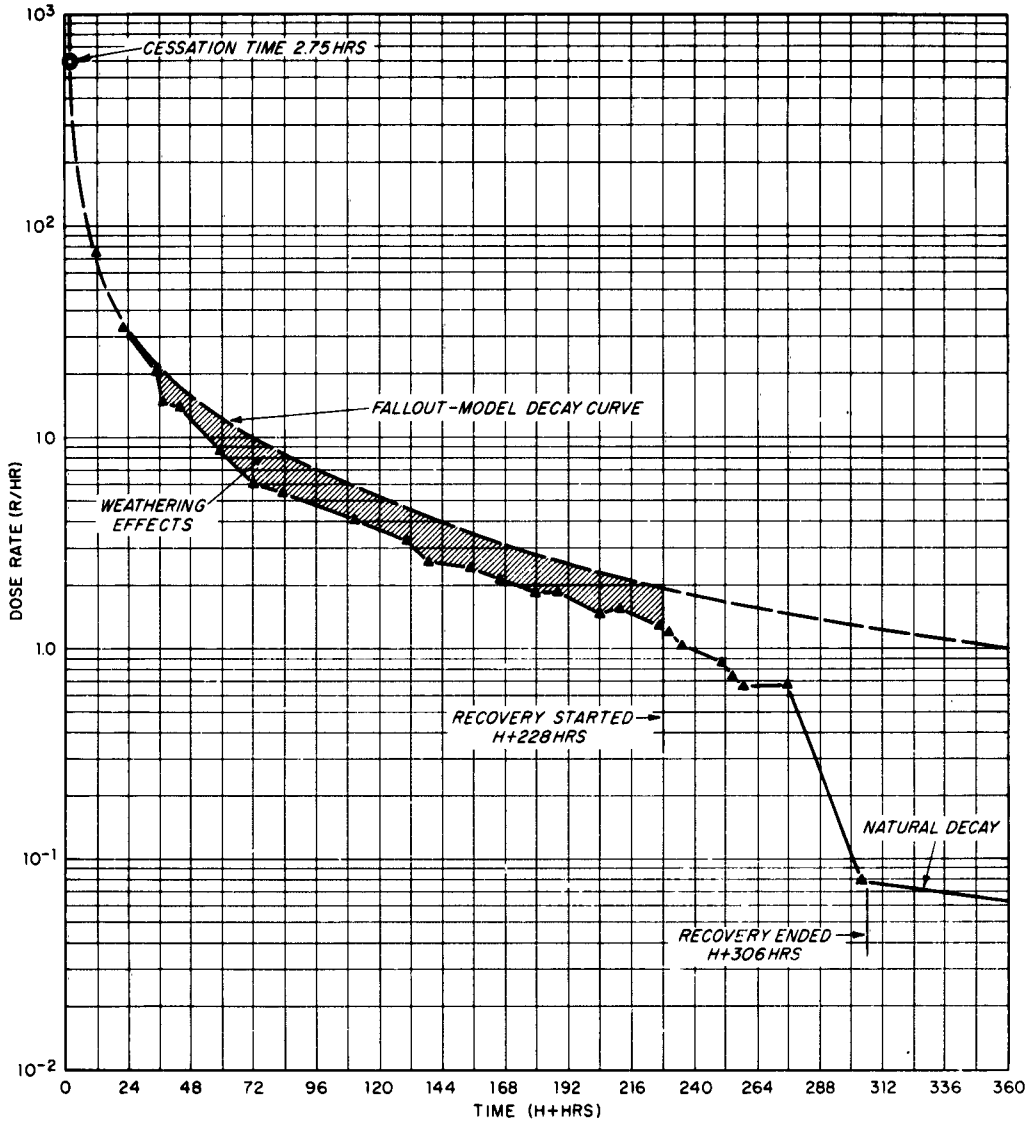

Fig. 3.6 Dose Rate History of Weathering and Recovery - Bldg. 570 (Station 17)

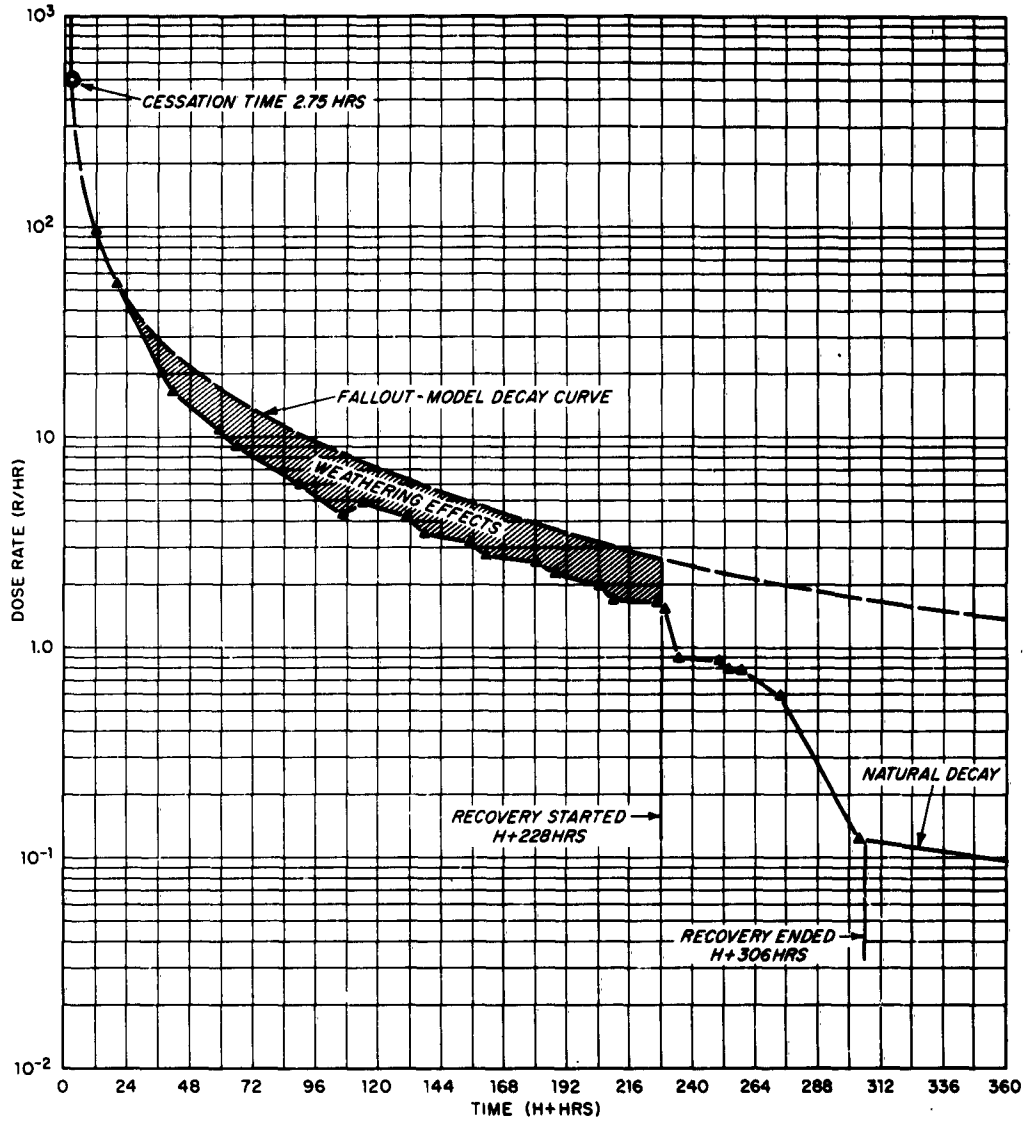

Fig. 3.7 Dose Rate History of Weathering and Recovery - Roof Bldg. 571 (Station 17R)

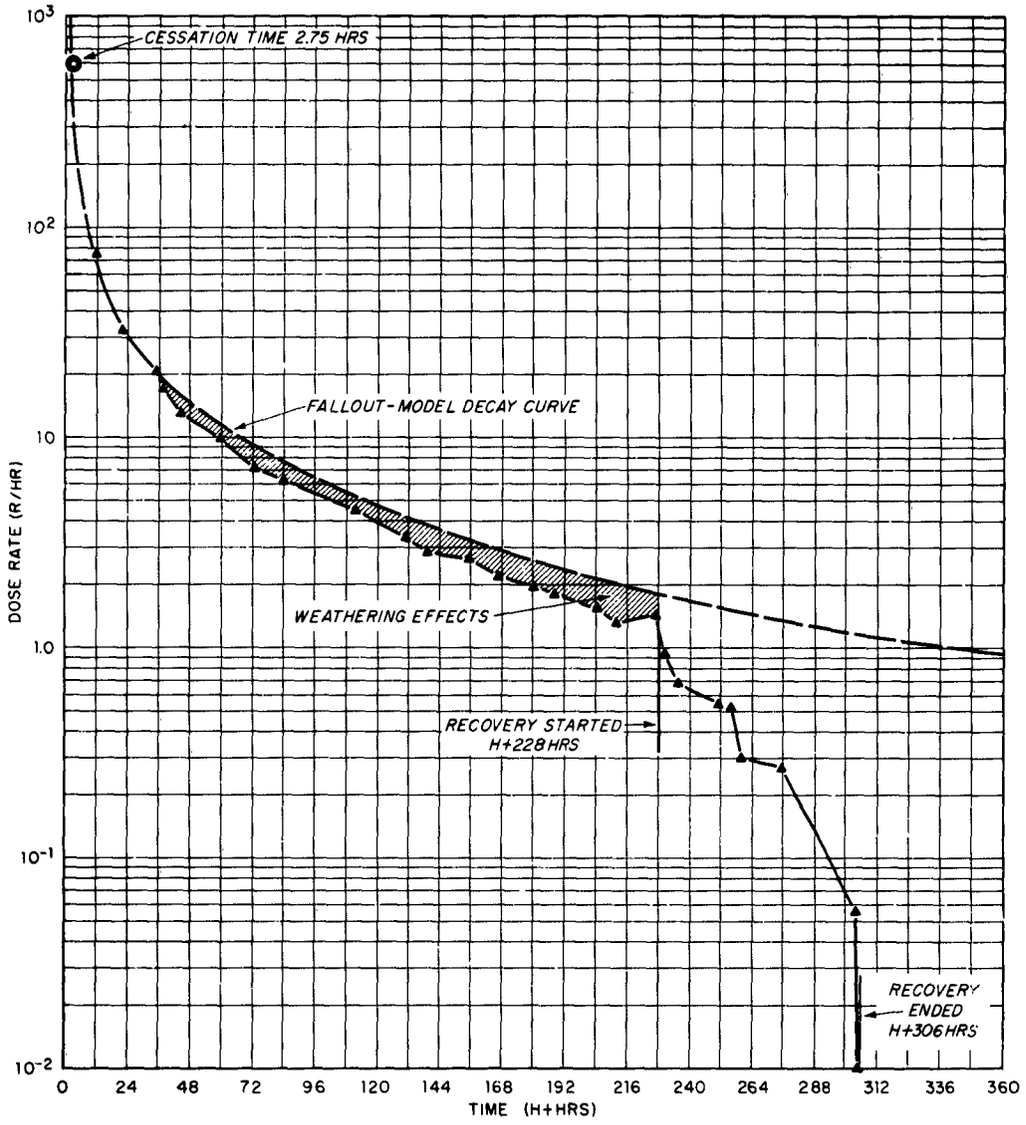

Fig. 3.8 Dose Rate History of Weathering and Recovery - Bldg. 571 (Station 14)

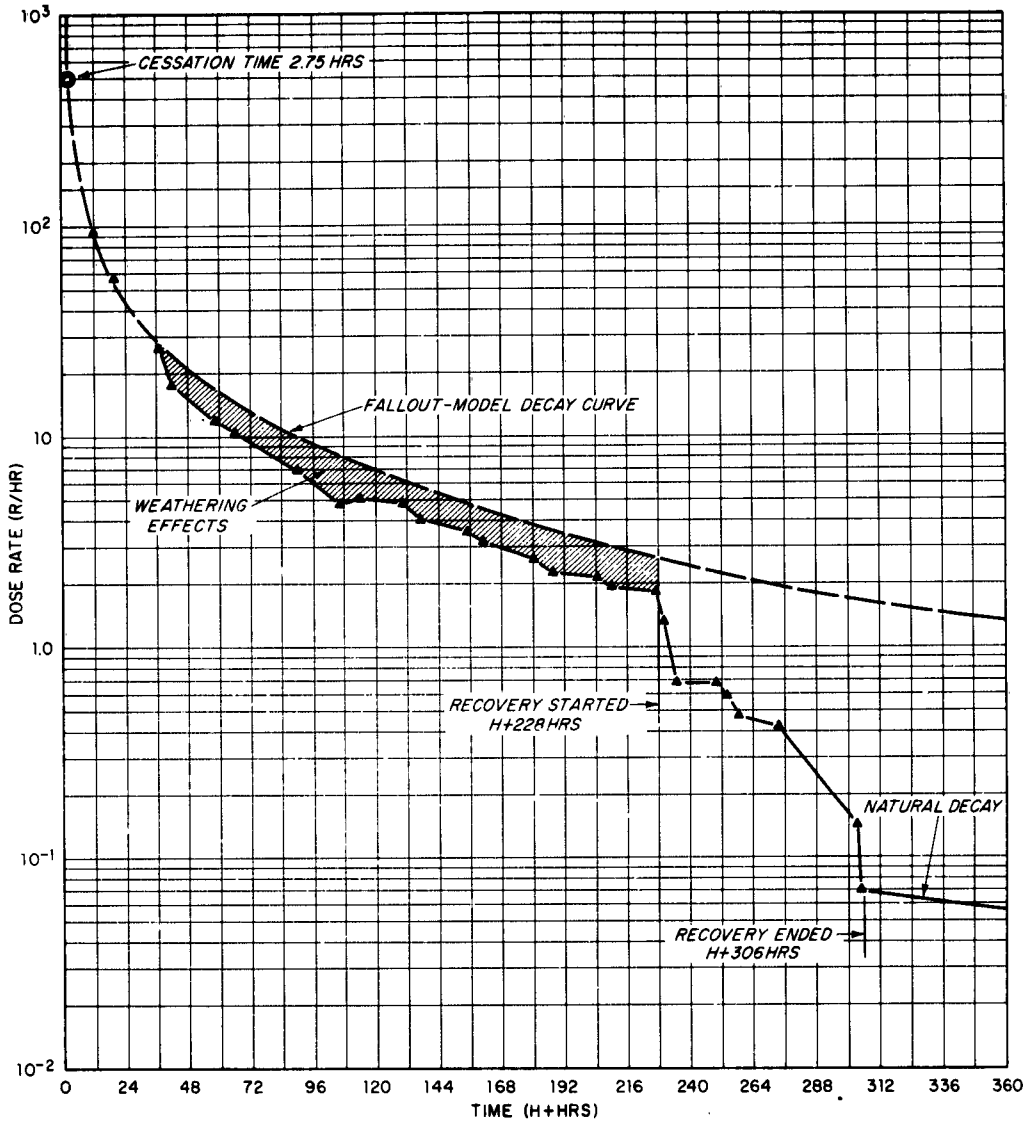

Fig. 3.9 Dose Rate History of Weathering and Recovery - Roof Bldg. 571 (Station 14R)

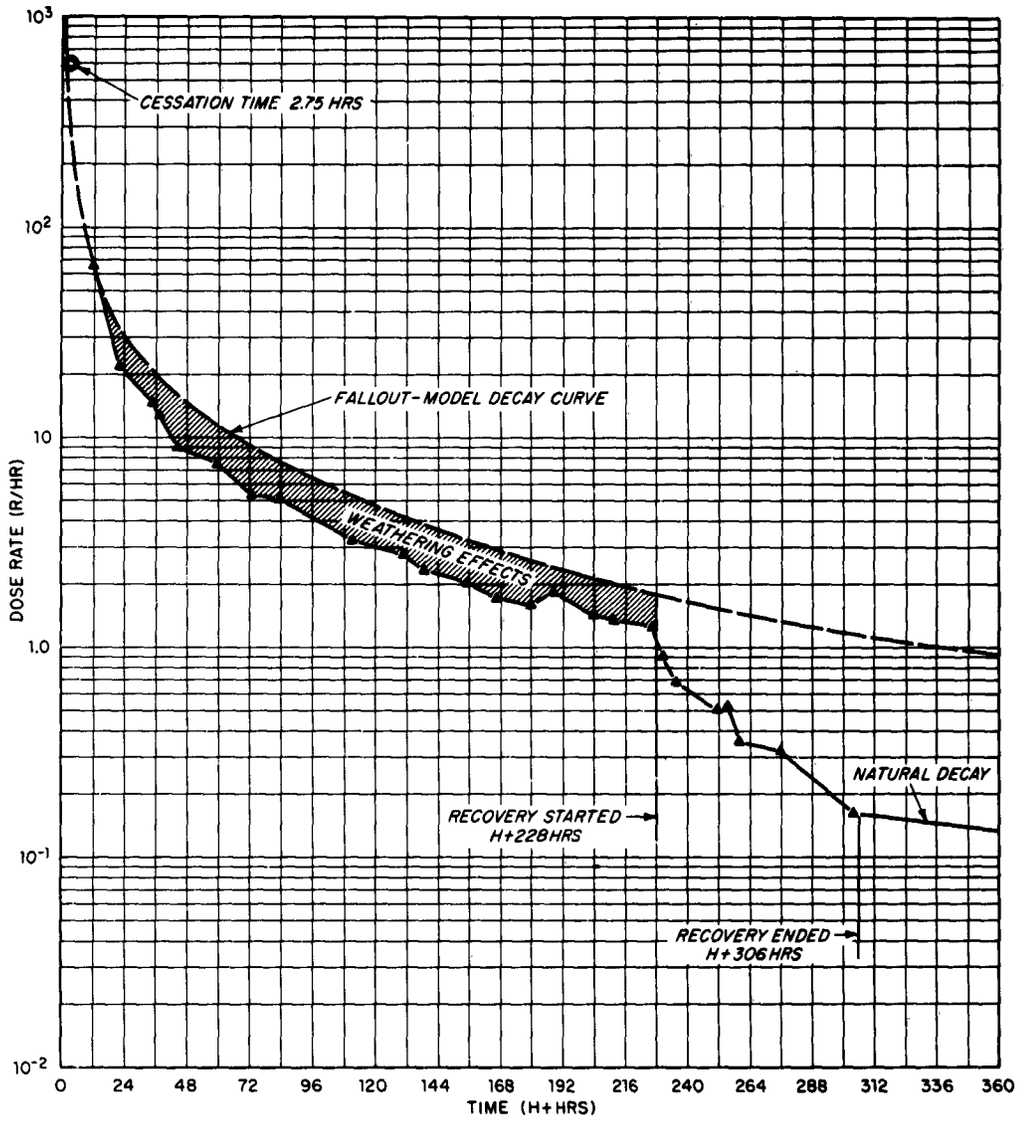

Fig. 3.10 Dose Rate History of Weathering and Recovery - Bldg. 572 (Station 7)

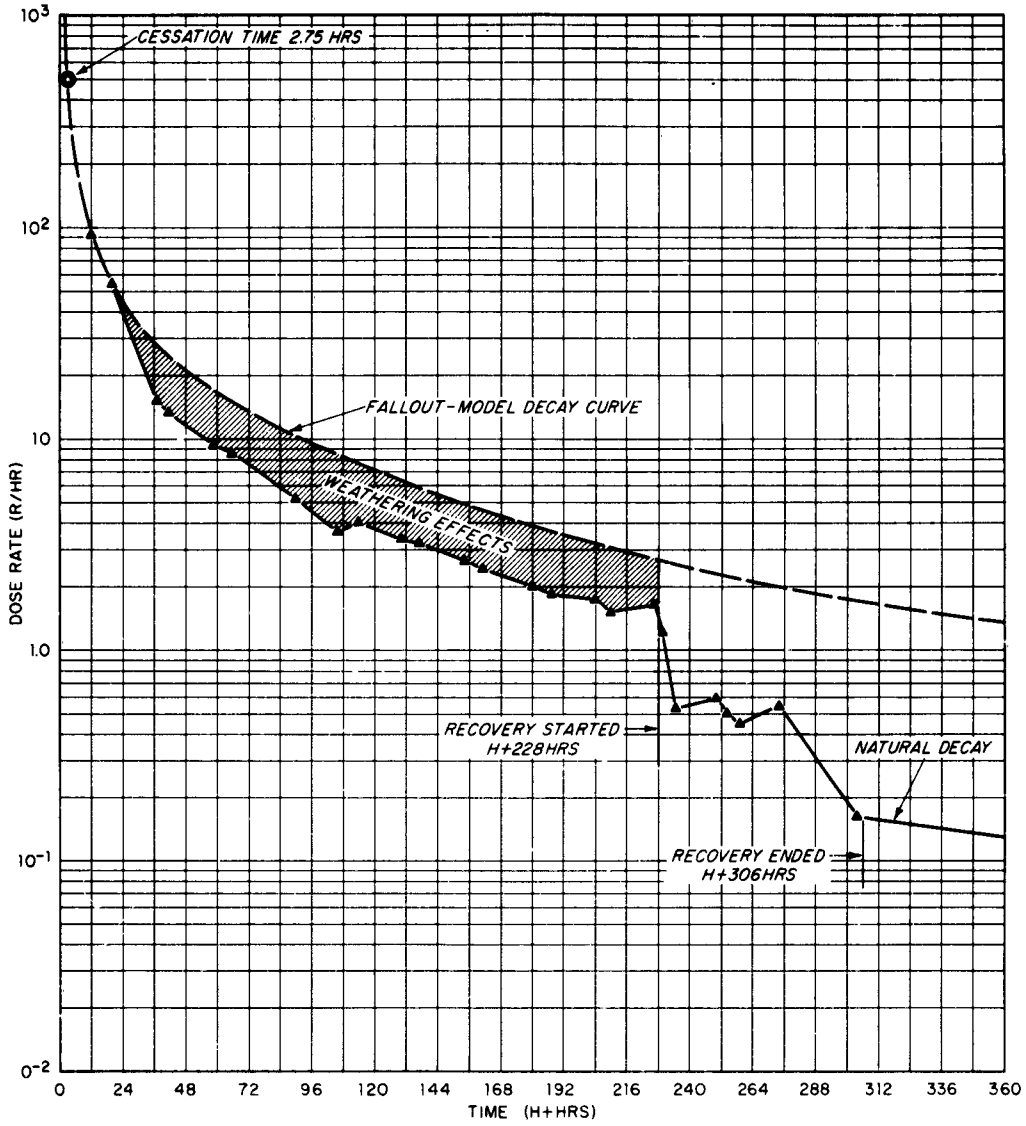

Fig. 3.11 Dose Rate History of Weathering and Recovery - Roof Bldg. 572 (Station 7R)

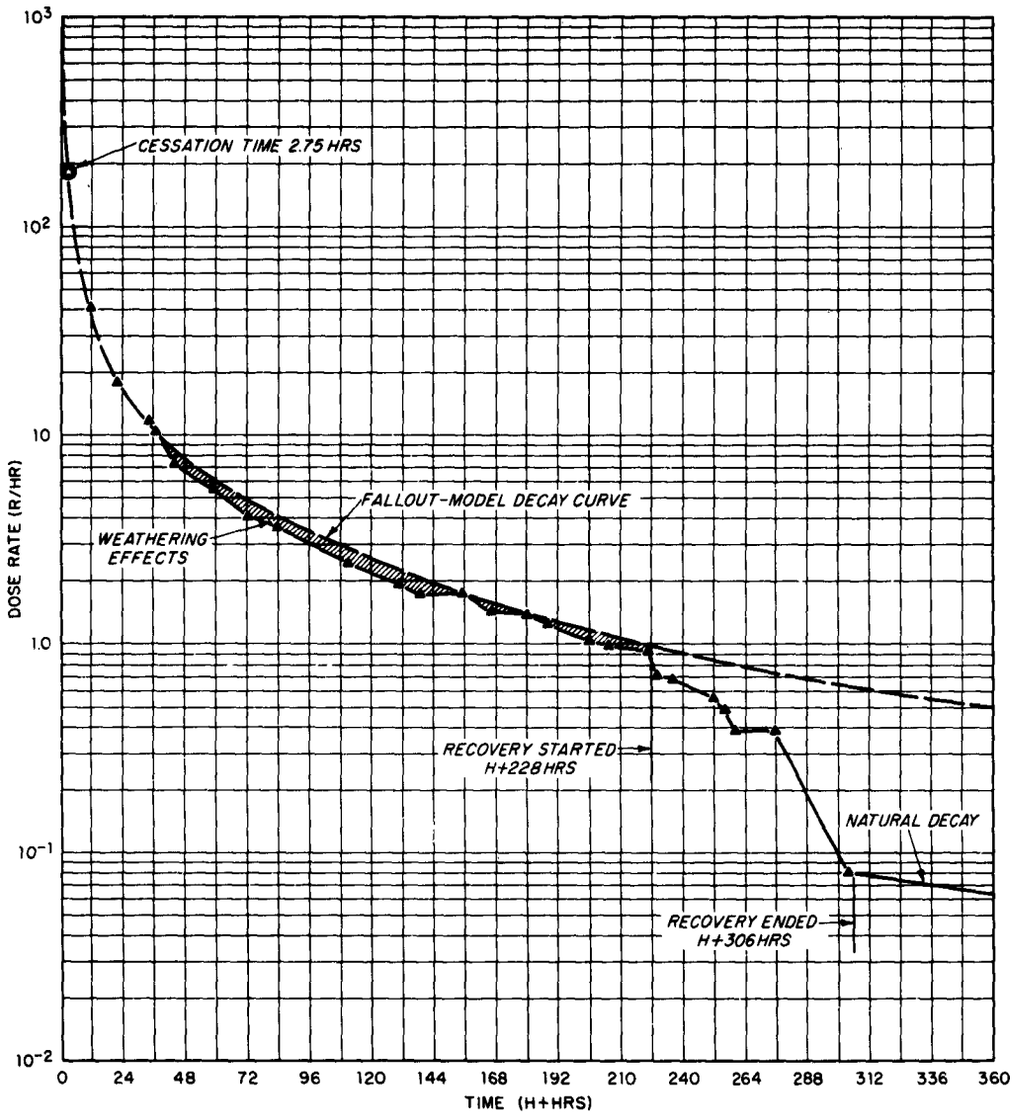

Fig. 3.12 Dose Rate History of Weathering and Recovery - 1st Floor Bldg. 573 (Station 12)

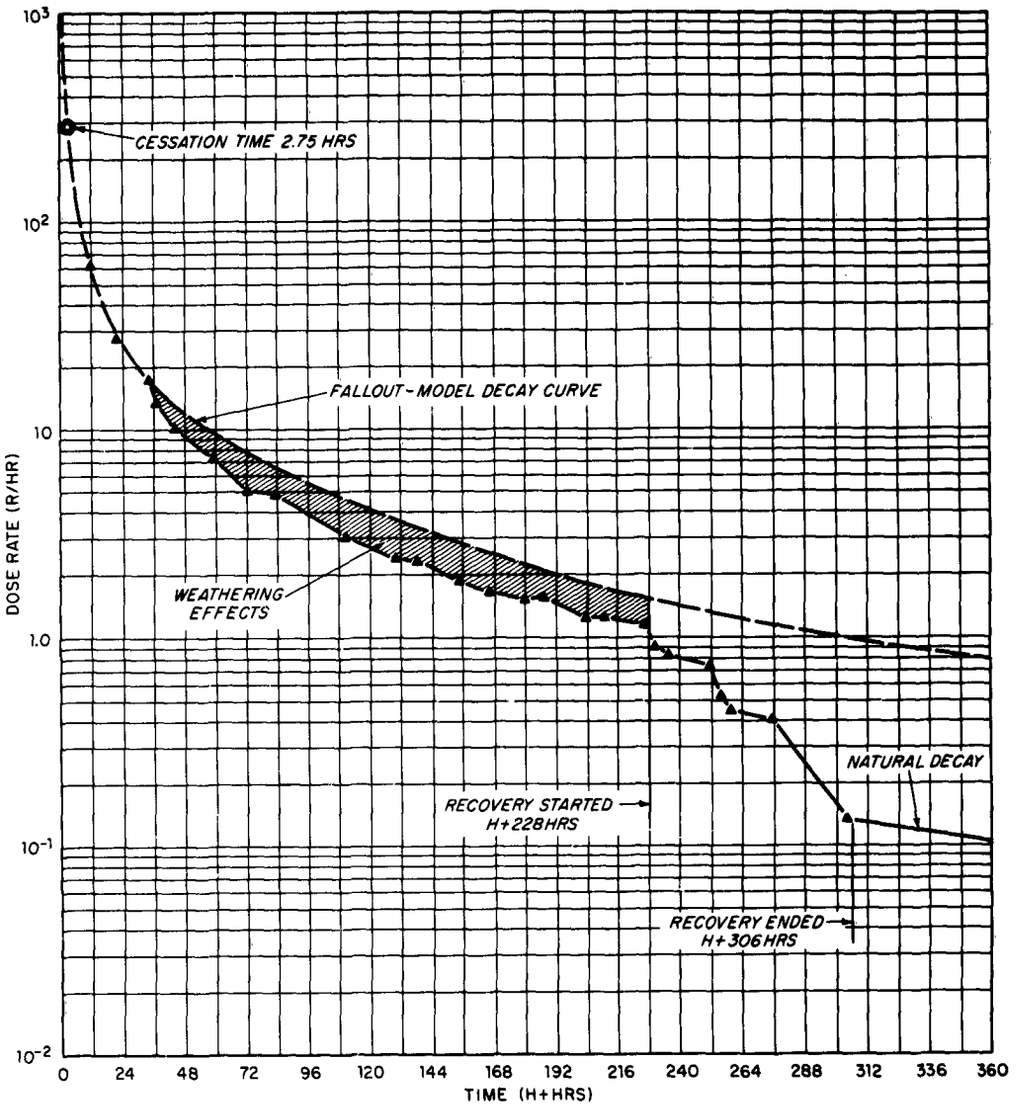

Fig. 3.13 Dose Rate History of Weathering and Recovery - 2nd Floor Bldg. 573 (Station 10)

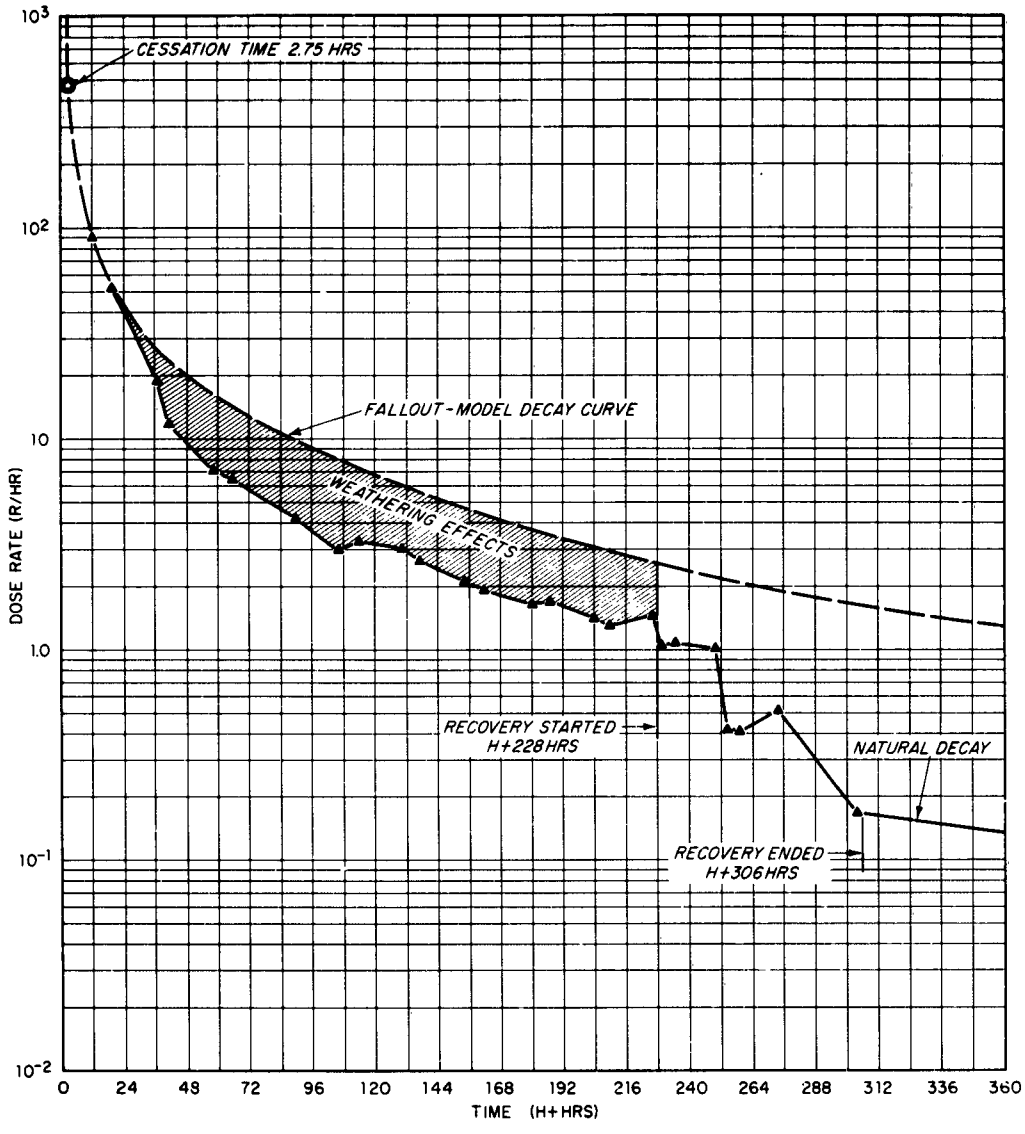

Fig. 3.14 Dose Rate History of Weathering and Recovery - Roof Bldg. 573 (Station 10R)

TABLE 3.6

Dose Rate Reduction by Weathering and/or Recovery

Surface or Space	Instrument Location	Station No.	Percent Reduction		
			Weathering	Recovery	Combined
Asphaltic concrete	10th St	19	34.9	62.1	97.0
Asphaltic concrete	Plaza	4	75.6	19.8	95.4
Land - no vegetation - flat surface	Terrace	2	51.8	30.6	82.4
Land - vegetation	East field	3	0	61.5	61.5
Bldg interior	Bldg 572	7	38.3	47.7	86.0
Bldg interior (upper floor)	Bldg 573-U	10	33.3	53.4	86.7
Bldg interior (lower floor)	Bldg 573-L	12	13.3	74.0	87.3
Bldg interior	Bldg 571	14	33.7	66.1	99.8
Bldg interior	Bldg 570	17	35.9	57.8	93.7
Tar and gravel roof	Bldg 572	7R	47.0	43.5	90.5
Tar and gravel roof	Bldg 573	10R	52.7	37.2	89.9
Tar and gravel roof	Bldg 571	14R	56.6	38.6	95.2
Tar and gravel roof	Bldg 570	17R	40.1	52.8	92.9

Removal effectiveness indicated by shielded gamma measurements for a given component may be quite high, but, because of the added contributions from the surrounding area, the resultant reduction in the unshielded dose rate will be considerably poorer. Conversely, the dose rate of the surroundings will decrease with improved recovery effectiveness in the given component.

The effect of weathering on the reduction of the dose rate at any location must be considered when planning the recovery operations. The redistribution of the dry fallout particles would affect the choice of recovery procedures. The excessive build-up of fallout along curbs may require successive passes by a street sweeper to effectively remove the fallout particles. Areas around buildings, in planting beds and lawns are usually the most difficult to decontaminate, since heavy equipment cannot operate efficiently in close quarters. These types of areas trap migrating fallout and consequently manual decontamination procedures are required to remove the fallout, resulting in greater manpower requirements.

The percentage reduction in the gamma dose rates in Table 3.6 due to weathering is the result of the migration of the dry fallout particles to and/or from the various sources that contribute to each location. For example, the reduction in the dose rates inside buildings is due not only to the migration of particles from the roof surfaces but also to the migration of particles from the sidewalks and streets surrounding the building. From the percentage decrease in dose rate on the various types of surfaces listed in Table 3.6, the various surfaces can be ranked in order of decreasing susceptibility to migration of fallout, as follows: (1) large asphaltic surfaces (Plaza), (2) unplowed land (Terrace), (3) tar and gravel roofs, (4) asphaltic street (10 St) and (5) plowed land (East Field).

The Complex III rankings differ somewhat from those determined during Complex I. These differences can be explained by the change in surface texture. Prior to Complex III the unplowed land (Terrace) was bladed and compacted, resulting in a smooth vegetation-free surface, whereas during Complex I the Terrace was covered with a heavy growth of vegetation. Also the East Field was covered with vegetation during Complex III and plowed at Complex I. The tar and gravel roofs, after two complex experiments, had all loose gravel removed. This, in effect, made the tar and gravel comparable to smooth compacted soil in its susceptibility to migration.

Type of Surface	Dose Rate Reduction by Weathering (%)	
	Complex I	Complex III
Large asphalt surface	41	76
Asphalt street	30	35
Tar and gravel roofs	8	49
Land, no vegetation, unplowed: Terrace	-	52
Land, no vegetation, plowed: East Field	2	-
Land, vegetation: Terrace	1	-
Land, vegetation: East Field	-	0

The dose rate history curves for the surfaces that experienced the greatest weathering effects all show a departure from the theoretical decay curves at approximately H+36 hours. The wind records showed exceedingly high winds during this period. Weathering results from Complex I agrees generally with the earlier findings of Chepil[8,9] relating to the erosion of soil by wind. Chepil stated that wind velocities greater than 10 knots (measured at a one ft height) are required to initiate erosion of soil particles in the 150 μ to 300 μ size range. Wind velocity measurements were obtained during Complex III at three different locations, all one foot above the surface of interest. Table 3.7 lists the times at which the wind velocity exceeded 10 knots during the weathering phase. The maximum wind speeds were experienced at all three locations between H + 28 to H + 48 hours, which brackets the period of greatest weathering.

Gamma radiation measurements taken during and after the weathering phase outside the perimeter of the target complex area indicated that negligible amounts of the dry fallout particles had left the confines of the target complex area. The winds redistributed the dry fallout particles to areas within the target complex where surface roughness, vegetation and obstructions trapped them more permanently. Even though this redistribution reduced the gamma dose rate at the various measuring locations, the recovery procedures employed still had to cope with the total mass of fallout material originally dispersed.

As a result of the recovery operation described in Section 2.7, a further reduction in dose rate occurred following the weathering phase. A tabulation of weathering and recovery effects in terms of percent reduction is given below. Dose rate reductions from Complex I are given for a basis of comparison.

TABLE 3.7

Times at Which Wind Velocity Exceeded 10 Knots During the Weathering Phase

Date	Time H +	Direction	Maximum Velocity (knots)
		Plaza	
Oct 8 (D+0)	10-18	West	17
Oct 9 (D+1)	28-48	North	31
Oct 10 (D+2)	50-64	South-West	14
Oct 11 (D+3)	85-88	West	14
Oct 12 (D+4)	106-115	West	15
Oct 13 (D+5)	133-139	West	14
Oct 14 (D+6)	156-159	North	15
	163-168	North	27
Oct 15 (D+7)	169-170	North	21
	172-179	North	28
Oct 16 (D+8)	211-212	West	10
		10th St and Hamilton	
Oct 8 (D+0)	11-16	West	15
Oct 9 (D+1)	32-41	North	20
	44-45	West	14
Oct 11 (D+3)	77-78	West	10
Oct 12 (D+4)	106-107	West	10
	110-114		12
Oct 13 (D+5)	137-138	West	10
Oct 14 (D+6)	157-158	North-West	10
	164-166	North	14
	167-168	North	13
Oct 15 (D+7)	168-169	North	10
	179-185	North-East	
Oct 16 (D+8)	221-222	North	10
		Roof Height	
Oct 8 (D+0)	10-18	West	21
	20-21	West	10
Oct 9 (D+1)	28-48	North	40
Oct 10 (D+2)	59-64	South-West	18
	66-67	West	10
Oct 11 (D+3)	83-90	West	16
Oct 12 (D+4)	105-115	West	20
Oct 13 (D+5)	133-139	West	19
Oct 14 (D+6)	156-160	West	15
	163-168	North	30
Oct 15 (D+7)	168-170	North	15
	177-188	North	29
Oct 16 (D+8)	203-204	West	10
	208-209	West	10
	211-212	West	13

	Complex III		Complex I	
	Station 14 Bldg 571	Station 19 10th St	Station 14 Bldg 571	Station 19 10th St
Weathering	33.7	34.9	27.3	33.6
Recovery	66.1	62.1	60.6	63.5
Combined	99.8	97.0	87.9	96.1
Residual	0.2	3.0	12.1	3.9

In each experiment the combined effects of weathering and recovery are nearly equal for the location on 10th St, but the total reduction achieved in building 571 during Complex III is greater than that of Complex I. This may be due to the condition of the roof, which contributes over 50 % of the dose rate at station 14. As pointed out in the previous section this roof provided a much different surface texture than at Complex I and consequently the dry fallout particles were easier to remove in Complex III. Regardless of complex experiment or location, weathering accounted for about 1/3 of the total reduction in dose rate.

The effects of weathering and recovery on the dose rate experienced in building 573, a two story building, can be summarized as follows:

	% Reduction		
Station	Weathering	Recovery	Combined
1st floor Station 12	13.3	74.0	87.3
2nd floor Station 10	33.3	53.4	86.7
Roof Station 10R	52.7	37.2	89.9

The reduction in dose rate by weathering was greatest on the roof and least at the 1st floor station and, conversely, the reduction during recovery was greatest at the 1st floor and least on the roof. However the combined effects at both locations (and the 2nd floor as well) were about the same. During weathering, fallout particles removed from the roof by winds were deposited on the areas surrounding the building and, consequently, the reduction in dose rate at the first floor level was not as high as that experienced on the roof.

The advantage of having paved areas instead of lawns around a structure is apparent from the total reductions in dose rate observed inside the three single story buildings. The latter are ranked below in order of increased percent reductions.

Building	Station No.	Relative Amount of Paved Area	% Dose Rate Reduction
572	7	Least	86.0
570	17	Intermediate	93.7
571	14	Most	99.8

In accordance with the above ranking: building 572 has lawns on two sides, a land area off the back, and a paved drive at one end; building 570 has lawns on all sides, but is backed closely by the Plaza; and building 571 has a lawn on part of one side only, the rest of the grounds are paved. From this evidence it would appear that maximum reduction of interior dose rates may be expected where surroundings are mostly paved.

3.3 RECOVERY DOSE

The target dose rate histories shown in the preceding section provide a graphic illustration of the radiation levels hypothesized for this experiment and that may be encountered in a real fallout situation. Of greater importance, however, is the radiation dose represented by the areas under these curves. Consider, for example, the dose rate history given in Fig. 3.2 for 10th St. Assuming a continuous exposure, an area summation under the recovery portion of the lower curve (from 228 to 306 hr) results in a radiation dose of 48 r. The dose to recovery crews would be somewhat smaller, since only 1/3 of the continuous 78 hr phase indicated would be devoted to actual recovery. Nevertheless, doses $\geq$ 48 r could be accrued by these same crews if it were necessary to start recovery considerably earlier. Therefore, a capability for estimating the expected dose to recovery personnel is an extremely important requirement of the advance recovery planning.

For the purposes of this study it is assumed that adequate shelters are available. Thus, the dose during the emergency phase may be considered negligible. The significant dose is that accrued during the recovery and mission phases following the emergency. This section deals with just the recovery phase and the determination of the recovery dose. A detailed treatment of dose determination for both the recovery and mission phases is given in Ref. 1.

3.3.1 Dose Determinations

In general, dose may be thought of as the product of dose rate and time. But, because dose rate is also a function of time, dose D is more properly expressed as

$$D = \int_{t_x}^{t_y} I(t)\, dt \qquad (2)$$

where I = the fallout radiation intensity in r/hr at a height of 3 ft
t = the time in H + hours.

Just how the dose rate I from fallout varies will depend upon the combined effects of radioactive decay, weathering, recovery and shielding.

Curves showing the expected decrease in dose rate due to decay effects only are available from field test data and/or theoretical considerations. The upper curve in Fig. 3.2 is a typical example. Graphical integration of the area beneath such a decay curve over a time interval from t_x to t_y corresponds to the right hand member of Eq. (2). The resultant dose D will represent the potential (hypothetically maximum) free field dose due to undisturbed fallout.

The potential dose over the 78 hr period cited earlier is found from Fig. 3.2 to be 230 r. The difference between this value and the 48 r dose mentioned previously for the same time interval is due to the additional effects of weathering and recovery. Unfortunately, dose rate history curves will not be available until after completion of recovery - too late for planning purposes. Other means must be employed to predict the recovery dose.

From the foregoing, two factors are worth emphasizing. First, potential dose D can be computed from appropriate fallout decay curves. Second, actual dose D' will be significantly less than D. The decrease between potential and actual doses is customarily represented by a dose reduction factor termed residual number RN. Thus, the dose during a particular reclamation task becomes

$$D_2' = RN_2\, D_2 \qquad (3)$$

where, through an established precedent, the subscript 2 denotes the recovery phase. (Subscripts 1 and 3 signify shelter and mission phases, respectively). Predicting recovery dose, then, is largely a problem of finding a suitable residual number.

The concept of an RN_2 value has meaning only with reference to a particular reclamation method. Because RN_2 values differ from method to method, they are a function of individual reclamation effectiveness. In addition, RN_2's are markedly influenced by cumulative recovery effectiveness, target shielding, and equipment shielding. The relationship between RN_2 and this combination of reduction factors can be shown to be

$$RN_2 = F_n S\ (RC) \tag{4}$$

where F_n = the cumulative recovery effectiveness, i.e., the average fractional radiation level remaining in the target area any time during the recovery phase. F_n approaches the final recovery effectiveness F as the recovery nears completion.

S = the target shielding factor, which is a constant for a given location within a built-up area.

RC = the reclamation coefficient, which is a complex function of reclamation effectiveness F_j and equipment shielding S_e.

F_n and S may be calculated from contribution factors which are defined and discussed in Section 3.4. RC values, however, must be derived from detailed dose rate histories of actual surface reclamation experiments. This is explained as follows.

If Eq. 3 is solved for RN_2 and set equal to Eq. 4, the general expression for reclamation coefficient becomes

$$RC = 1/F_n\ (D_2'/SD_2) \tag{5}$$

In an isolated reclamation experiment involving one target component F_n becomes unity and may therefore be dropped from Eq. 5 in determining RC. D_2' will equal the area under the experimental dose rate history curve. The product SD_2 corresponds to the potential (free field) dose from Eq. 2 corrected for target shielding effects. Thus the experimentally derived RC value may be expressed as the ratio of two doses

$$RC = D_2'/D_2^o \tag{6}$$

where D_2' = actual dose to reclamation crews during a time interval Δt.

D_2^o = SD_2, the dose that would result without the benefit of reclamation over the same time interval.

When experiments employ relatively long lived radiotracers like Ba^{140}-La^{140}, D_2^s may be obtained, to a good approximation, from the product of the time interval Δt and radiation intensity i_o^* at the start of a given reclamation test. This is especially true of the complex experiments, since reclamation periods were limited to a few hours for any one method. For longer periods, i_o might have to be corrected for radioactive decay effects. It should also be noted that the shielding factor S is contained inherently in both numerator and denominator of Eq. 6, hence its effects cancel.

Finally, from Eq. 6, the expression for experimental RC value becomes

$$RC = D_2'/i_o \Delta t \qquad (7)$$

Solution to Eq. 7 is obtained directly from specific dose rate history data. This in turn may then be used to solve Eq. 4 for the corresponding RN_2 value.

3.3.2 Typical Dose Rate Histories

In order to establish RC (and eventually RN_2) values, a dose rate history was recorded for each reclamation method-surface combination encountered during the recovery phase of the complex experiment. Portable radiacs were used to monitor the changing gamma dose rate alongside recovery personnel. Where necessary, measurements were taken as often as once every minute. The dose rate history of each reclamation method was plotted to provide curves for determining the required D_2' values.

Figures 3.15 through 3.23 contain typical dose rate curves for eight basic reclamation methods. In all cases the curves are extremely irregular. They rise and fall as reclamation progresses, depending upon:

(a) The procedural pattern employed by teams with respect to the surface being reclaimed.
(b) The temporary interruption of strong radiation contributions (from outside the work surface), due to shielding by heavy equipment, buildings and other obstructions.
(c) The repeated filling and dumping of simulant collectors such as sweeper hoppers and loader buckets.

*Lower case i represents experimental mr/hr intensities as distinct from anticipated r/hr fallout intensities represented by upper case I.

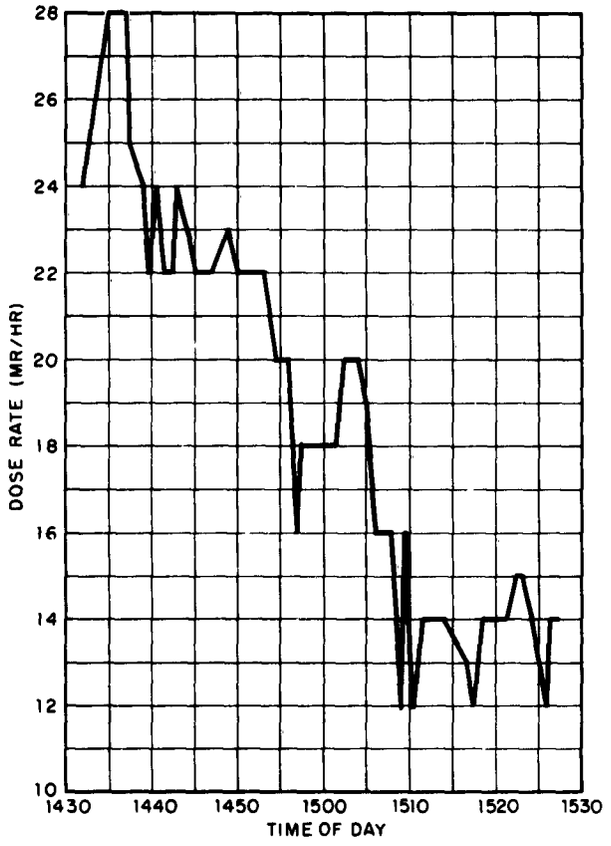

Fig. 3.15 Dose Rate History for Firehosing Roof - Bldg 571

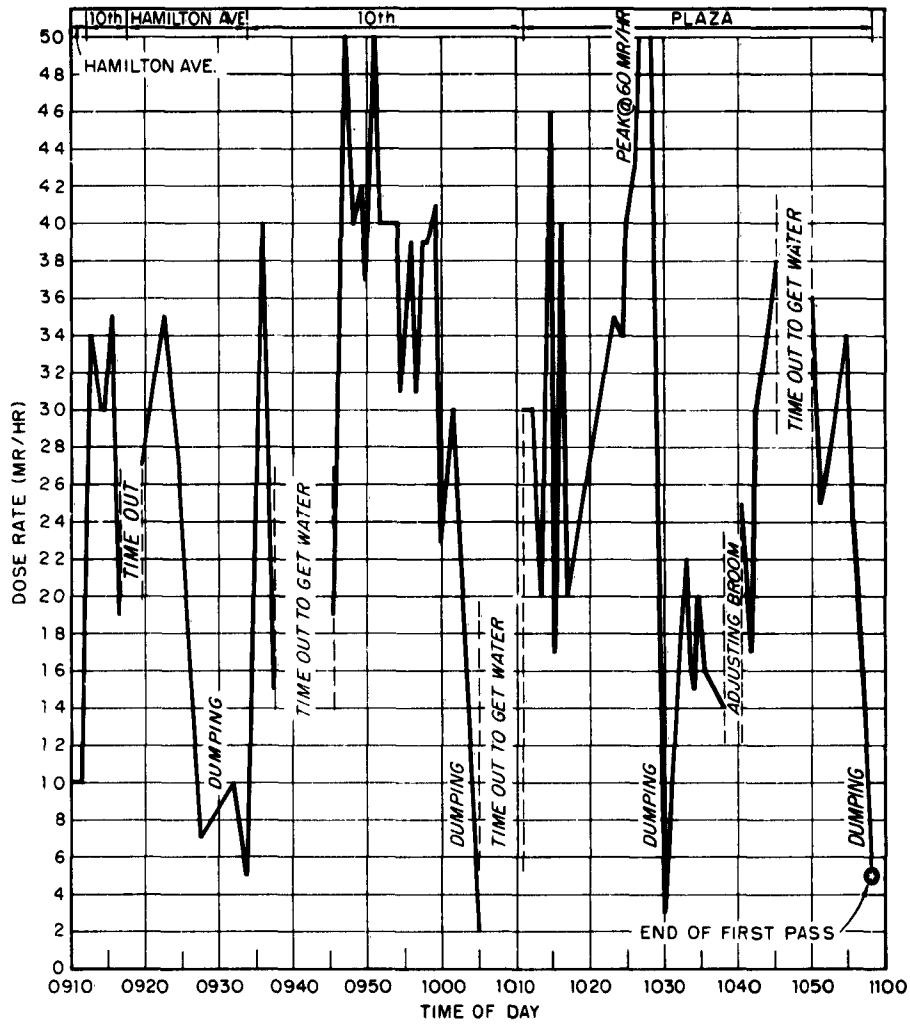

Fig. 3.16 Dose Rate History for Motor Sweeping - First Pass

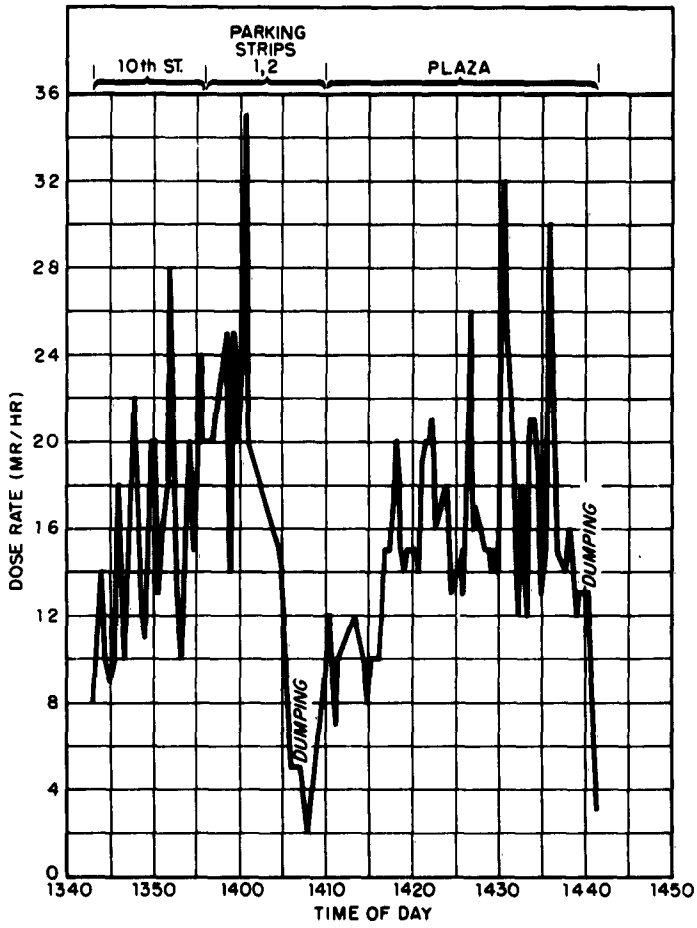

Fig. 3.17 Dose Rate History for Motor Sweeping - Second Pass

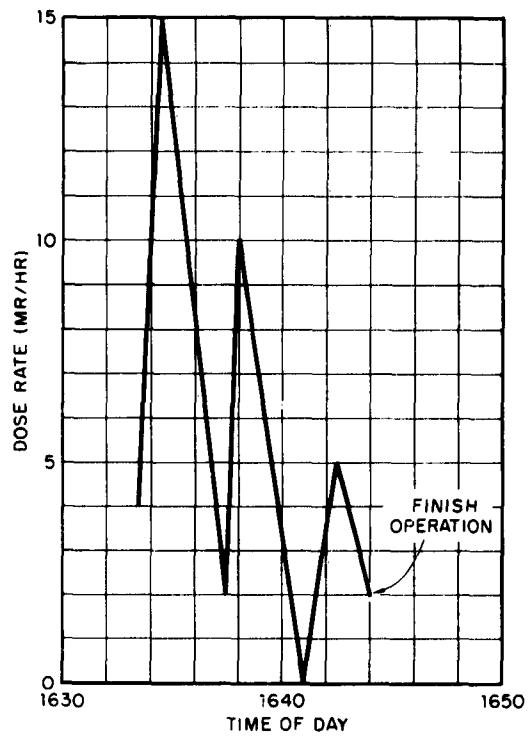

Fig. 3.18 Dose Rate History for Motor Flushing Plaza

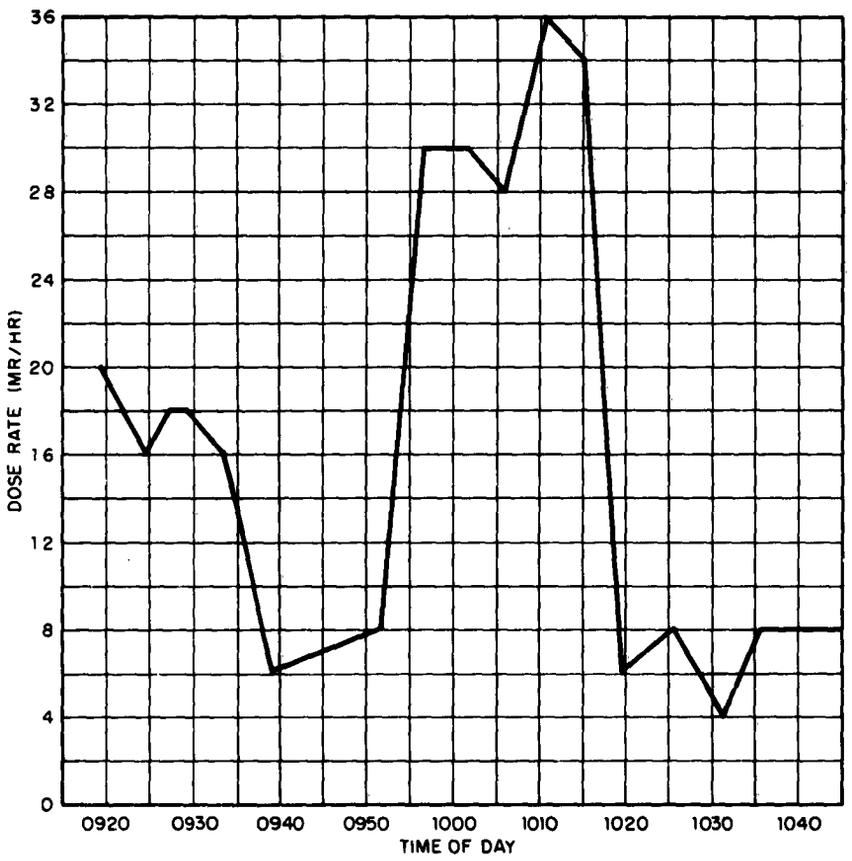

Fig. 3.19 Dose Rate History for Motor Grading Terrace

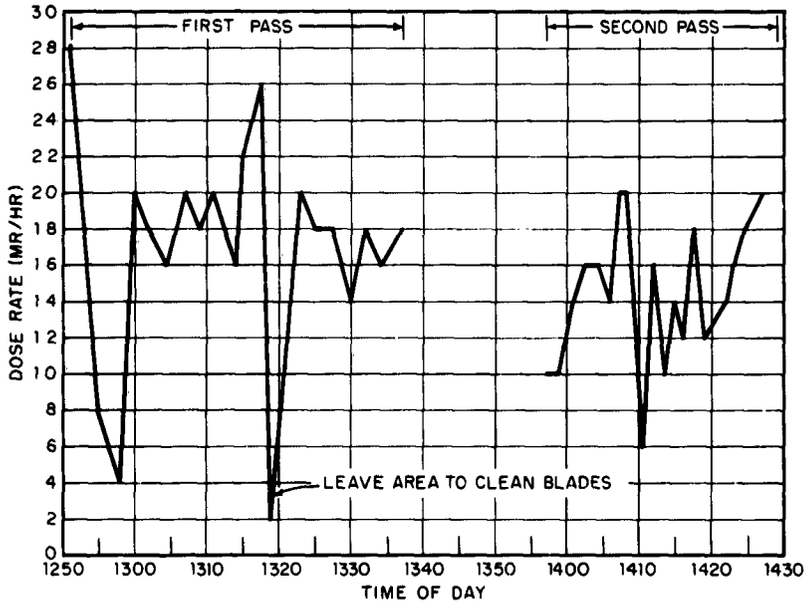

Fig. 3.20 Dose Rate History for Rototilling East Field

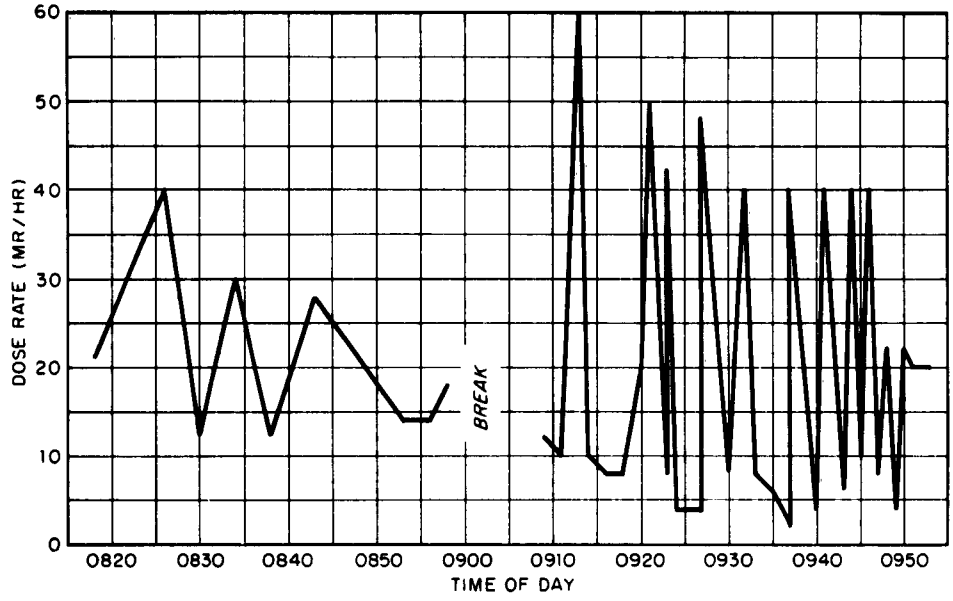

Fig. 3.21 Dose Rate History for Tractor Scraping Lawns

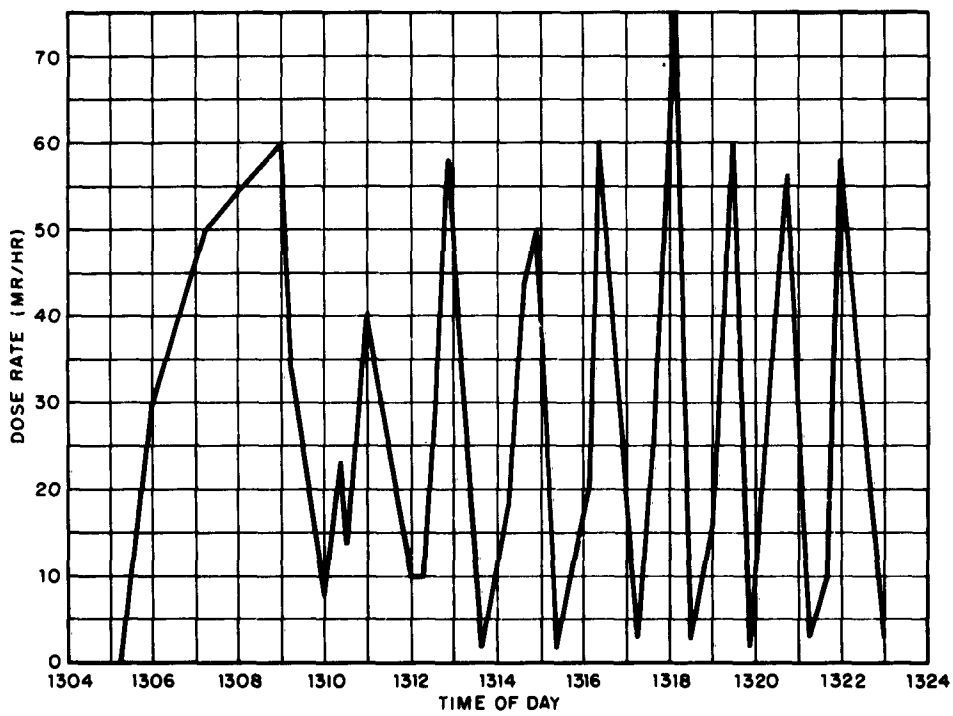

Fig. 3.22 Dose Rate History for Loading Spoil

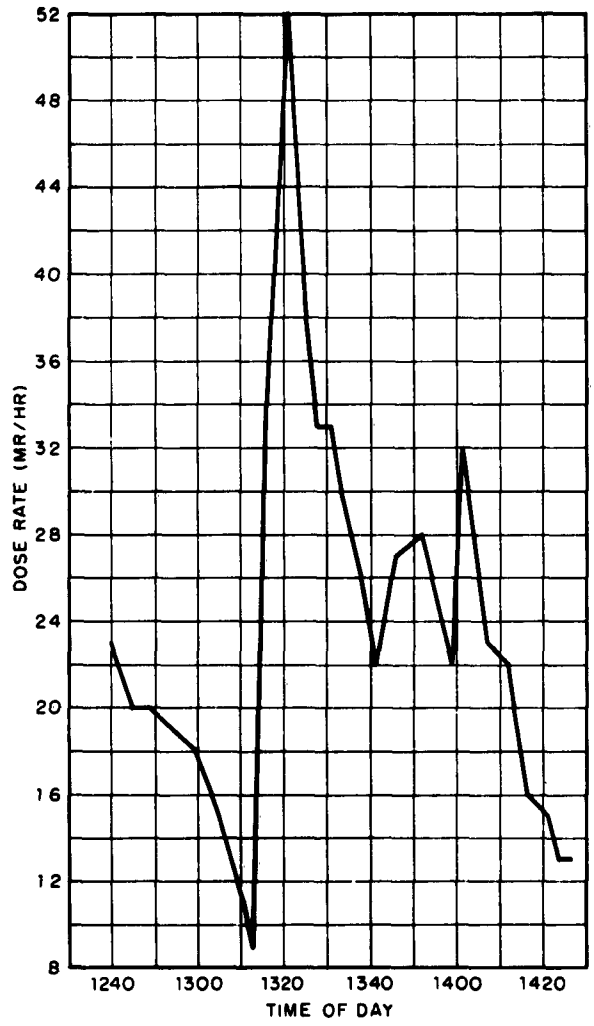

Fig. 3.23 Dose Rate History for Shoveling Lawns

Because of variations and interactions among the above factors, there appears to be no set trends in the dose rate histories, except in the case of sweeping and possibly loading.* The sweeper history in Figs. 3.16 and 3.17 shows a succession of jagged humps. As would be expected, the dose rate builds up with the accumulation of simulant and drops sharply when the hopper is emptied. The loader exhibits a saw tooth history (see Fig. 3.22) with maxima when the bucket is full and minima when the bucket is dumped.

3.3.3 Derived Reclamation Coefficients

From the dose rate histories it was possible to solve Eq. 7 for the desired RC values. These are given (together with the calculations) in Tables 3.8 through 3.12 for eleven separate reclamation operations. The notation $(RC)_j$ is used to distinguish individual or step coefficients from the average or composite RC values. Where available, results from Complex II are also listed.

A comparison of the entries in these tables shows only rough agreement between Complex II and Complex III results. This is to be expected, since the two experiments were dissimilar in a number of respects affecting reclamation coefficients. For instance,

(1) Simulant mass loading differed between complex experiments by a factor of three.

(2) Leaching of the radiotracer from the tagged sand during the weathering phase of Complex II altered the reclamation effectiveness of certain methods.

(3) The sequence of procedural techniques for the various reclamation methods was not consistent between the two experiments.

Where replicate results were obtained for a given method during Complex III, the RC values are quite variant. Standard deviations of around 5 % are associated only with sweeping (for one pass) and shoveling (of planter beds). The remaining operations exhibit standard deviations ranging from $\pm$ 9 % for firehosing roofs to $\pm$ 40 % for loading spoil. Deviations of this magnitude are not unusual, however, considering the small number of data samples (4 or less per method).

*The apparent trend exhibited by firehosing in Fig. 3.15 is misleading. Comparison with other histories for this method indicates the trend to be highly unpredictable.

TABLE 3.9

Reclamation Coefficients, RC, for Sweeping and Flushing

Location	Δt (hr)	i_o* (mr/hr)	D_2^o (mr)	D_2' (mr)	$(RC)_j$	RC ($\pm$ % σ)	RC for Complex II
			Sweeping				
Hamilton Ave							
One Pass	0.29	26	7.55	4.81	0.64	0.64	2.23
10th St							
1st Pass	0.47	23	10.80	16.50	1.53	1.53	2.39
2nd Pass	0.50	21.1	10.55	6.50	0.62		
Two Passes			21.35	23.00		1.08	1.62
Plaza							
1st Pass	0.62	16	9.93	16.34	1.65	1.65	1.18
2nd Pass	0.47	15.3	7.20	7.24	1.01		
Two Passes			17.13	23.58		1.37	0.83
Totals and Average for 1 Pass			20.73	32.84		1.58 $\pm$ 6	1.42
Totals and Average for 2 Passes			38.48			1.21 $\pm$ 16	1.03
			Flushing				
Plaza	1.55	17	26.40	4.32	0.16		

*All intensities are averages of 3 ft ground readings taken just before start of sweeping or flushing.

TABLE 3.10

Reclamation Coefficient, RC, for Grading and Rototilling

Location	Δt (hr)	i_o* (mr/hr)	D_2^o (mr)	D_2' (mr)	$(RC)_j$	RC ($\pm$ %σ)
			Motor Grading			
Lawns - Bldg 571	0.290	45.0	13.05	2.83	0.217	
Lawns - Bldg 573	0.267	85.0	22.70	3.70	0.163	
Terrace	1.475	63.0	92.25	22.75	0.247	
Totals and Average			128.00	29.28		0.23 $\pm$ 22
			Rototilling			
East Fields						
First Pass	0.716	41	29.40	11.26	0.383	0.38**
Second Pass	0.533	41	21.87	7.85	0.359	0.36
Totals and Average			51.27	19.11		

* All intensities are averages of 3 ft ground readings taken just before start of grading or rototilling.

**Same as average value reported for plowing - Complex II.

TABLE 3.11

Reclamation Coefficients, RC, for Soil Removal Operations

Location	Δt (hr)	i_o* (mr/hr)	D_2^B (mr)	D_2' (mr)	$(RC)_j$	RC ($\pm$ % σ)
			Tractor Scraping			
Bldg 570 - lawns	2.24	40	89.6	35.41	0.395	
Bldg 572 - lawns	2.20	53	116.6	39.02	0.335	
Bldg 573 - lawns	1.26	120	151.20	49.99	0.331	
Totals and Average			357.40	124.42		0.35 $\pm$ 11**
			Loading (Payloader)			
Bldg 570 - lawns	3.270	45	147.15	22.60	0.154	
Bldg 572 - lawns	2.167	52	112.08	20.23	0.179	
Bldg 573 - lawns	0.600	120	72.0	6.08	0.084	
Sub totals and Average			331.23	48.91		0.15 $\pm$ 40
Bldg 571 - beds	1.283	22	28.27	8.64	0.306	
Terrace	0.317	33	10.46	1.08	0.103	
10th St	0.846	35	29.61	7.77	0.262	
Sub totals and Average			68.34	17.49		0.26 $\pm$ 46
Grand totals and Average			406.62	71.07		0.18 $\pm$ 40

* All intensities are average 3 ft ground readings taken just before start of the given soil removal method.
**Complex II value was 0.42.

TABLE 3.12

Reclamation Coefficients, RC, for Manual Tasks

Location	Δt (hr)	i_o* (mr/hr)	D_2^o (mr)	D_2' (mr)	$(RC)_j$	RC ($\pm$ % σ)	RC for Complex II
			Hand Shoveling				
Bldg 570 - Lawns	1.658	50	82.90	45.34	0.547		
Bldg 571 - Lawns	1.383	39	53.94	38.51	0.714		
Totals and Average			136.84	83.85		0.61 $\pm$ 16	0.82
Bldg 570 - Beds	0.392	47	18.42	17.37	0.938		
Bldg 571 - Beds	0.280	31	8.69	8.34	0.961		
Bldg 572 - Beds	0.316	26	8.22	7.23	0.879		
Bldg 573 - Beds	0.630	37	23.31	22.80	0.978		
Totals and Average			58.63	55.74		0.95 $\pm$ 4	0.86
			Shoveling Assist to Scraper				
Bldg 572 - Lawns	2.15	16	34.40	38.23	1.111		
Bldg 573 - Lawns	1.31	25	32.75	23.11	0.706		
Terrace	0.316	10	3.16	2.95	0.934		
East Field	0.166	18	2.99	2.42	0.766		
Totals and Average			73.30	66.71		0.91 $\pm$ 22	0.64
			Shoveling Assist to Loader				
Bldg 570 - Lawn	0.283	11	3.11	3.01	0.968		
Terrace	0.250	33	8.25	10.63	1.288		
10th St	1.066	35	37.31	22.76	0.610		
Totals and Average			48.67	36.40		0.75 $\pm$ 53	

*All intensities are average 3 ft ground readings taken just before start of the given task.

In spite of these deviations, the relative magnitudes of the RC values are consistent within classes of reclamation methods. For instance, manual methods display average RC values between 0.5 and 1.0. With the exception of sweeping, motorized methods result in average RC values significantly less than 0.5. This is, of course, due to the shielding which the equipment provides the operator. Sweeping represents a unique case where the advantage of equipment shielding is cancelled by the buildup of simulant within the hopper. As a result, average RC values, for the first two passes at least, are greater than one. An exception is noted in Table 3.9 where an RC value less than one was obtained for Hamilton Ave. The analysis in the following section shows the worth of this particular result to be highly questionable.

3.3.4 Reclamation Coefficient Versus Effort

Results from the Complex II experiment[1] showed that, for firehosing roofs and sweeping pavements, RC decreased with the continued expenditure of reclamation effort. In each instance the surface was subjected to repeated passes by the respective reclamation method. Sweeping data from Complex III indicated a similar relationship. Findings from both experiments are presented in Fig. 3.24. Within the respective effort ranges shown the data points describe straight lines having a common slope of -1/2. The general equation fitting these curves is

$$RC = KE^{-1/2} \qquad (8)$$

where E represents the appropriate unit effort and K is a combined constant of proportionality and decay factor. Values of the latter are shown for each curve.

Four of the data points from Complex III and six from Complex II exhibit a strongly correlated trend defined by the lower curve. In view of this close correlation, the one outlying data point (corresponding to the result from Hamilton Ave.) may be ignored. That this point is of dubious value is further indicated by the fact that three Complex II data points from Hamilton Ave. fall on or very near the equated curve.

The upper curve represents Complex II results from sweeping 10th St only. The decreasing trend of this curve substantiates that of the lower curve, since both curves have a slope of -1/2. There is no ready physical explanation for the displacement of the two curves. If such differences as mass loading, hopper accumulation rate, surface roughness, surface shape, operator skill, etc. were influencing, then the

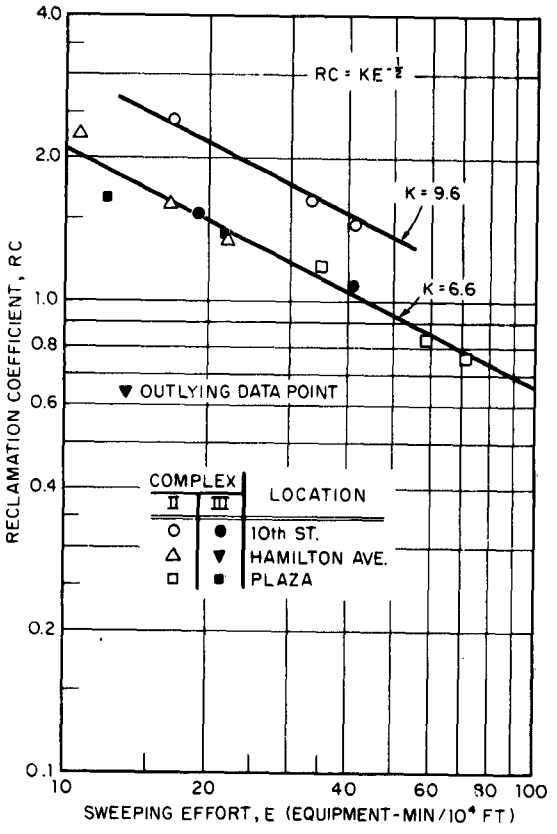

Fig. 3.24 Influence of Sweeping Effort on Reclamation Coefficients

points defining the lower curve should have shown no correlation at all. It can only be assumed that the displacement indicated by the K values shown in Fig. 3.24 may vary 30 to 50 %. Within this range, however, the present data demonstrates a reasonably predictable decrease in RC value with an increase in unit effort.

It should be pointed out that the curves shown in Fig. 3.24 should not be extrapolated in either direction. Extending them to the left results in unit effort values less than the minimum required for complete surface coverage. Continuing the curves to the right approaches prohibitive values of unit effort and unachievably small RC values. The fact must also be emphasized that, in spite of the decrease in RC value with the expenditure of time and effort, the dose to reclamation personnel continues to increase.

3.4 RADIATION CONTRIBUTIONS

An essential requirement of a reliable recovery planning procedure is a method for predicting the radiation contribution of each component to the overall radiation level within a potential target complex. Without this capability it becomes extremely difficult, if not impossible, to make acceptable estimates of such important planning variables as:

(a) Target shielding factor, S.
(b) Overall recovery effectiveness, F.
(c) Dose reduction factors, RN_2 and RN_3.

A simplified method for predicting contributions was devised in 1959 and used in Complex experiments I and II. Upon comparing the predicted values with those derived experimentally, it was concluded that, in spite of the apparent disagreement between a number of paired contributions (predicted versus measured), the general trend of correspondence demonstrated the prediction method to be basically sound. An attempt was made, therefore, to improve upon this method and recheck it against Complex III measurements.

3.4.1 Contribution Factors

In planning a recovery operation it is convenient to know the individual radiation contributions of the various target components to some common location usually near the center of the general working area. For a perfectly circular complex area the calculation of contributions to the center is relatively easy. Ignoring air absorption or self-absorption, the radiation intensity I from a uniformly contaminated area of radius r to a point at height h above the center is, according to Evans,[10]

$$I = k \frac{a}{r^2} \ln \left(1 + \frac{r^2}{h^2}\right) \qquad (9)$$

where a = the total activity in curies
k = the intensity at unit distance from a unit amount of activity.

The concentration of activity q in curies/ft^2 is equal to $a/\pi r^2$. Substituting πq for a/r^2 in Eq. 9

$$I = \pi k q \ln \left(1 + \frac{r^2}{h^2}\right) \qquad (10)$$

The product kq in Eq. 10 is equal to the intensity I* at a unit distance from a unit area. For uniform concentrations of contaminant I* will be constant. Therefore, the ratio I/I* will be proportional to radiation contributions from the surroundings. This ratio is defined as the contribution factor. Rewriting Eq. 10, the contribution factor for a circular area becomes

$$cf\ (circle) = \pi \ln \left(1 + \frac{r^2}{h^2}\right) \qquad (11)$$

For a circle having an area equal to that of the complex, the radius r would equal 212 ft. Setting h equal to 3 ft, Eq. 11 may be solved to give a value of 26.8 as the total contribution factor for the equivalent circle.

In calculating the cf values for the target complex, Eq. 11 was used for a circular area immediately surrounding the reference location, station 19 in the middle of 10th St. This centrally located area is designated as sector T6 in Fig. B.8 of the Appendix. Its diameter is 32 ft corresponding to the width of 10th St.

Contributions from sectors lying beyond this 32 ft circle were computed from an approximate formula based on the inverse square relation. That is, the contribution factor for a given sector of the target was assumed to be nearly equal to the ratio of the sector area A and the square of its distance d from the receiving point. Thus

$$cf\ (sector) \simeq A/d^2 \qquad (12)$$

The contribution factors predicted by Eq. 11 and 12 do not contain the effects of shielding from intervening materials. Therefore, in the case of a target complex, it is necessary to correct the cf value by a shielding reduction factor s. The shielded contribution factor

cf_s for a given radiation source then equals the product of s and cf. Table 3.13 lists the various contribution factors predicted by the above equations for all target components referred to station 19. Both the unshielded (cf) and shielded (cf_s) values are shown. More complete computations for the individual target sectors comprising each target component are given in Appendix E.

Appearing alongside each tabulated contribution factor computed for Complex III is another value in parenthesis. The latter is taken from Complex II calculations. Together they indicate differences resulting from several factors neither readily apparent from nor directly attributed to Eq.'s 11 and 12. That is, the equations used were the same in both experiments. But, physical improvements within the test target area (see Section 2.2), more accurate measurements, and refined theoretical considerations combined to change the magnitude of the variables used in the Complex III calculations.

For instance, comparison of the cf values shown in Table 3.13 reveals differences between pairs ranging from 13 to 34 % for the Plaza, the Terrace, the lawns and the walks and planters. These significant cf differences may be attributed almost entirely to comparable differences (14 to 38 %) in the estimates of A, the component area. In some cases, the size of a given component was changed during test site improvements. In other cases, the 1962 topological survey showed Complex II area estimates to be in error. The differences exhibited by the eight remaining cf pairs tabulated are, in general, too small to correlate with any known discrepancies in the two variables of Eq. 12; namely, area A and distance d.

It is of interest to note that the total cf value (25.95) shown at the foot of Table 3.13 is within about 3 % of the value (26.8) calculated earlier from Eq. 11. Such close agreement tends to justify the use of the inverse square approximation given by Eq. 12 for sectors beyond the central 32 ft circle at station 19.

In addition to discrepancies in area estimates between Complex II and Complex III, Table 3.13 discloses an even stronger source of disagreement, the shielding factor s. This is demonstrated by the differences in the paired cf_s values listed. With the exception of 10th St, where shielding was negligible, these differences ranged from 8 to 210 %. In connection with the four components cited earlier, these differences were due to the combined effects of area changes and shielding factor changes. The latter, however, was almost totally responsible for those differences exhibited by the remaining target components.

TABLE 3.13

Predicted Contribution Factors for Station 19, 10th St*

Component and Location	cf	cf_s
Roofs		
Bldg 570	0.3020 (0.2949)	0.0544 (0.1655)
Bldg 571	0.3970 (0.4252)	0.0803 (0.2359)
Bldg 572	0.3640 (0.3712)	0.1465 (0.2001)
Bldg 573	0.4030 (0.4199)	0.1111 (0.2190)
Sub Totals	1.466 (1.511)	0.392 (0.820)
Pavement		
Hamilton Ave	0.3232 (0.3118)	0.1198 (0.0345)
10th St	14.1375 (14.1430)	14.1188 (14.0918)
Plaza	1.2358 (1.0715)	0.6456 (0.4687)
Parking Strips	1.6570 (1.6877)	1.4349 (1.6837)
Sub Totals	17.354 (17.214)	16.319 (16.279)
Fields		
East Land	0.3130 (0.3220)	0.2408 (0.3077)
Terrace	1.0300 (1.3869)	0.7228 (1.0541)
Sub Totals	1.343 (1.657)	0.964 (1.315)
Grounds		
Lawns	4.0494 (3.6161)	3.9303 (2.9480)
Walks and Planters	1.7421 (1.1869)	1.3779 (1.1083)
Sub Totals	5.792 (4.724)	5.308 (4.056)
Grand Totals	25.95 (25.24)	22.98 (22.52)

*Contribution factors in parentheses are from Complex II calculations.

The magnitude of the discrepancies between s values used in the two experiments is illustrated in Fig. 3.25 by the prominent spacing between the shielding curves. The straight line, semi-log form of the two broken curves was dictated by the well known equation for simple shielding, $s = e^{-ux}$. The slope of these lines was determined by two half-thickness values taken from the 1957 edition of the Effects of Nuclear Weapons. At the time of Complex II no better information was available. The half-thicknesses selected were reported as approximate values for gamma radiation from fission products. Since the average photon energy of fission products (after the first few hours) is comparable to that of the Ba^{140}-La^{140} simulant employed during the experiment, the half-thickness values were considered appropriate.

Unfortunately, the shielding curves as originally plotted and used during Complex II showed s versus T in inches of shielding material. In this form the two curves for wood and concrete appeared in a perfectly logical relation to one another. However, when s is plotted against mass thickness τ in lb/ft^2 (as in Fig. 3.25), the curves become immediately open to question. They reverse positions so that now, pound for pound, wood appears to be a better shielding material than concrete. Even if this is conceivable, special shielding measurements made after Complex III further indicated that the curve for wood, at least, sloped too steeply. The importance of this finding can only be appreciated when it is realized that the wooden buildings accounted for most of the shielding encountered in the target complex.

In order to approximate the curve fitting these measurements, a build-up factor was introduced into the shielding equation. The solid curve in Fig. 3.25 labeled Complex III, is the result. Contribution factor calculations made no allowances for air absorption, self-absorption, terrain roughness or broad beam attenuation effects. However, Complex III calculations reflect a scattering correction by virtue of the build-up factor used in establishing the solid curve. Computational details and associated theory used in the determination of this more reliable curve are presented in Appendix F.

Another refinement, introduced to further improve contribution factor predictions appears in Appendix G. This comprises a consistent system for calculating effective shielding thicknesses in support of the shielding curve developed in Appendix F.

3.4.2 Fractional Contributions

In order to gain a measure of confidence in the predicted cf_s factors listed in Table 3.13, it was necessary to make repeated radiation surveys during the dispersal phase of the complex experiment. The

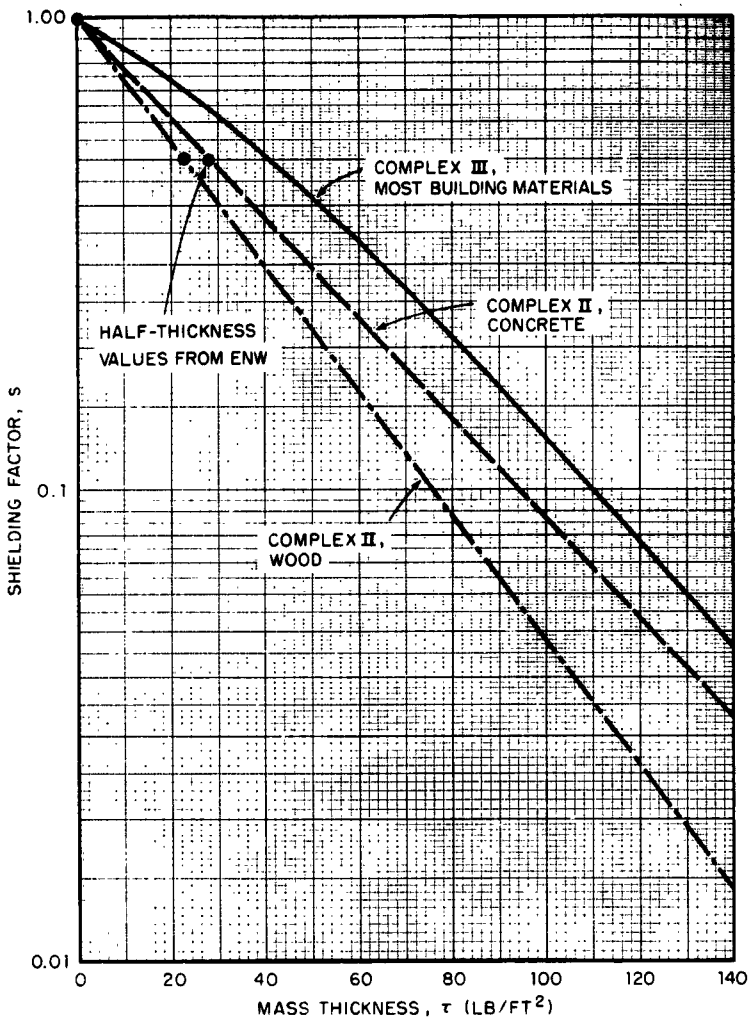

Fig. 3.25 Comparison of Shielding Effects Curves Used in Obtaining cf_s Values

dispersal operation followed the 14-step sequence shown in Table 3.14. Radiation readings were taken after each step at all 20 RAMS stations. From these survey data it was then possible to derive factors indicative of the actual contributions from the various target components.

Before comparing the above factors with predicted values, the latter were adjusted for the non-uniform distribution of radioactivity over the various target complex surfaces. This was accomplished by multiplying the cf_s values (predicted in Table 3.13) by the ratio:

$$\frac{q\ \mu c/ft^2 \text{ measured unit activity}}{854\ \mu c/ft^2 \text{ average unit activity}}$$

so that

$$(cf_s)_a = \frac{q}{854}\,(cf_s) \qquad (13)$$

Table 3.14 lists the adjusted predicted contribution factors $(cf_s)_a$ and develops a means for comparing predicted and measured contributions to station 19. A column-by-column explanation of the table appears below:

Column 1 - cf_s, the shielded contribution factor computed from Eqs. 11 and 12.
Column 2 - q, simulant concentration in $\mu c/ft^2$ as actually dispersed.
Column 3 - $(cf_s)_a$, adjusted value of cf_s according to Eq. 13.
Column 4 - f_p, predicted fractional contribution, i.e., the ratio of the individual contribution factor for a given surface to that for the entire complex.
Column 5 - e_p, percent error in f_p values of column 4.
Column 6 - $\Sigma_c i$, the decay-corrected mr/hr intensity at the reference location as affected by the cumulative contribution from successively contaminated surfaces during dispersal.
Column 7 - Δi, the incremental intensity ascribed to an individual surface and equal to the difference between two successive values of $\Sigma_c i$ in column 6.
Column 8 - f_m, measured fractional contribution, i.e., the ratio of an individual Δi to the final $\Sigma_c i$ measured after completion of dispersal.
Column 9 - e_m, percent error in f_m values of column 8.

Near the bottom of the table, under columns 4 and 8, are shown the grouped fractional contributions for the four surface types found in the complex, namely: roofs, fields, grounds (lawns and beds) and paved areas (walks and parking strips, streets and Plaza).

TABLE 3.14

Comparison of Predicted Vs Measured Fractional Contributions (f) to Station 19, 10th St.

Contributing Components In Order of Dispersal Sequence	1 Contribution Factor cf_s (Table 3.13)	2 Simulant Concentration q ($\mu c/ft^2$)	3 Adjusted Contribution $(cf_s)_a$ ①×②/854	4 Predicted Fractional Contribution f_p ③/24.851	5 Percent Error in f_p $\pm e_p$	6 Observed Cumulative Intensity* $\Sigma_c i$ (mr/hr)	7 Incremental Intensity Δi Δ⑥	8 Measured Fractional Contribution f_m ⑦/97.9	9 Percent Error in f_m $\pm e_m$
Roof: Bldg. 571	.0803	883	.0830	.0033	101	.56	.56	.0057	20
Bldg. 570	.0544	828	.0527	.0021	115	.86	.30	.0031	68
Bldg. 572	.1465	836	.1434	.0058	25	1.65	.79	.0081	47
Bldg. 573	.1111	823	.1070	.0043	123	2.53	.88	.0090	67
East Field	.2408	814	.2295	.0092	50	3.19	.66	.0067	124
Lawns & Beds: Bldg. 573	.8597	1046	1.0529	.0424	24	7.78	4.59	.0429	37
Bldg. 572	.7027	717	.5899	.0237	21	8.70	0.92	.0094	254
Bldg. 571	1.8600	785	1.7097	.0688	23	10.10	1.40	.0143	189
Bldg. 570	.6756	921	.7286	.0293	56	12.10	1.90	.0194	166
Terrace	.7228	902	.7634	.0307	59	14.80	2.80	.0286	137
Walks & Parking Strips	2.6450	854	2.6450	.1063	33	29.80	15.00	.1530	44
10th Street	14.1188	967	15.9869	.6433	23	90.20	60.40	.6170	32
Plaza	.6456	850	.6426	.0259	73	97.30	7.10	.0724	380
Hamilton Ave.	.1198	830	.1164	.0047	67	97.90	0.60	.0061	460
			24.851						
Grouped Values by Component Type									
Roofs				.0155	25			.0259	14.5
Fields				.0399	33			.0353	83
Lawns & Beds				.1642	8			.0900	28.5
Walks & Parking Strips				.1063	33			.1530	44
Pavements				.6739	13			.6955	36

*As read from RAMS data, station 19, 10th St.

From the above development it is seen that any comparisons of measured and predicted values depend on the fractional contribution f rather than on the contribution factor cf. Although the latter is satisfactory as a predicted value, its counterpart in the measured case cannot be conveniently derived from the RAMS measurements of column 5. This observed data can be readily expressed in terms of the fractional contribution f_m. By converting the adjusted cf_s values to f_p values, the fractional contribution then becomes a common basis for comparison.

Ideally the paired fractional contributions of columns 4 and 8 in Table 3.14 should equal each other. Obviously this is not the case. Assuming (for the moment)* that the f_m values are a true indication of the actual fractional contributions, the discrepancies in the f_p values may be classed as shown in the table:

No. of f_p Values	Factor of Difference From f_m	Percent of Total Contributions
4	2.1 - 4.8	10.5
7	1.3 - 1.7	20.5
3	1.04 - 1.10	69.0

The f_p values divide themselves into three classes according to whether they differ from their paired f_m values by factors of more than 2, less than 2, or nearly unity, i.e., almost equal to their respective f_m values. It is apparent that an inverse relationship exists between the size of the discrepancies and their importance. That is, the most errant class of f_p values comprise but a small part of the total contribution; while the least errant represents the major, hence, controlling portion of the total contribution.

Figures 3.26 and 3.27 provide an even clearer indication of how significant the differences between f_p and f_m values really are. Plots are shown for both the individual and grouped contributions taken from Table 3.14. Referring to Fig. 3.26, for perfect agreement between predicted and observed values all points should fall on the 45° dashed line. Except for the grounds (lawns and beds) of bldg. 571 and the Plaza, all points follow the directional trend of the idealized line. Fortunately the sum of the measured contributions from the two outlying points make up barely 9 % of the total.

Obviously the points of greatest significance are the two representing 10th St. and the walks and parking strips. Together they

*That is, in spite of the percent errors shown in column 9.

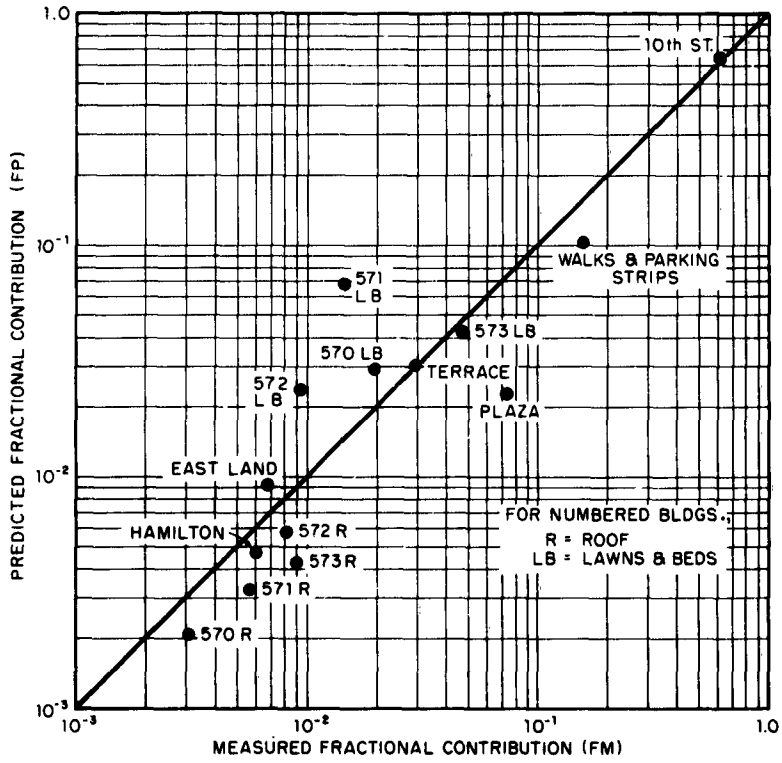

Fig. 3.26 Comparison of Predicted vs Measured Values for Individual Contributions to Station 19

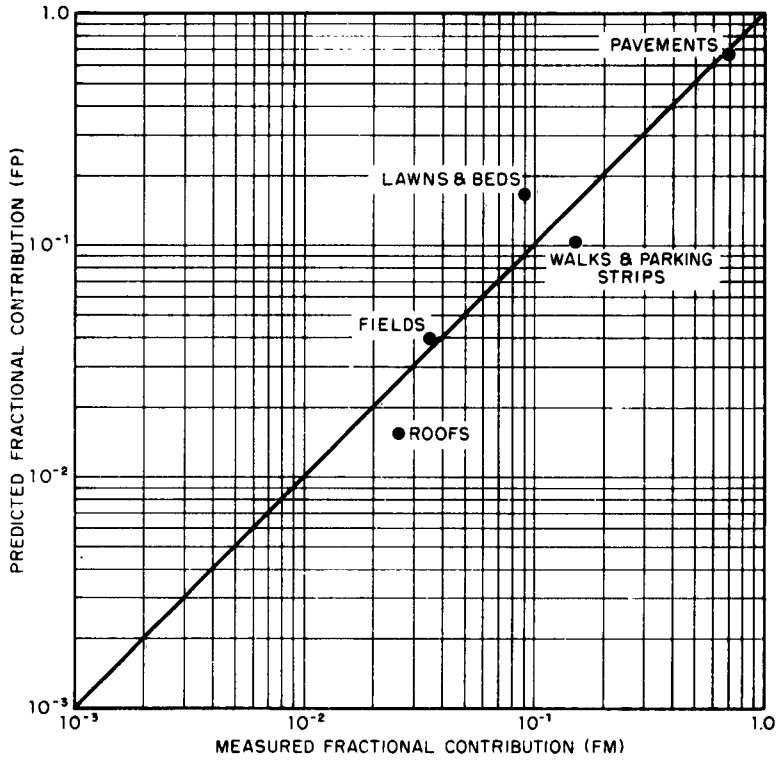

Fig. 3.27 Comparison of Predicted vs Measured Values for Grouped Contributions to Station 19

account for 77 % of the total contribution to station 19. The 10th St point, because of its nearness to the dashed line, indicates an especially close agreement between f_p and f_m coordinates. It is interesting to note that the six points grouped in the lower left hand corner, between fractional contributions of 10^{-3} to 10^{-2}, comprise only about 4 % of the total contribution. They include all of the roofs plus Hamilton Ave. and the East Field.

A plot of grouped fractional contributions (from the bottom of Table 3.14) are shown in Fig. 3.27. Here the point pattern is more closely confined to the dashed line than in the previous plot of Fig. 3.26. The compensation of errors accrued in the individual f_p and f_m values is responsible. This is borne out by the entries in Table 3.14 (columns 5 and 9) which show the reduction in the percent error between individual and grouped fractional contributions.

The foregoing demonstrates the improved reliability of the predicted results when the individual f values are combined according to the four basic surface types found in the target complex. Grouping the data in this way carries a special significance, since recovery planning is also keyed to the combination of surface types, not to single target components. For this reason, the strong trend shown by the point pattern in Fig. 3.27 (and Fig. 3.26 as well) indicates that the method employed for predicting contribution factors is sufficiently accurate for recovery planning. Furthermore, comparison of these predictions with those of Complex II represents a definite improvement.

3.4.3 Analysis of Error

Estimates of the percent error in the predicted and measured f values are given in columns 5 and 9 of Table 3.14. The errors in a number of cases are quite large due to the cumulative effects of specific errors in the variables involved. For instance, f_p is a function of at least six variables, each of which is a source of error. It can be shown statistically that e_p (the percent error in f_p) is proportional to the square root of the sum of the squares of the relative errors in these variable. Of these relative errors, that associated with the shielding factor s was found to be controlling. On the average this one source of error was responsible for 98 % of the collective effect ascribed to the six relative errors investigated.

The percent error e_m in the measured fractional contribution f_m was also the result of additive effects. From Table 3.14 it is apparent that each f_m was determined from the difference Δi between two successive RAMS readings. Therefore a given e_m is proportional to the square root of the sum of the squares of the errors (not relative errors) in these

dose rate readings. In calculating e_m a relative error of 20 % was assumed for all RAMS readings. This was based on RAMS instrument calibrations and performance information.*

Comparing the two kinds of error terms in Table 3.14, e_p values are generally much less than e_m values. For three of the four sets of roof values the situation is reversed. These exceptions are probably caused by the greater reduction in potential roof contributions due to shielding (see Table 3.13). Increased shielding is signified by a decrease in the shielding factor s. But the relative error in s and, hence, the percent error e_p increases as s decreases. Therefore, the percent error for roofs tends to be larger than for the other components in direct proportion to the increased shielding.

Grouping the percent errors, as shown at the bottom of Table 3.14 reduces the differences among e_p's and e_m's. Differences between paired e_p and e_m values also decrease markedly. As noted earlier these grouped estimates are smaller than in the individual cases because of compensating effects among error terms.

*See Ref. 4 for explanation of RAMS performance characteristics.

CHAPTER 4

CONCLUSIONS AND RECOMMENDATIONS

4.1 CONCLUSIONS

As indicated in Section 1.1 of the introduction, Complex III is the culmination of a series of three Target Complex experiments. The test series has been a unique undertaking considering the full scale proportions of each experiment, the mass production and dispersal of ton quantities of fallout simulant, the realism and success of the recovery operations performed and the overall planning and technical requirements leading to the final achievement of the test objectives.

The results of each succeeding complex experiment has borne out, amplified or added to the findings of the previous experiment(s). Taken together, the three tests have demonstrated two very important axioms; (1) Radiological recovery of a target complex can be an accomplished fact requiring no unusual or exotic tools, (2) The performance of a safe recovery operation (within prescribed dose limits) is assured by following a definite schedule based on a radiological recovery planning procedure.

The specific conclusions related to this final test in the series, Complex III, are enumerated below:

1. Support functions such as emptying sweeper hoppers, filling flusher tanks, and setting up, moving and rolling up firehosing equipment account for at least 1/5 of the total working time allotted to these recovery methods.

2. For disposal sites located more than 3 miles from a given target complex, the time required in hauling spoil becomes controlling in a soil removal operation.

3. In a built-up area similar to the test target complex, a soil removal operation may be expected to account for half the total recovery effort.

4. Predictions of the overall recovery time and recovery effort should be multiplied by a correction factor of 1.1 to compensate for the optimism which consistently colors the various reclamation time estimates.

5. Estimates of expected reclamation times based on isolated tests of individual methods must be upgraded in accordance with full-scale operational-recovery data when planning the recovery of a target complex.

6. From the standpoint of support time required: street sweeping, street flushing, firehosing roofs and hauling spoil are the least efficient methods; motor grading, loading spoil, shoveling sod, sweeping walks and rototilling are the most efficient; tractor scraping is intermediate.

7. Although the migration and redistribution of fallout simulant by winds during the weathering phase may reduce the radiation levels by 1/3 or more, in general, the bulk of the fallout material still can be expected to remain within the confines of the immediate area.

8. The effects of weathering upon radiation levels in exposed areas (roofs and grounds) are resisted by surface irregularities in texture and configuration and by obstructions such as curbs, fences and buildings.

9. Reduction of radiation levels indoors is improved by paved surroundings which encourage increased weathering effects.

10. For wind velocities no greater than those observed during the weathering phase, the ultimate removal of redistributed fallout material must be achieved by the recovery effort.

11. The combined effects of weathering and recovery may reduce the general radiation level in a built-up area as much as 97 %.

12. The calculation of a recovery dose reduction factor, RR_2, from a particular dose rate history must take into account the cumulative target recovery effectiveness, F_n (in addition to target shielding factor and reclamation coefficient).

13. Reclamation coefficients are a function of the method-surface combination. They are also dependent upon reclamation effectiveness and equipment shielding.

14. To date, reclamation coefficients for a given method-surface combination are quite variant from one complex recovery operation to another and from one target component to another.

15. For street sweeping, reclamation coefficients display a trend that is inversely proportional to the square root of the unit effort.

16. Because of the strong correlation between predicted and measured values, the improved method for predicting contribution factors can be used for recovery planning purposes.

17. Conventional street cleaning, fire fighting and construction equipment represent an available (but not the ultimate) means for achieving the effective recovery of a target complex.

18. The approach used in the operational recovery and the planning factors obtained are applicable to residential installations having geometry and shielding characteristics comparable to the test complex.

19. Application of Complex III results to industrial facilities may be quite limited in view of the difficulties anticipated in predicting contribution factors for such a target.

4.2 RECOMMENDATIONS

The following investigations are recommended:

1. Conduct firehosing tests on tar and gravel surfaces to improve the reclamation performance with respect to improved effectiveness and reduced support time.

2. Determine the feasibility of reclaiming lawn areas with sod cutting machines and measure the performance characteristics.

3. Formulate a recovery planning procedure for an industrial target complex experiment.

4. Develop and test an aerial dispersal system capable of more realistic distribution of fallout simulant over target surfaces.

5. Conduct a target complex experiment on a more heavily constructed facility representative of light industrial and/or outlying business districts.

In addition it is recommended that a series of tests be performed on typical full-sized target components for the purpose of:

1. Obtaining time-and-motion data which will establish relationships between productive effort and the various forms of support effort; thereby improving future estimates of expected reclamation times.

2. Constructing accurate reclamation dose-rate histories in order to derive more precise reclamation coefficients (RC) and to further study the dependency of RC values upon unit effort and fallout mass loading.

3. Measuring the dose rate reduction and fallout removal capabilities of weathering due to rains and high velocity winds.

4. Observing weathering effects during aerial dispersal.

5. Detecting adverse effects of a non-visual simulant on reclamation performance.

6. Obtaining better contribution factor estimates.

REFERENCES

1. W. L. Owen, J. D. Sartor. Radiological Recovery of Land Target Components - Complex I and II. U. S. Naval Radiological Defense Laboratory Technical Report, USNRDL-TR-570, 25 May 1962.

2. H. Lee. Estimating Cost and Effectiveness of Decontaminating Land Targets. U. S. Naval Radiological Defense Laboratory Technical Report, USNRDL-TR-435, 6 June 1960.

3. C. F. Miller. Fallout and Radiological Countermeasures. Distribution of Fallout Particles Following a Nuclear Detonation. Vols. I and II. Stanford Research Institute, Project No. IM-4021, January 1963.

4. P. A. Covey. A Method of Compensating for Temperature Dependence of a Remote Area Gamma Monitoring System. U. S. Naval Radiological Defense Laboratory Technical Report, USNRDL-TR-604, 27 November 1962.

5. W. L. Owen, J. D. Sartor, W. H. Van Horn. Performance Characteristics of Wet Decontamination Procedures - Stoneman II. U. S. Naval Radiological Defense Laboratory Technical Report, USNRDL-TR-335, 21 July 1960.

6. H. Lee, J. D. Sartor, W. H. Van Horn. Performance Characteristics of Dry Decontamination Procedures. U. S. Naval Radiological Defense Laboratory Technical Report, USNRDL-TR-336, 6 June 1959.

7. H. Lee, J. D. Sartor, W. H. Van Horn. Performance Characteristics of Land Reclamation Procedures. U. S. Naval Radiological Defense Laboratory Technical Report, USNRDL-TR-337, 12 January 1959.

8. W. S. Chepil. Soil Conditions That Influence Wind Erosion. U. S. Department of Agriculture, Technical Bulletin No. 1185, June 1958.

9. W. S. Chepil, N. P. Woodruff. Estimations of Wind Erodibility From Farm Fields. U. S. Department of Agriculture Research Service, Product Research Report No. 25, March 1959.

10. R. D. Evans. The Atomic Nucleus. McGraw-Hill Book Co., York, Pa., 1955, page 743.

11. D. E. Clark, Jr., W. C. Cobbin. Some Relationships Among Particle Size, Mass Level, and Radiation Intensity of Fallout From a Land Surface Nuclear Detonation, U. S. Naval Radiological Defense Laboratory Technical Report, USNRDL-TR-639, 21 March 1963.

12. H. Goldstein, J. E. Wilkins, Jr. Calculation of the Penetration of Gamma Rays. U. S. Atomic Energy Commission, Final Report, NYO 3075, June 1954.

13. L. V. Spencer. Structure Shielding Against Fallout Radiation From Nuclear Weapons. National Bureau of Standards, Monograph 42, June 1962.

APPENDIX A

SELECTION OF FALLOUT EVENT

The Camp Parks complex experiments were the first large-scale tests wherein the sand-simulant particle size ranges and distributions were held reasonably constant. This stable condition made it possible to use the Miller fallout model[3] to describe a typical fallout event (for the observed test particle sizes) in terms of weapon yield, distance downwind, standard intensity, and mass loading. The results are shown in Table 2.1 of Chapter 2.

In general, the technique for selecting a fallout event consists of matching a histogram of observed particle sizes to a family of fallout model curves* for the assumed weapon yield. The histogram, Fig. A.1, of particle sizes indicated that the sand dispersed for this experiment contained particles between 150 and 350 μ. The standard intensity curves bracket the particle sizes presumed to accompany a 1-MT burst for various distances downwind. At the peak intensity of approximately 2700 r/hr, the predicted fallout particle size range (150 to 300 μ) includes 86.8 % (by weight) of the test sand.

From the fallout model, curves may be constructed showing the relation between downwind distance and particle size for different weapon yields. Figure A.2 shows the curves for the lower and upper particle size limits associated with a 1-MT detonation. Projecting the 150 and 300 μ values vertically, they are seen to intersect the curves at a common distance reading of 1.75×10^5 ft, or about 33 miles. This, then, is the predicted distance from ground zero where the peak standard intensity of 2700 r/hr should occur.

One of the more important fallout conditions is that of mass loading, i.e., the concentration of fallout material in g/ft^2. This mass loading is proportional to the standard intensity and is determined from the mass contour ratio. According to Miller, this ratio is approximately 33 mg/ft^2 for every r/hr of standard intensity. Thus the mass level M

*The method for developing these curves is given in Reference 11.

equals the product of the standard intensity I_s and the mass contour ratio. For this experiment

$$M = 2700 \text{ r/hr} \times (0.033 \text{ g/ft}^2)/\text{r/hr}$$

$$M = 90 \text{ g/ft}^2$$

which was the nominal loading dispersed.

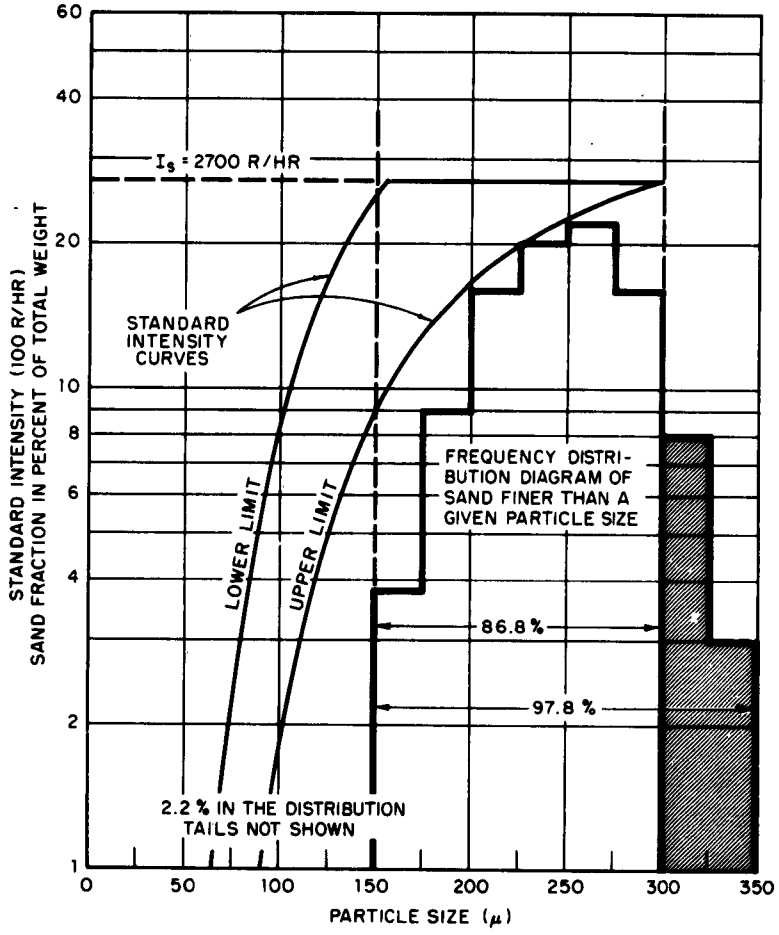

Fig. A.1 Fitting Range of Sand Particle Sizes to That Encompassed by Fallout Particles From a 1-MT Land-Surface Detonation

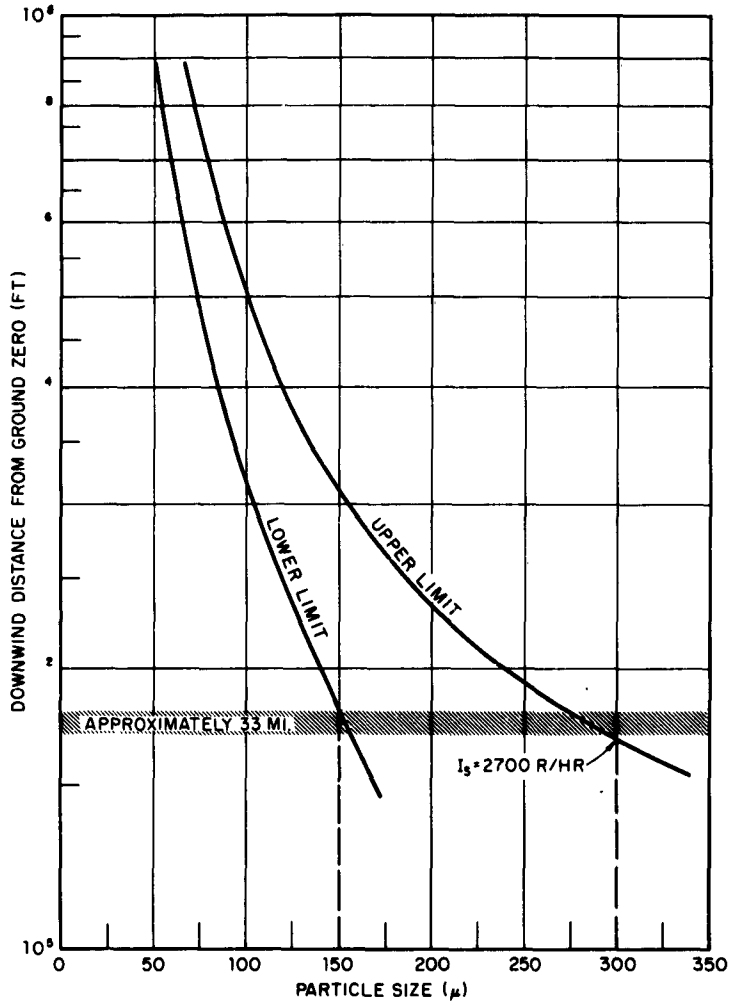

Fig. A.2 Establishing Downwind Distance From 1-MT Detonation for Particle Size Range of 150 to 300 Microns

APPENDIX B

DESCRIPTION OF EXPERIMENTAL LAND TARGET COMPLEX

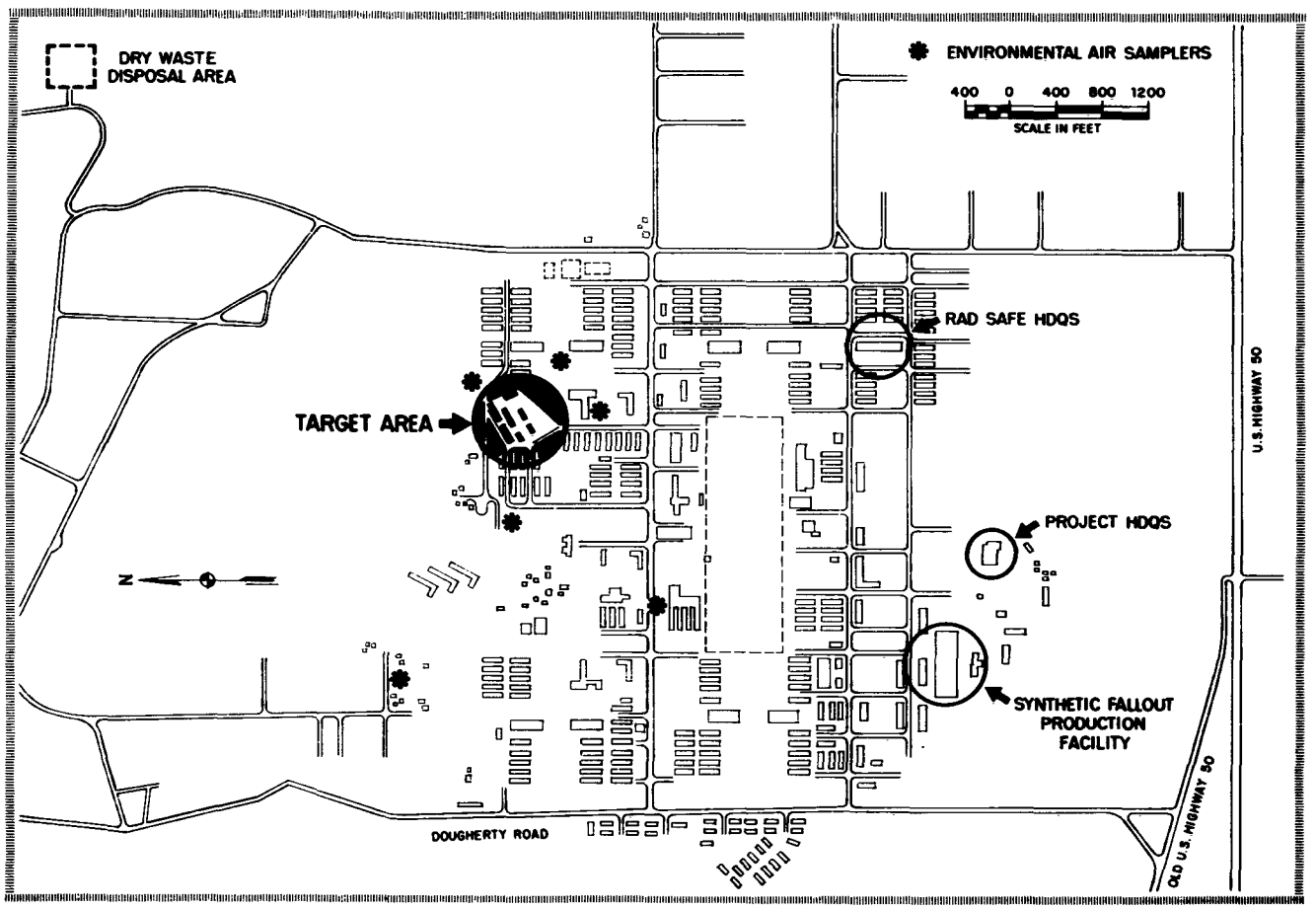

Fig. B.1 Location of Land Target Complex in Camp Parks

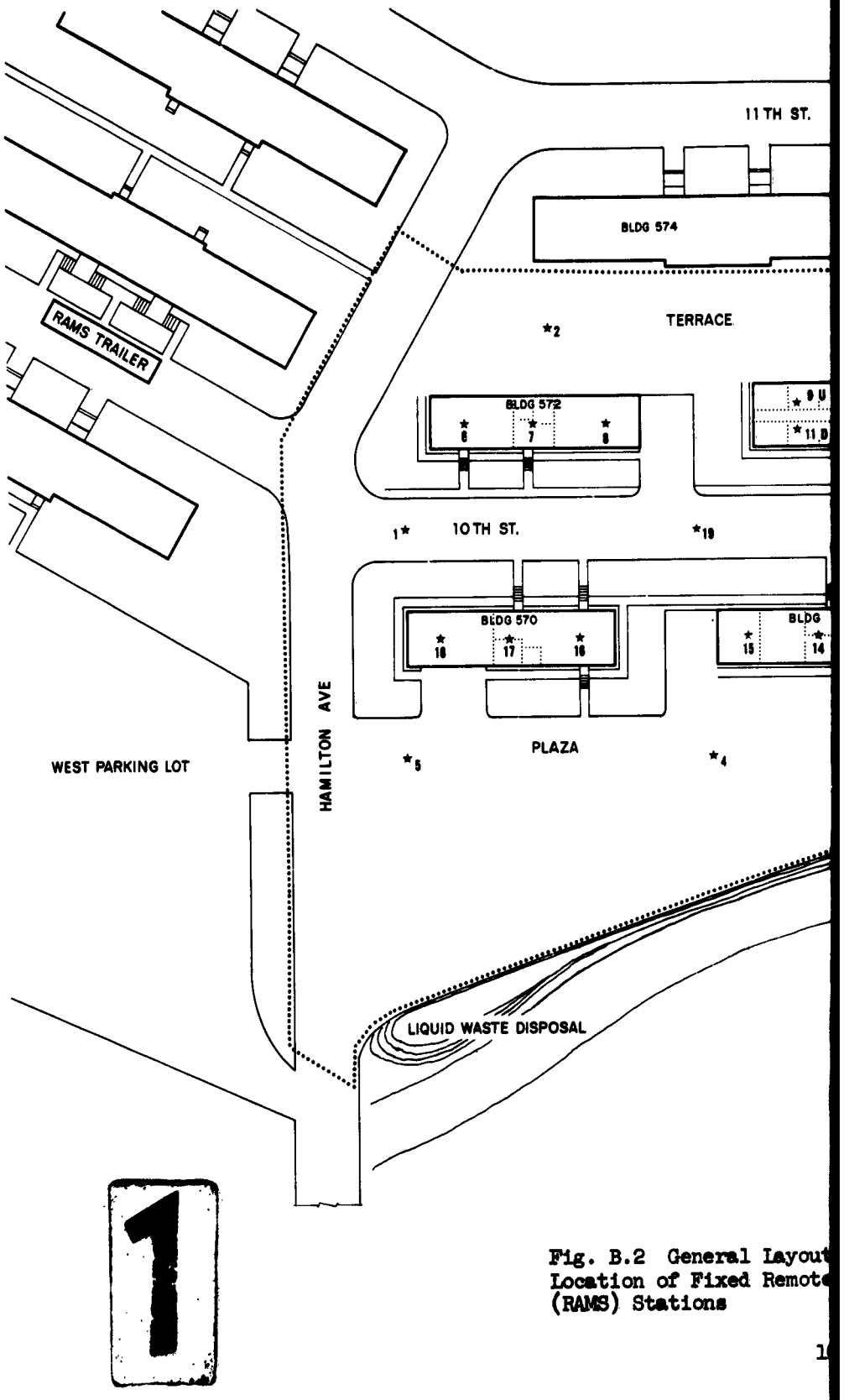

Fig. B.2 General Layout
Location of Fixed Remote
(RAMS) Stations

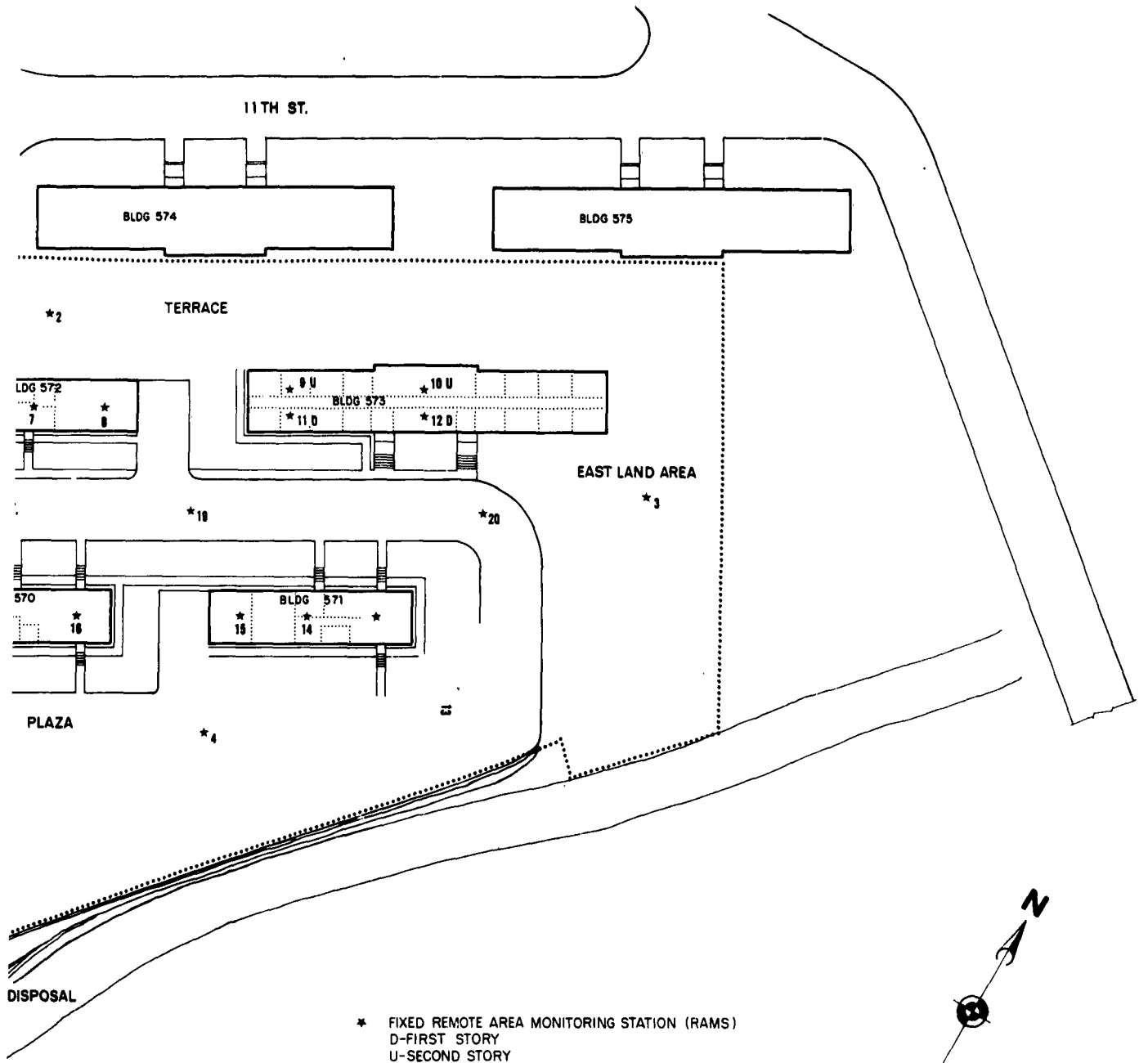

Fig. B.2 General Layout of Target Complex Showing Location of Fixed Remote Area Monitoring System (RAMS) Stations

2

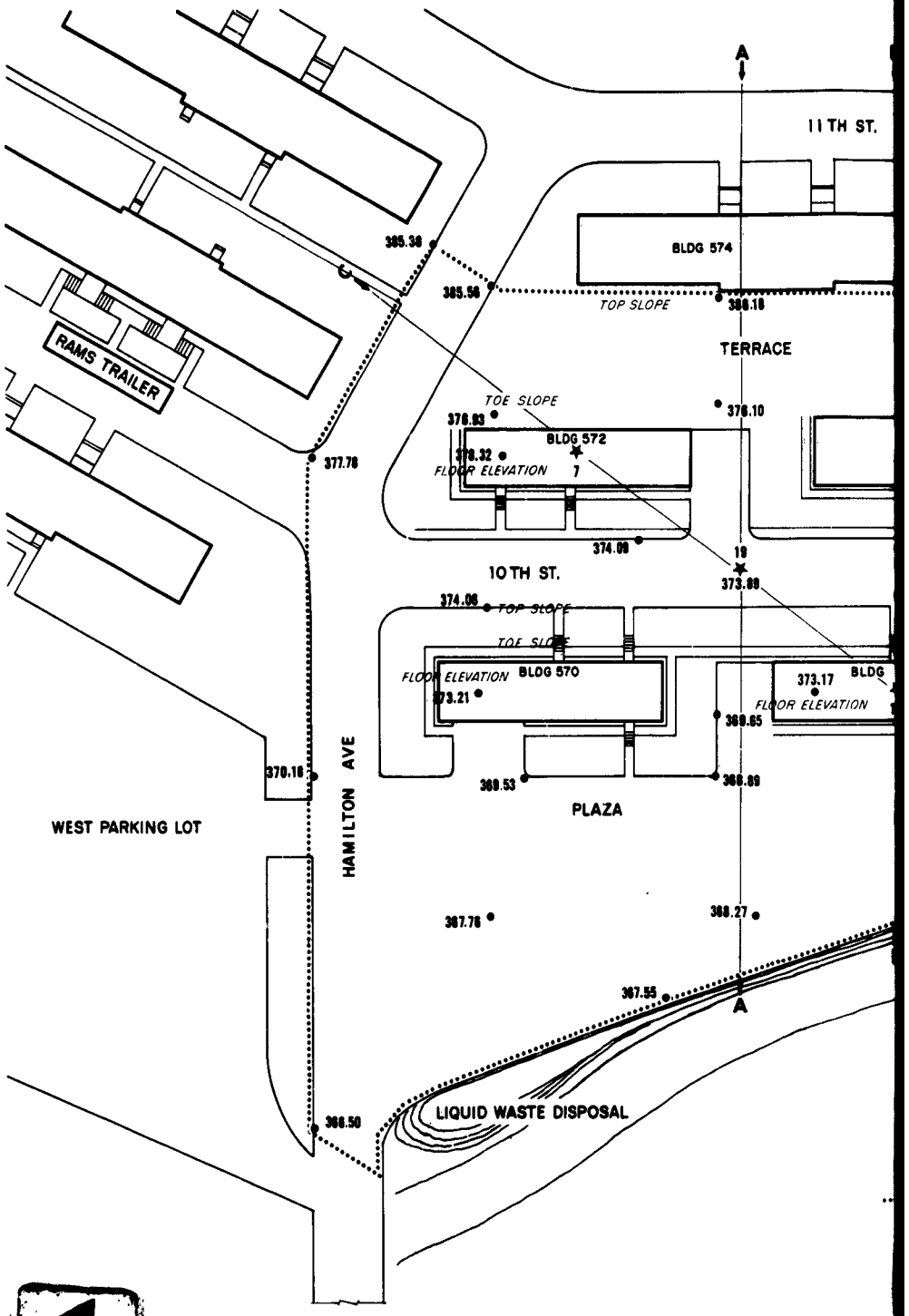

1

Fig. B.3 Elevations (

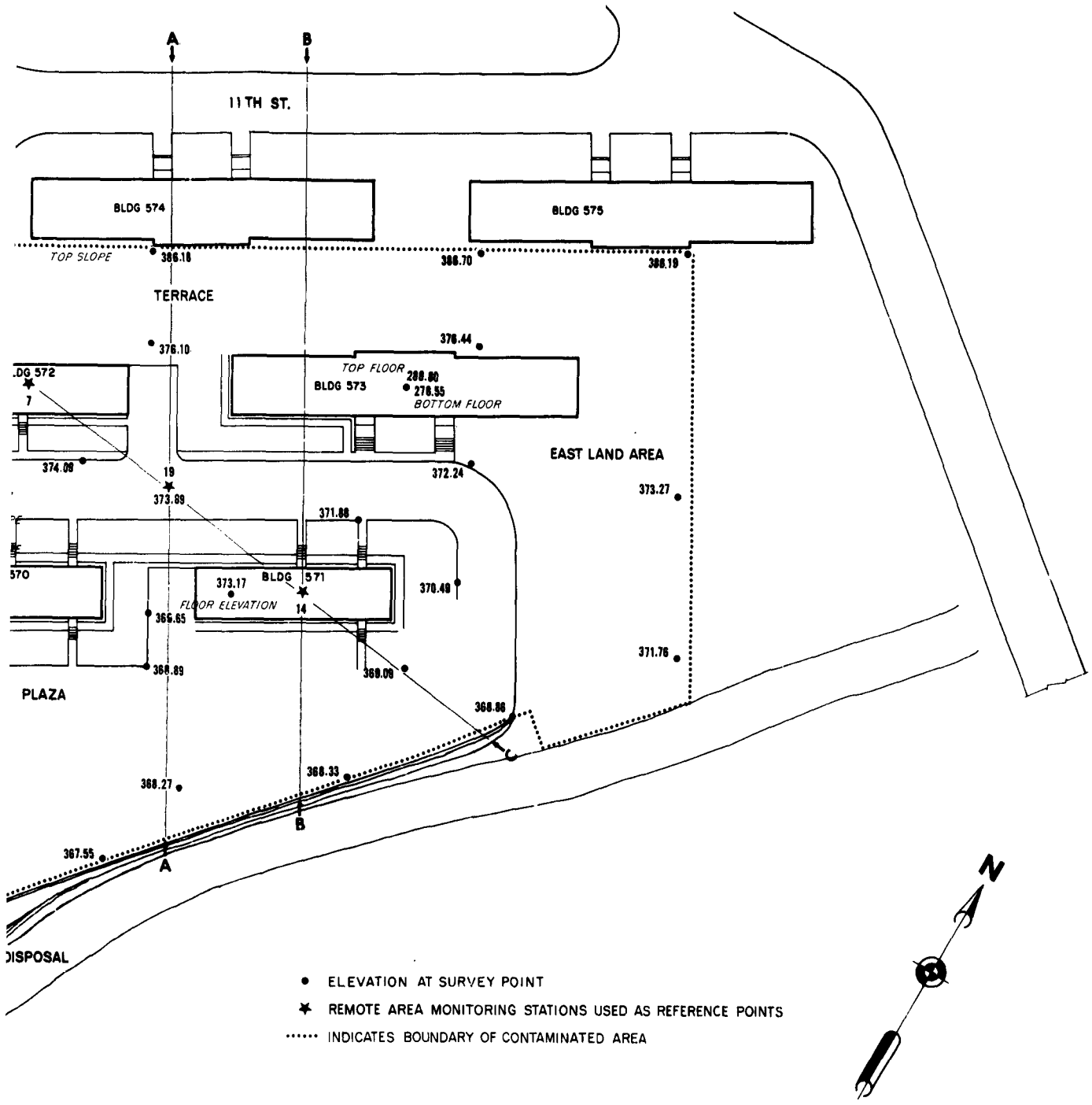

Fig. B.3 Elevations (ft) of the Component Surfaces of the Complex

2

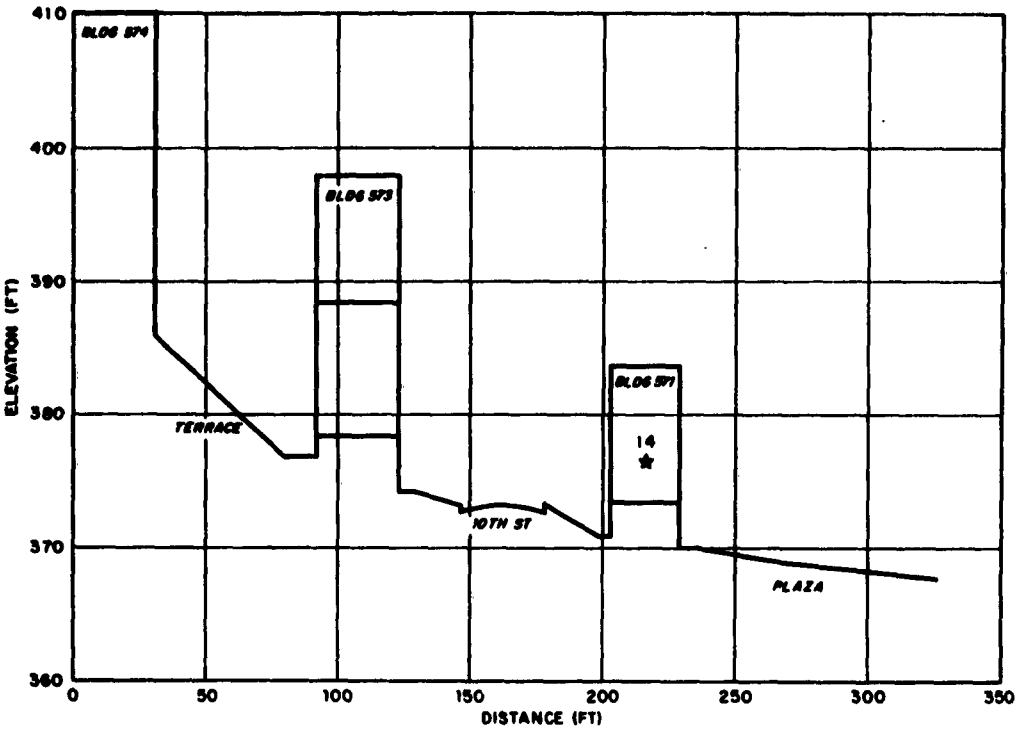

Fig. B.4 Profile Through Section B-B in Fig. B.3. Reference point at RAMS station 14.

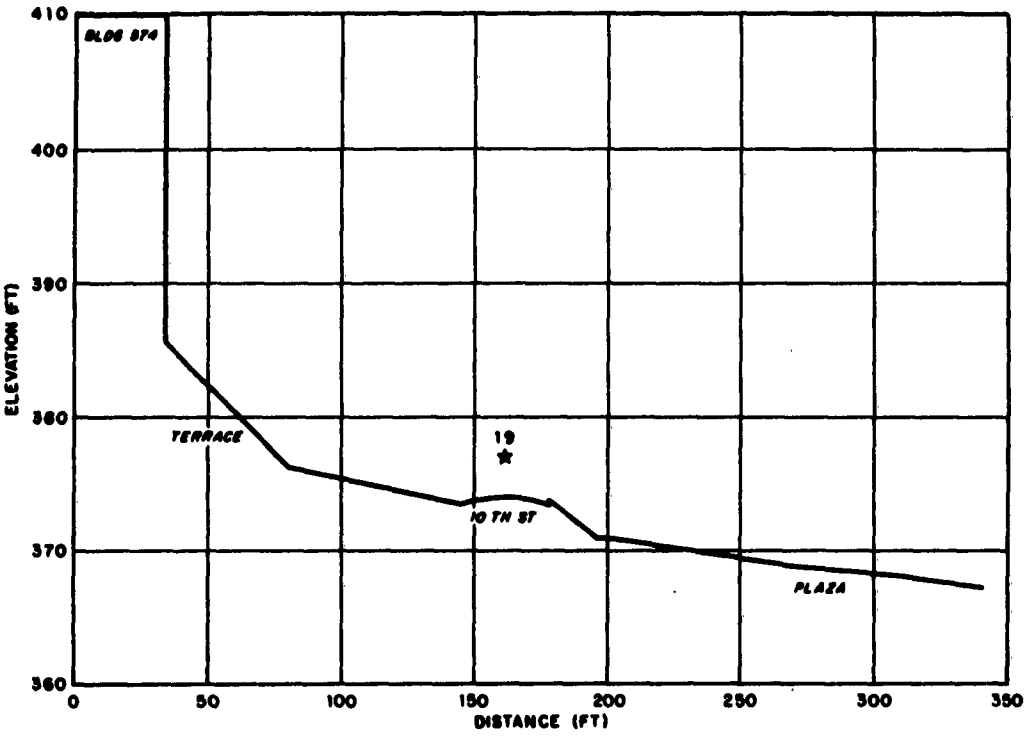

Fig. B.5 Profile Through Section A-A in Fig. B.3. Reference point at RAMS station 19.

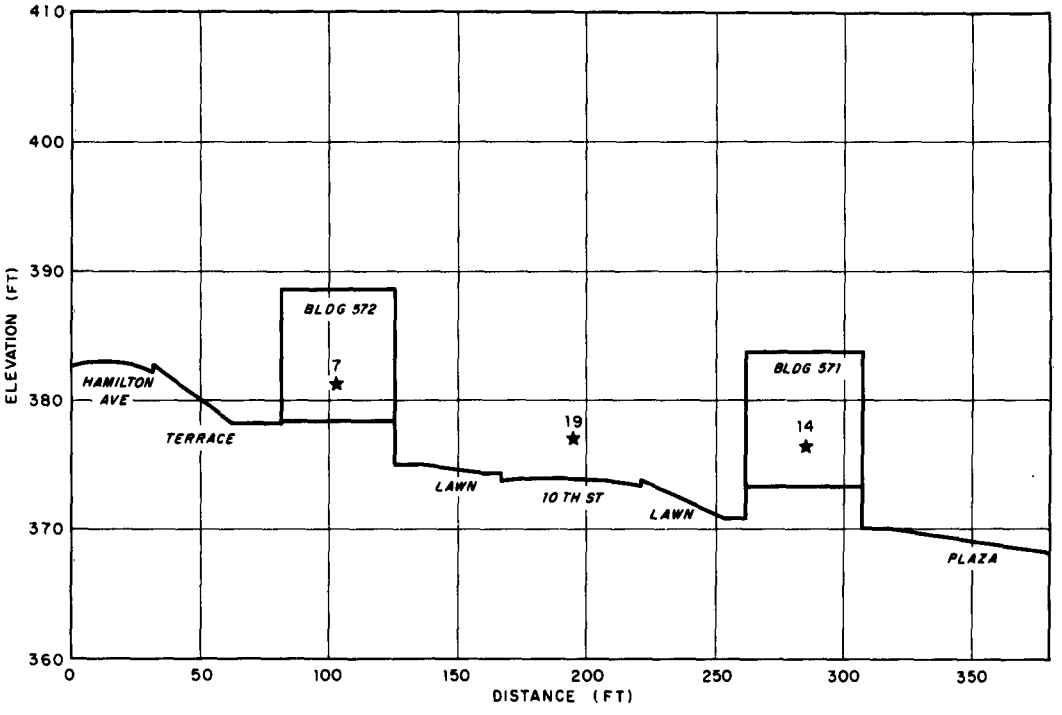

Fig. B.6 Profile Through Section C-C in Fig. B.3. Reference points at RAMS stations 14 and 19. RAMS station 7 also shown.

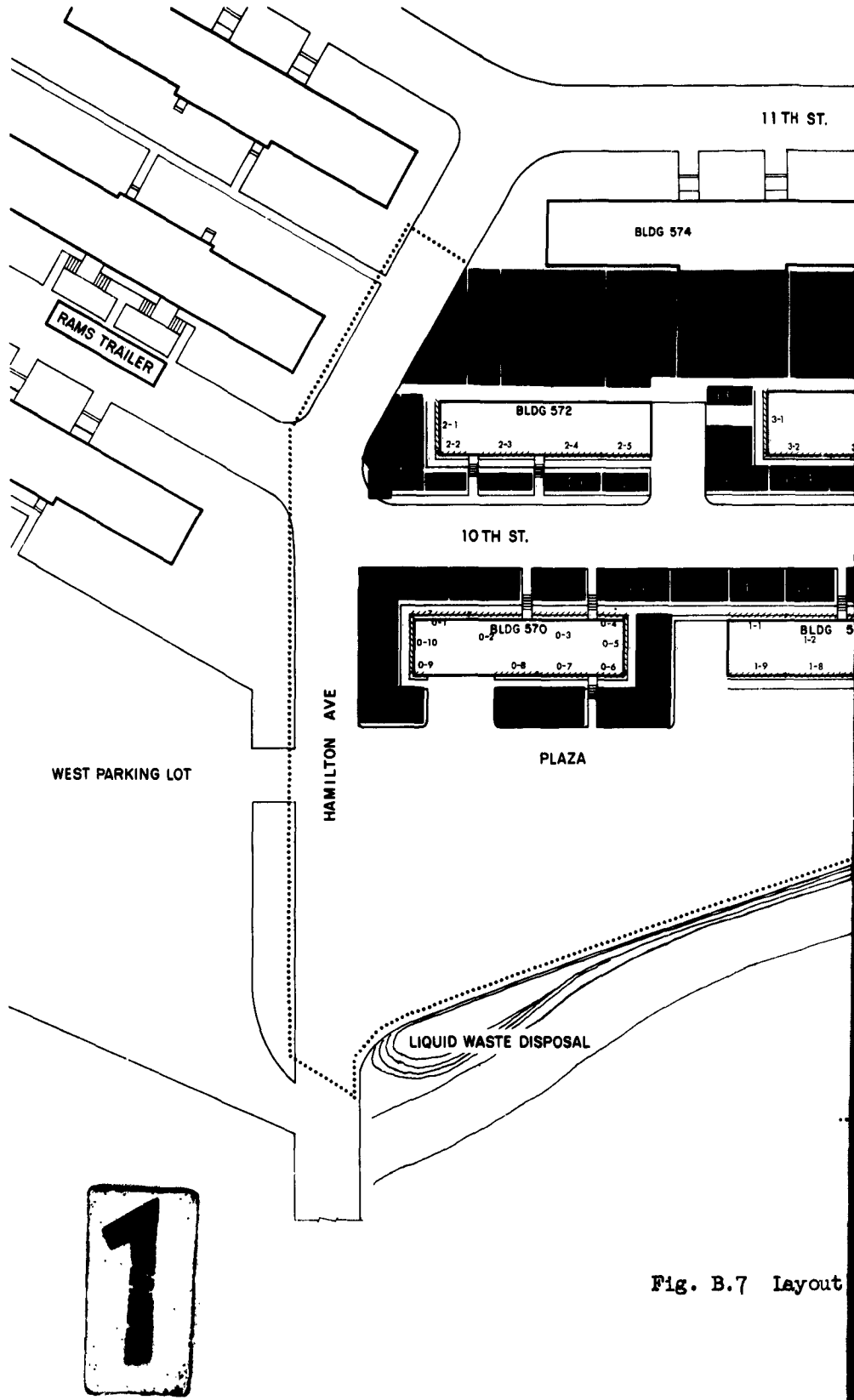

Fig. B.7 Layout

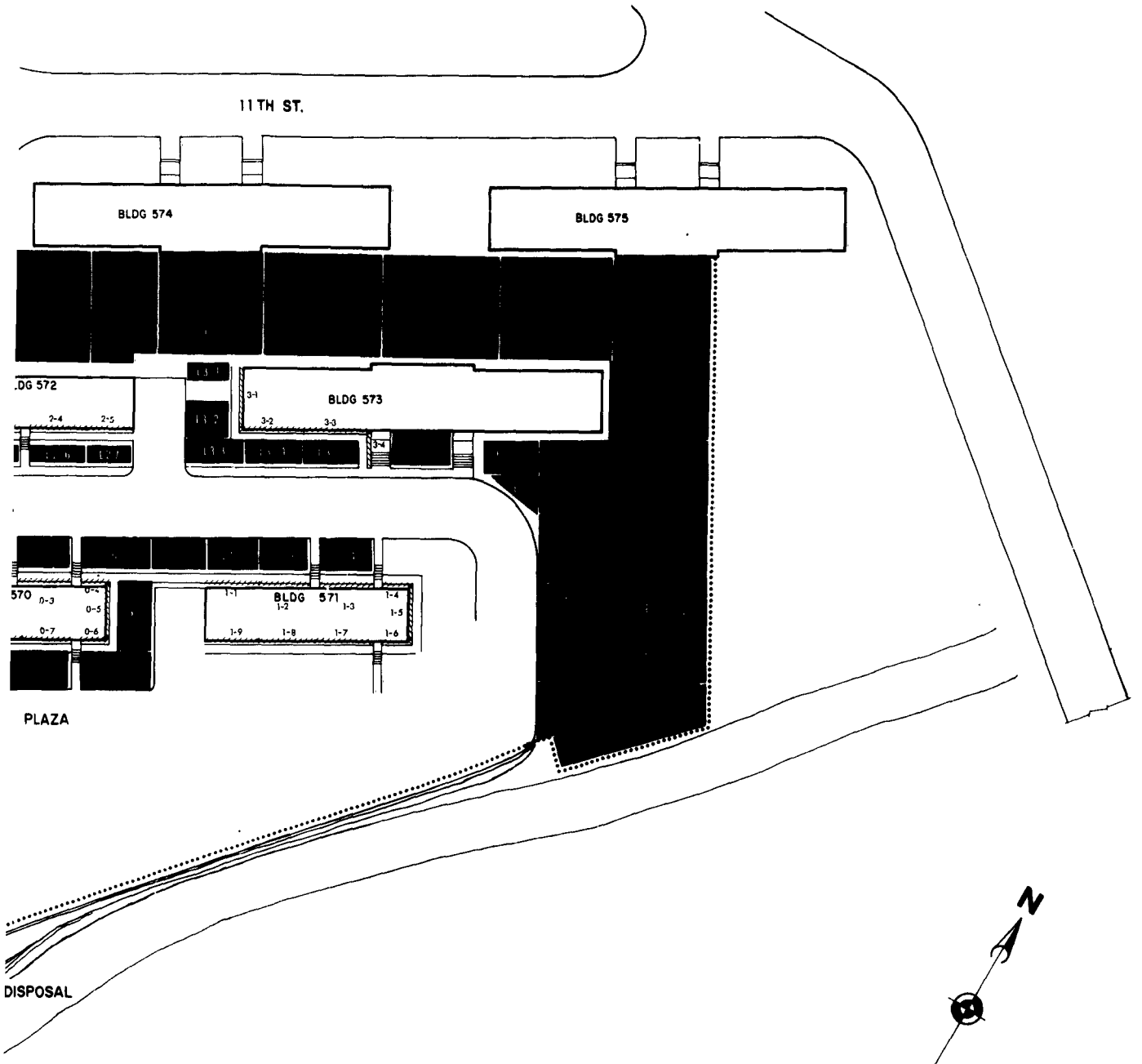

····· INDICATES BOUNDARY OF CONTAMINATED AREA

Fig. B.7 Layout of Unpaved Ground Test Surfaces

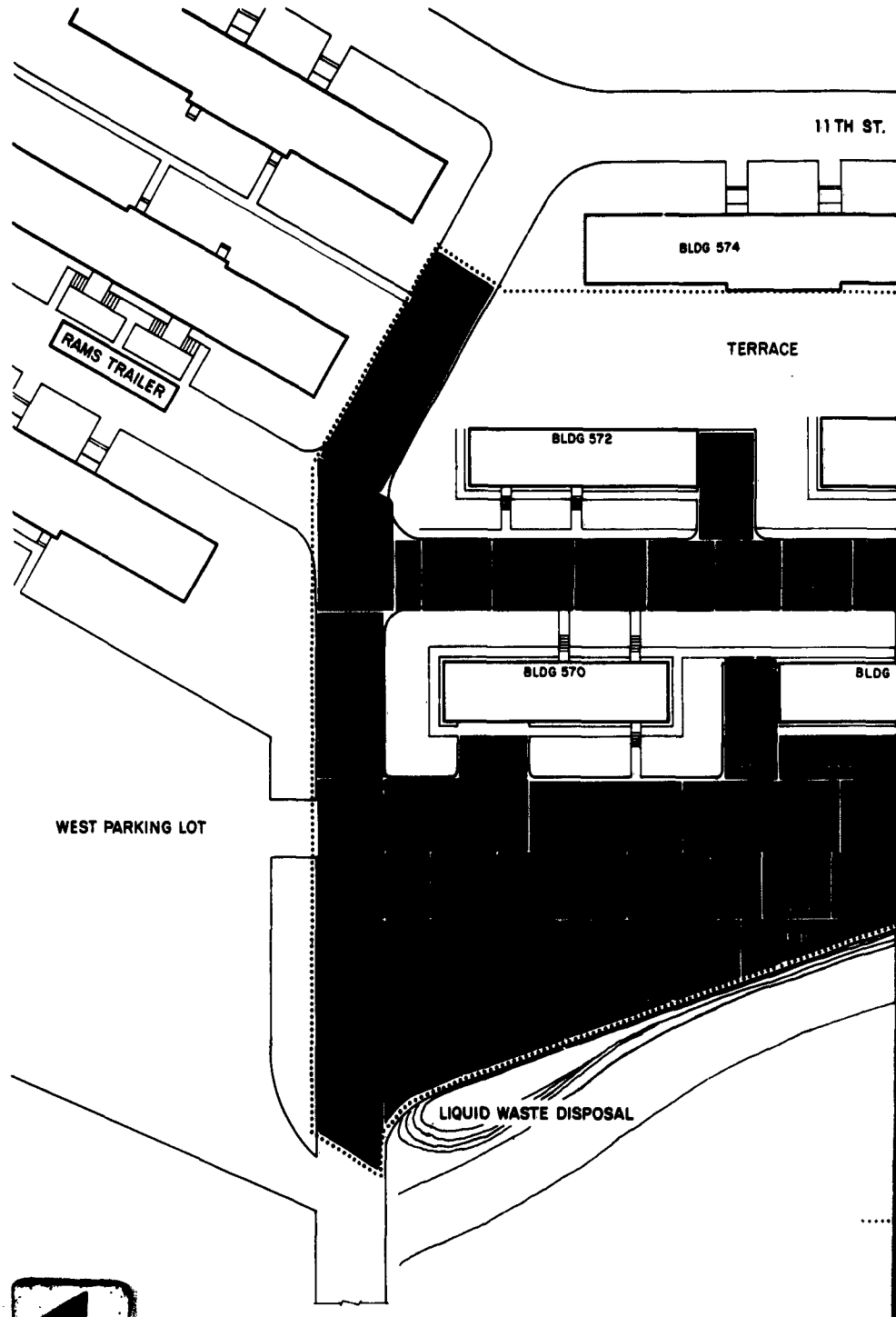
11TH ST.
BLDG 574
TERRACE
RAMS TRAILER
BLDG 572
BLDG 570
BLDG
WEST PARKING LOT
LIQUID WASTE DISPOSAL

Fig. B.8 Layou

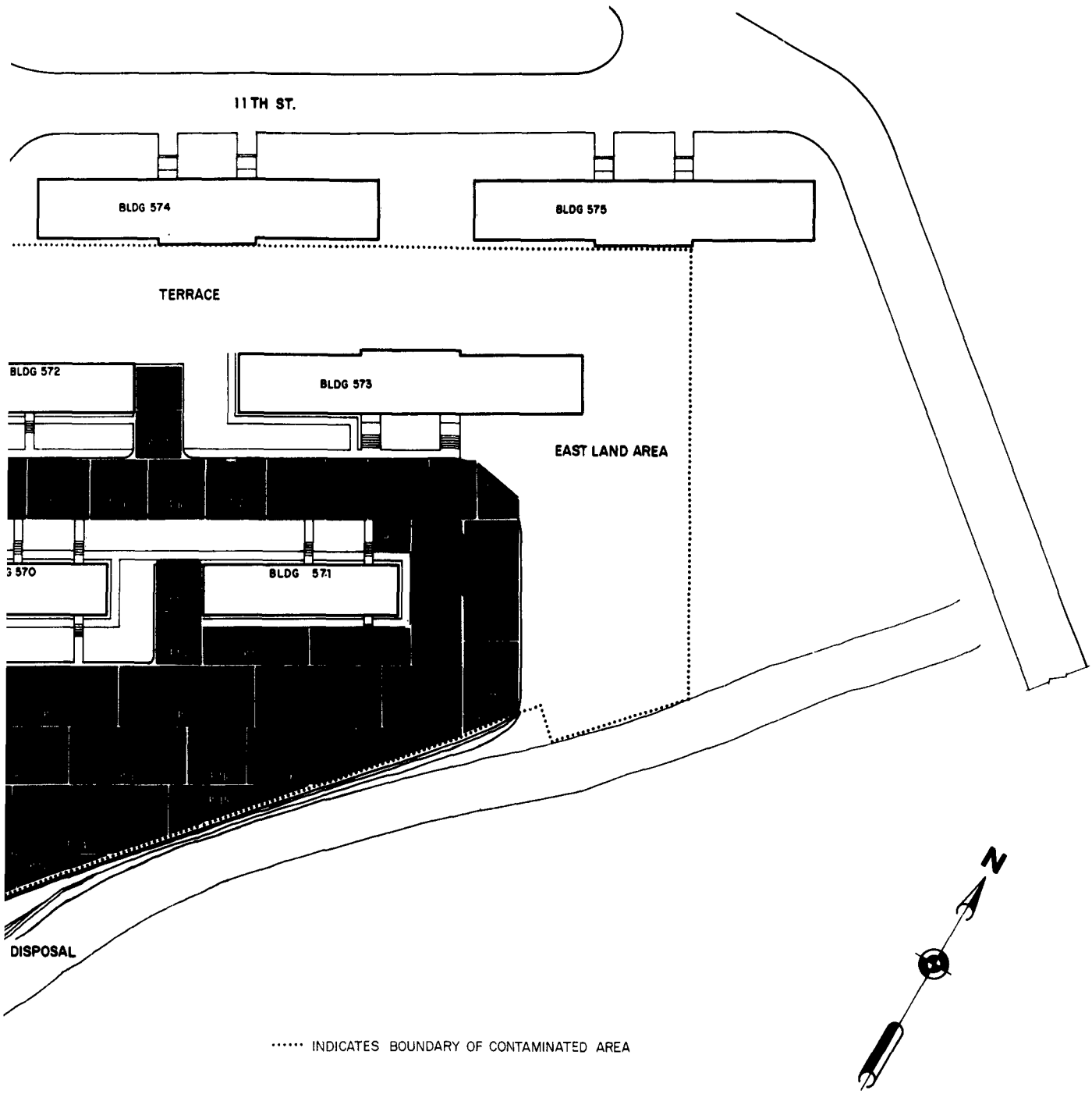

Fig. B.8 Layout of Paved Ground Test Surfaces

2

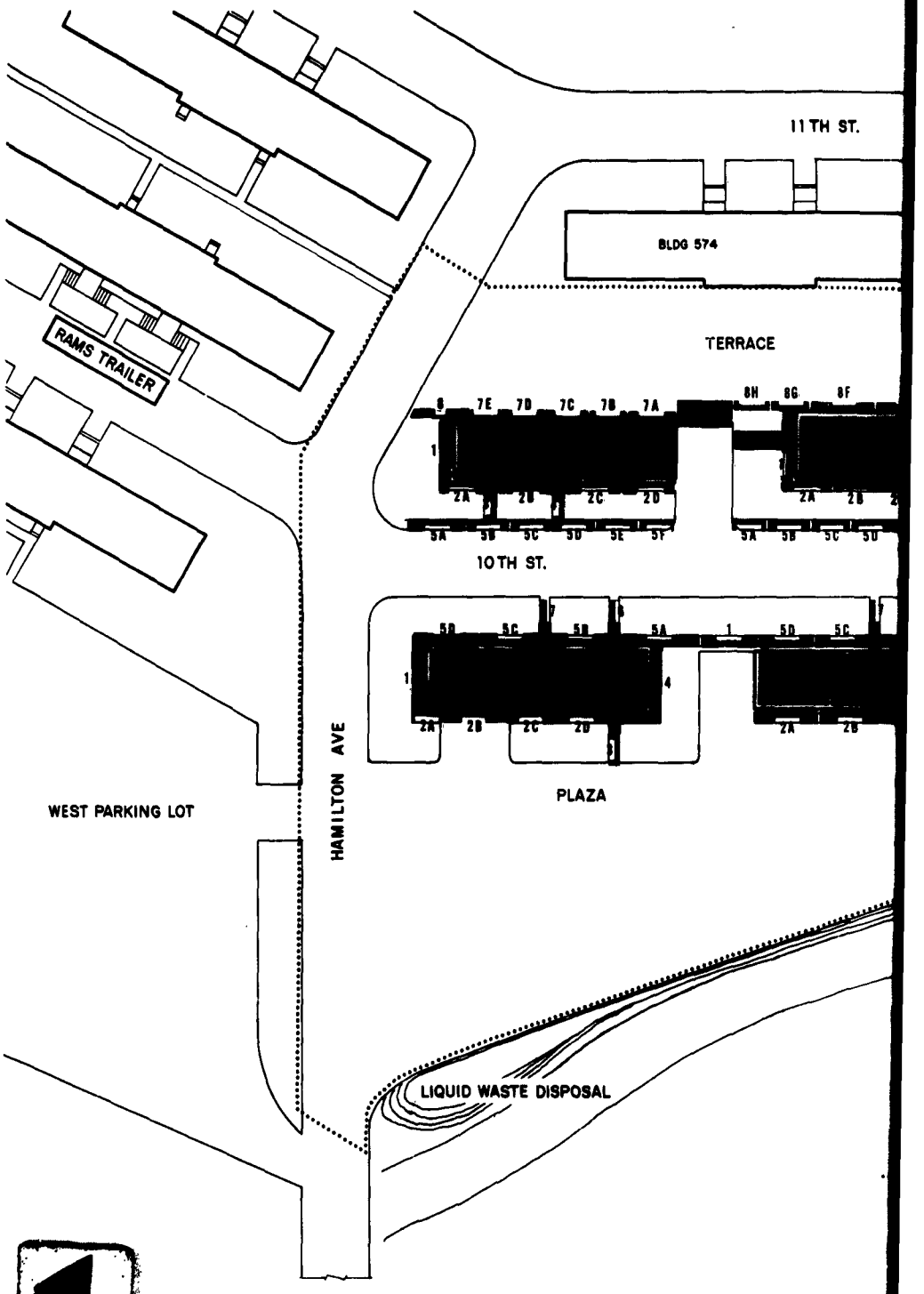

Fig. B.9 Layout of Tar and

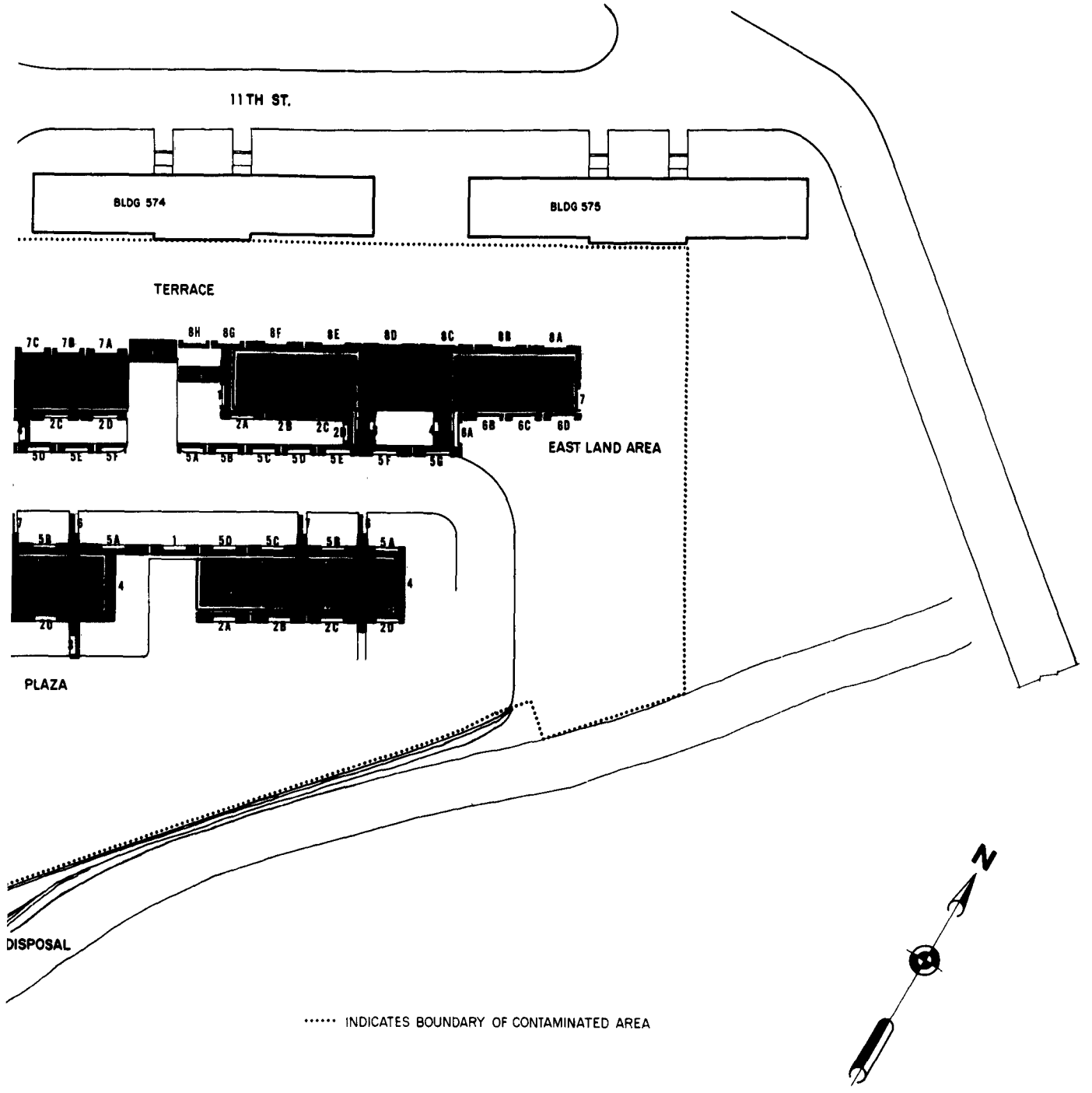

Fig. B.9 Layout of Tar and Gravel Roofs and Paved Walks

APPENDIX C

REMOTE AREA MONITORING SYSTEM (RAMS) DATA

3-ft gamma intensity readings are decay-corrected to 0000 hours of D+0.

TABLE C-1

Gamma Intensity Via RAMS During Dispersal Phase

Sequence of Dispersal	Date	Time	RAMS Station No. 1	2	3	4	5	6	7	8	9	10
Roof Bldg. 571	5 Oct 1960	0940	.086	.224	.078	.905	.147	.224	.267	.224	.905	1.21
Roof Bldg. 570	(D-3)	1150	.955	.468	.095	1.26	1.32	.651	.651	.442	1.04	1.34
Roof Bldg. 572		1200	2.17	1.56	.130	1.34	1.13	30.4	36.4	35.1	1.30	1.43
Roof Bldg. 573		1435	2.18	2.70	.74	1.48	1.13	26.2	33.2	39.3	32.3	37.1
After Rain		2045	1.81	3.10	1.94	1.33	.97	22.1	28.3	33.6	23.0	27.4
Morning Survey	6 Oct 1960	0735	1.92	3.66	2.01	1.37	.96	24.6	28.3	35.6	22.8	28.3
East Field E-1 - E-10	(D-2)	0930	2.28	3.65	105	1.93	1.19	24.6	30.1	36.5	22.8	32.0
Lawns and Beds - Bldg. 573		1030	2.56	4.58	105	2.20	1.65	24.7	30.2	37.6	27.5	35.7
Lawns and Beds - Bldg. 572		1140	11.0	6.42	105	2.11	1.37	34.9	36.7	40.3	28.4	35.7
Lawns and Beds - Bldg. 571		1300	11.0	6.41	105	3.75	1.47	32.1	35.7	42.1	28.4	35.7
Lawns and Beds - Bldg. 570		1420	13.8	6.46	106	4.70	4.89	36.0	38.8	43.3	39.5	36.9
Terrace (Land Areas Contam.)		1630	16.2	83.5	106	5.29	5.10	46.3	46.3	54.7	33.4	43.6
Morning Survey	7 Oct 1960	0710	13.4	86.4	110	5.28	4.80	43.2	42.2	49.9	22.1	41.3
Walks Bldgs. 572 and 573	(D-1)	0840	18.2	84.5	105	5.09	4.99	56.6	48.0	65.3	34.6	42.3
Walks Bldgs. 570 and 571		1000	19.2	81.6	105	12.5	7.78	49.9	48.0	66.2	35.5	44.1
10th St.		1125	79.6	78.7	105	13.4	8.93	59.5	57.6	72.0	39.4	48.0
Plaza		1515	87.5	87.5	117	96.3	107	68.1	58.4	73.9	40.8	49.6
Hamilton Ave. (Entire Complex Completed)		1730	96.0	107	117	112	117	57.8	59.7	78.3	39.2	50.9

Sequence of Dispersal	Date	Time	11	12	13	14	15	16	17	18	19	20
Roof Bldg. 571	5 Oct 1960	0940	.164	.172	39.6	35.4	37.9	5.38	.078	.94	.560	1.72
Roof Bldg. 570	(D-3)	1150	.182	.182	42.5	35.6	38.2	34.7	29.5	35.6	.859	1.82
Roof Bldg. 572		1200	.217	.200	40.8	35.6	38.6	34.7	30.4	35.6	1.65	1.82
Roof Bldg. 573		1435	9.6	15.7	41.0	27.9	34.9	35.8	27.0	27.9	2.53	5.24
(After Rain)		2045	6.9	15.9	31.8	23.9	28.3	36.1	25.6	24.8	2.48	5.31
Morning Survey	6 Oct 1960	0735	7.21	14.6	36.6	23.7	27.4	37.4	27.4	23.7	2.56	5.48
East Field E-1 - E-10	(D-2)	0930	7.48	16.4	39.2	25.6	29.2	37.4	29.2	24.6	3.19	11.9
Lawns and Beds - Bldg. 573		1030	11.0	19.2	39.4	25.6	29.3	38.4	30.2	25.6	7.78	17.4
Lawns and Beds - Bldg. 572		1140	11.0	20.1	39.4	26.6	31.1	38.5	30.2	25.6	8.70	17.4
Lawns and Beds - Bldg. 571		1300	11.0	19.2	45.8	32.0	37.5	39.4	30.2	25.6	10.1	18.3
Lawns and Beds - Bldg. 570		1420	11.1	20.3	46.1	33.2	42.4	59.9	46.1	46.1	12.0	19.4
Terrace (Land Areas Contam.)		1630	18.5	27.8	44.5	32.4	40.8	55.6	42.6	45.4	14.8	20.4
Morning Survey	7 Oct 1960	0710	17.3	16.3	43.2	32.6	30.7	59.5	43.2	43.2	14.4	19.2
Walks Bldgs. 572 and 573	(D-1)	0840	20.2	29.8	46.1	34.6	42.2	64.3	45.1	44.1	25.0	25.9
Walks Bldgs. 570 and 571		1000	20.2	29.8	62.4	41.3	52.8	69.1	53.8	54.7	29.8	32.6
10th St.		1125	24.0	34.6	69.2	44.1	58.6	69.2	57.6	58.6	90.2	97.8
Plaza		1515	25.3	35.0	77.8	49.6	64.2	85.6	68.1	72.0	97.3	117
Hamilton Ave. (Entire Complex Completed)		1730	26.5	36.2	72.4	58.7	65.6	82.2	64.6	66.6	97.9	97.9

TABLE C-2

Gamma Intensity Via RAMS During Weathering Phase

Date	Time	RAMS Station No. 1	2	3	4	5	6	7	8	9	10
8 Oct 1960 (D + 0)	0845	97.0	96.0	123	123	128	62.3	59.2	82.7	42.9	54.1
	1900	72.9	104	156	115	93.8	58.4	58.4	80.3	39.6	50.0
9 Oct 1960 (D + 1)	0725	73.9	88.9	129	118	98.5	58.9	50.4	76.1	42.9	51.4
	1030	49.5	101	108	46.3	28.0	50.6	43.1	66.7	40.9	43.1
	1725	39.6	109	121	38.4	22.5	52.7	42.8	57.1	34.0	38.4
10 Oct 1960 (D + 2)	0825	38.6	108	115	37.6	23.9	52.3	37.6	56.8	38.6	37.6
	2200	37.4	104	123	36.2	21.0	46.7	36.2	54.9	35.1	33.9
11 Oct 1960 (D + 3)	0845	39.0	104	122	37.8	25.6	54.9	37.8	56.1	39.0	37.8
12 Oct 1960 (D + 4)	0945	41.8	106	125	38.0	22.8	58.2	38.0	57.0	35.4	35.7
	1215	38.3	112	128	39.6	21.7	56.1	38.2	56.1	35.7	34.4
	1545	27.0	113	127	39.8	21.8	63.0	41.1	57.8	36.0	37.3
13 Oct 1960 (D + 5)	0750	38.8	112	123	38.8	22.7	56.1	34.8	54.8	38.8	33.4
	1620	38.0	106	122	36.6	23.1	59.6	38.0	55.6	35.3	35.3
14 Oct 1960 (D + 6)	0825	38.2	98.9	126	36.7	22.6	62.1	36.8	57.9	36.8	33.9
	1930	39.2	97.2	132	40.6	21.8	65.3	46.4	56.5	34.8	33.4
15 Oct 1960 (D + 7)	0900	41.8	104	131	37.3	22.4	61.2	38.8	55.2	35.8	34.3
	1710	39.6	119	132	38.0	22.8	76.1	48.7	59.4	44.1	38.1
16 Oct 1960 (D + 8)	0930	36.2	96.0	127	36.2	22.0	66.1	39.3	55.1	39.3	34.6
	1655	38.4	114	127	40.1	22.4	72.2	48.1	57.8	40.1	36.9

		11	12	13	14	15	16	17	18	19	20
8 Oct 1960 (D + 0)	0845	25.5	36.8	75.6	67.4	66.4	87.8	66.4	69.4	112	107
	1900	27.1	32.3	71.9	58.4	67.7	78.1	59.4	63.5	104	102
9 Oct 1960 (D + 1)	0725	24.6	34.3	69.6	61.1	57.9	84.7	58.9	58.9	99.6	79.3
	1030	14.0	33.4	54.9	54.9	56.0	66.7	47.4	52.7	72.1	79.6
	1725	21.9	27.4	46.1	49.4	54.9	54.9	52.7	53.8	62.6	56.0
10 Oct 1960 (D + 2)	0825	22.8	28.4	45.4	51.1	52.3	62.5	44.3	50.0	65.9	57.9
	2200	19.9	26.9	44.4	47.9	52.6	59.6	39.7	50.2	57.3	53.8
11 Oct 1960 (D + 3)	0845	22.0	28.1	43.9	48.8	52.5	58.6	42.7	51.2	61.0	58.6
12 Oct 1960 (D + 4)	0945	21.5	26.6	44.3	45.6	53.1	58.2	43.1	51.9	62.1	59.5
	1215	22.9	26.8	43.4	49.7	53.6	62.4	44.6	52.3	57.4	54.8
	1545	21.8	27.0	46.3	46.3	57.9	57.9	56.6	52.6	64.3	60.4
13 Oct 1960 (D + 5)	0750	22.7	26.8	44.1	46.8	53.5	60.2	45.4	52.1	61.5	57.5
	1620	21.7	25.8	44.7	43.4	55.6	55.6	39.4	54.3	61.0	57.0
14 Oct 1960 (D + 6)	0825	22.6	31.1	43.8	48.0	53.6	57.9	43.8	52.3	62.2	59.4
	1930	23.2	29.0	44.9	44.9	58.0	60.9	43.5	58.0	63.8	60.9
15 Oct 1960 (D + 7)	0900	22.4	31.3	44.7	44.7	55.2	61.2	41.8	55.2	59.7	58.1
	1710	25.9	30.4	45.6	44.1	60.8	57.8	45.6	62.4	54.8	51.7
16 Oct 1960 (D + 8)	0930	25.2	28.3	40.9	42.5	53.5	61.4	40.9	56.7	50.4	48.8
	1655	25.7	28.9	41.7	38.4	57.8	56.1	46.5	59.4	54.5	49.7

TABLE C-3

Gamma Intensity Via RAMS During Recovery Phase

Sequence of Recovery	Date	Time	RAMS Station No.									
			1	2	3	4	5	6	7	8	9	10
Pre-Recovery	17 Oct 1960 (D + 9)	0750	36.6	116	116	36.6	23.2	73.2	40.0	61.6	38.3	36.6
Terrace and Curbs		1130	23.4	21.8	126	21.8	16.7	61.9	30.1	46.9	36.8	30.1
Streets and Roofs 570, 571, 572		1635	22.0	22.0	119	23.7	16.9	49.1	23.7	37.3	35.6	32.2
Morning Survey	18 Oct 1960 D + 10)	0800	22.8	22.8	114	22.8	19.3	42.2	19.3	31.6	31.6	28.1
Roof Bldg. 573		1235	21.2	21.2	115	23.0	19.4	42.4	21.2	35.3	23.0	21.2
Street Flushed		1650	11.6	23.2	57.2	28.6	43.0	39.4	14.3	28.6	23.2	17.9
Morning Survey	19 Oct 1960 (D + 11)	0830	18.0	22.1	64.4	33.1	46.0	40.5	14.0	31.3	23.9	18.0
All Areas Recovered	20 Oct 1960 (D + 12)	1300	0.4	18.7	45.3	3.0	3.0	15.8	8.1	8.7	3.7	6.7
Flower Beds - Bldg. 571		1505										

			11	12	13	14	15	16	17	18	19	20
Pre-Recovery	17 Oct 1960 (D + 9)	0750	25.0	30.0	43.3	46.6	58.2	66.6	63.2	61.6	49.9	49.9
Terrace and Curbs		1130	20.1	23.4	40.2	31.8	43.5	53.6	40.2	58.6	41.8	45.2
Streets and Roofs 570, 571, 572		1635	22.0	23.7	32.2	23.7	32.2	45.7	35.6	49.1	37.3	42.4
Morning Survey	18 Oct 1960 (D + 10)	0800	21.1	21.1	29.8	21.1	29.9	47.4	33.4	24.6	35.2	36.9
Roof Bldg. 573		1235	15.2	19.4	30.0	21.2	31.8	42.4	30.0	44.1	40.6	44.1
Streets Flushed		1650	13.6	15.2	21.4	12.3	25.0	37.6	26.8	37.6	23.2	28.6
Morning Survey	19 Oct 1960 (D + 11)	0830	14.7	16.6	22.1	12.0	25.8	42.3	29.4	38.6	23.9	31.3
All Areas Recovered	20 Oct 1960 (D + 12)	1300	2.9	4.0	6.3	2.8	4.5	7.7	4.0	5.9	3.4	8.1
Flower Beds - Bldg. 571		1505			3.4	0.1	2.6	0	0	0	3.2	6.9

APPENDIX D

PORTABLE RADIAC SURVEY (CUTIE PIE) DATA

3 ft gamma intensity readings are decay corrected to 0000 hours of D+0.

TABLE D-1

Gamma Intensity Via Radiacs During Dispersal Phase

Sequence of Dispersal	Date	Time	At RAMS Station No.									
			1	2	3	4	5	6	7	8	9	10
Roof Bldg. 571	5 Oct 1960	0930	.097	.167	.222	.65	.088	.10	.12	.16	.83	.72
Roof Bldg. 570	(D-3)	1045	---	.25	.23	---	---	.22	.26	.27	.96	---
		1110	.74	---	---	.79	.79	---	---	---	---	---
Roof Bldg. 572		1220	1.46	1.13	.28	.79	.63	28.3	30.7	33.3	1.00	.84
Roof Bldg. 573		1430	1.56	1.58	.93	.95	.67	21.0	26.0	36.6	24.5	32.7
	6 Oct 1960	0730	1.48	1.81	1.85	.87	.65	21.0	27.6	38.4	19.4	31.5
East Field E-1 - E-10	(D-2)	0925	1.58	1.83	102	1.23	.69	23.2	26.9	37.3	21.6	34.9
Lawns L3-1 - L3-6		1035	1.82	2.22	99.1	1.36	.97	21.7	28.4	41.5	24.4	36.6
Lawns L2-1 - L2-7		1140	8.3	2.8	96.8	1.27	.83	31.2	35.3	47.0	25.8	36.2
Lawns L1-2 - L1-4		1255	8.06	2.93	92.2	1.52	.83	32.2	35.2	46.6	24.7	36.4
Lawns L0-1 - L0-9		1425	11.3	3.11	99.0	2.83	2.70	32.2	35.0	46.1	26.3	37.3
Terrace (Finish Land Areas)		1630	13.5	102	99.0	3.10	2.76	42.6	45.0	60.5	30.2	44.3
	7 Oct 1960	0650	13.4	105	105	3.05	2.98	42.0	44.4	57.4	31.0	43.1
Walks Bldgs. 572 and 573	(D-1)	0845	18.0	108	101	3.02	2.89	48.5	49.2	69.1	22.3	46.8
Walks Bldgs. 570 and 571		1005	16.8	103	105	9.4	6.5	47.8	48.2	70.1	33.4	46.1
10th St.		1125	88.6	102	108	99	72.5	52.9	53.9	77.3	37.4	50.2
Plaza		1515	92.4	113	105	107	111	55.0	56.2	78.8	37.7	53.7
Hamilton Ave.		1640	97.0	109	110	112	120	57.3	58.8	79.8	39.4	52.6
(Entire Complex Completed)												

Sequence of Dispersal	Date	Time	11	12	13	14	15	16	17	18	19	20
Roof Bldg. 571	5 Oct 1960	0930	.21	.20	35.4	37.4	36.7	.22	.13	.075	.66	.90
Roof Bldg. 570	(D-3)	1045	.25	.23	---	---	---	---	---	---	---	---
		1110	---	---	34.7	36.6	36.8	29.0	32.5	31.6	.85	.85
Roof Bldg. 572		1220	.27	.23	34.2	36.4	26.2	28.5	30.9	30.5	1.37	.96
Roof Bldg. 573		1430	9.11	14.3	32.5	30.8	28.4	29.2	25.3	20.6	2.10	2.82
	6 Oct 1960	0730	8.34	15.3	30.1	26.6	25.5	31.5	25.7	19.2	2.1	29.8
East Field E-1 - E-10	(D-2)	0935	9.04	15.5	34.8	29.0	26.9	32.2	26.4	20.2	2.4	10.2
Lawns L3-1 - L3-6		1035	10.4	19.4	34.1	28.1	27.2	30.9	26.5	20.1	8.3	14.1
Lawns L2-1 - L2-7		1440	11.1	20.5	34.8	28.6	27.6	32.5	27.2	21.2	8.5	14.5
Lawns L1-2 - L1-4		1255	12.7	19.4	37.8	34.3	33.9	34.8	27.9	21.9	10.1	14.5
Lawns L0-1 - L0-9		1425	11.3	20.8	39.2	35.7	36.6	51.9	40.6	38.0	13.6	16.6
Terrace (Finish Land Areas)		1630	18.3	27.4	40.1	38.5	39.0	53.1	43.4	39.4	16.5	17.4
	7 Oct 1960	0650	18.4	27.9	38.9	36.5	37.2	52.0	40.8	38.4	15.7	18.1
Walks Bldgs. 572 and 573	(D-1)	0845	20.9	29.8	40.8	39.4	39.6	55.0	43.7	40.3	27.2	22.6
Walks Bldgs. 570 and 571		1005	20.6	29.8	54.0	45.1	47.8	61.2	48.5	45.1	28.6	27.8
10th St.		1125	24.9	34.3	62.3	51.0	54.1	65.7	52.6	49.3	98.8	96.6
Plaza		1515	26.3	36.7	72.7	59.1	65.9	79.8	62.7	59.3	99.7	97.3
Hamilton Ave.		1640	26.9	37.2	71.7	59.0	65.6	81.5	64.6	65.4	97.9	97.9
(Entire Complex Completed)												

TABLE D-2

Gamma Intensity Via Radiacs at Roof Height During Dispersal Phase

Sequence of dispersal	Date	Time	Above RANS Station No.											
			6R	7R	8R	9R	10R	21R	13R	14R	15R	16R	17R	18R
Roof Bldg. 571	5 Oct 1960 (D-3)	1010	---	---	---	---	---	---	73.0	76.31	71.2	---	---	---
Roof Bldg. 570		1045	1.00	1.13	1.18	1.24	1.03	.74	---	---	---	---	---	---
		1110	---	---	---	---	---	---	72.2	75.0	66.5	58.2	63.4	58.8
Roof Bldg. 572		1220	57.6	70.9	65.4	1.46	1.11	.61	71.1	74.1	66.7	57.1	63.0	57.8
Roof Bldg. 573		1430	42.7	54.0	67.6	55.3	67.9	68.5	62.5	64.4	46.8	56.8	47.7	38.8
	6 Oct 1960 (D-2)	0730	44.2	57.2	70.6	51.6	67.8	72.7	55.8	50.9	46.4	61.4	47.8	35.8
East Field E-1 - E-10		0925	45.7	57.7	68.8	49.4	69.1	75.4	60.3	52.4	44.5	61.5	47.1	36.2
Lawns L3-1 - L3-6		1035	45.0	58.6	70.1	50.7	70.1	75.4	60.6	52.3	43.1	47.7	62.0	36.0
Lawns L2-1 - L2-7		1140	50.5	67.0	73.5	52.3	69.4	75.1	61.5	53.7	43.8	62.0	47.5	35.7
Lawns L1-2 - L1-4		1255	49.6	60.9	72.1	52.8	70.8	75.8	63.1	57.1	48.9	62.4	47.5	36.3
Lawns L0-1 - L0-9		1425	50.9	63 1	73.5	51.9	70.8	75.8	63.4	57.6	52.3	76.3	58.1	47.7
Terrace (Finish Land Areas)		1630	63.8	75.8	88.0	58.0	74.2	81.6	65.4	60.3	57.0	79.1	60.5	50.3
	7 Oct 1960 (D-1)	0650	66.7	84.6	92.7	62.0	77.7	84.1	65.8	59.6	52.9	79.1	60.3	50.3
Walks Bldgs. 572 and 573		0845	66.5	79.0	106	51.9	77.3	82.6	66.5	60.5	55.4	83.3	63.8	53.5
Walks Bldgs. 570 and 571		1005	67.9	81.8	103.2	66.0	78.0	84.7	77.0	67.2	67.4	87.1	66.2	56.9
10th St.		1125	71.5	83.3	101.4	68.3	83.3	87.4	81.4	71.5	69.1	93.7	71.5	61.3
Plaza		1515	74.2	85.6	107.0	67.1	81.9	86.8	90.9	82.2	82.4	97.3	82.4	70.3
Hamilton Ave. (Entire Complex Completed)		1640	77.1	88.6	100.4	71.2	83.0	87.9	92.8	85.0	85.0	97.9	86.4	77.9

TABLE D-3

Gamma Intensity via Radiacs During Weathering Phase

Date	Time	At RADS Station No.																			
		1	2	3	4	5	6	7	8	9	10	11	12	13	14	15	16	17	18	19	20
8 Oct 1960 (D + 0)	0830	100	102	110	117	126	54.1	56.1	78.6	37.8	51.1	25.5	34.7	74.5	60.2	67.4	82.6	64.4	69.4	107	107
	1645	74	114	123	111	105	54	54	78	36	50	26	35	76	58	67	81	62	59	98	113
9 Oct 1960 (D + 1)	0935	44	110	109	39	25	43	42	65	34	42	24	30	54	54	58	66	47	49	70	81
	1640	37	114	110	30	20	40	36	47	30	33	22	24	38	45	51	52	40	45	62	55
10 Oct 1960 (D + 2)	0810	34	108	102	28	18	38	36	49	28	31	22	24	38	44	51	57	43	47	53	51
	1500	32	107	100	28	17	37	35	47	28	31	21	23	37	44	51	52	38	43	52	51
11 Oct 1960 (D + 3)	1500	31	103	100	28	17	36	35	46	26	29	22	24	36	41	49	50	36	40	50	49
12 Oct 1960 (D + 4)	0720	27	86	82	23	14	30	29	40	23	25	17	19	31	35	42	43	33	36	44	42
	1515	30	102	101	28	18	35	34	49	27	33	20	23	35	43	51	52	39	42	52	49
13 Oct 1960 (D + 5)	0740	31	112	106	31	16	35	35	51	29	35	21	27	36	47	52	54	40	44	56	54
	1445	31	106	98	28	18	37	34	49	27	28	20	23	37	43	52	53	37	41	50	50
14 Oct 1960 (D + 6)	0740	32.6	106	102	28.3	18.4	36.8	32.6	45.2	29.6	34.0	22.6	24.0	35.4	42.4	49.5	55.1	41.0	45.2	52.3	50.9
	1500	30.1	106	98.8	27.2	18.6	34.4	31.5	44.4	25.8	28.6	18.6	21.5	34.4	43.0	48.7	47.3	37.3	43.0	45.8	50.1
15 Oct 1960 (D + 7)	0900	35.1	107	99.9	29.1	20.5	37.6	32.8	47.0	26.8	29.4	19.8	21.2	35.1	42.9	50.7	51.5	37.6	43.6	47.0	44.0
	1635	31.6	102	116	27.0	17.5	36.6	32.8	47.8	30.1	30.8	21.7	23.6	35.4	43.4	49.8	50.6	36.9	41.1	38.8	36.9
16 Oct 1960 (D + 8)	0900	33.1	113	101	35.1	18.9	40.9	37.8	53.5	33.1	34.6	22.0	28.4	34.6	42.5	53.5	55.1	39.4	42.5	37.8	33.1
	1510	30.4	112	99.2	27.2	17.6	38.4	35.2	51.1	30.4	33.6	25.6	28.8	35.2	43.2	51.2	46.4	36.8	44.8	38.4	35.2

TABLE D-4

Gamma Intensity via Radiacs at Roof Height During Weathering Phase

Date	Time	Above RAMS Station No.										
		6R	7R	8R	9R	10R	13R	14R	15R	16R	17R	18R
8 Oct 1960 (D + 0)	0900	74.5	85.7	102	70.4	83.7	91.9	87.8	88.8	107	89.8	82.7
	1645	76	89	111	70	84	99	93	93	114	88	84
9 Oct 1960 (D + 1)	0955	56	61	70	59	59	83	83	83	73	63	62
	1705	46	47	59	51	42	55	62	68	65	58	56
10 Oct 1960 (D + 2)	0810	44	48	57	49	36	49	61	63	64	55	52
	1500	46	50	46	50	38	48	61	61	62	53	52
11 Oct 1960 (D + 3)	1500	42	46	54	47	37	46	60	60	62	52	51
12 Oct 1960 (D + 4)	0720	35	38	44	39	31	41	50	50	51	44	43
	1515	43	47	54	47	38	47	59	59	63	56	53
13 Oct 1960 (D + 5)	0740	43	47	54	51	43	56	67	66	67	58	55
	1445	43	49	56	47	40	49	61	61	60	53	50
14 Oct 1960 (D + 6)	0740	42.4	48.0	56.5	49.5	38.2	50.9	63.6	65.0	65.0	56.6	55.1
	1500	44.4	47.3	57.3	50.1	37.2	47.3	61.6	60.1	61.6	53.0	48.6
15 Oct 1960 (D + 7)	0900	44.0	45.5	54.1	51.8	37.3	49.6	59.6	62.7	61.5	57.5	54.8
	1635	43.8	45.3	54.1	50.2	41.5	44.9	55.6	60.1	60.5	54.6	51.0
16 Oct 1960 (D + 8)	0900	47.2	48.8	58.2	47.2	39.4	44.1	59.8	59.8	67.9	55.1	53.5
	1510	44.8	44.8	57.6	48.0	38.4	44.8	57.6	60.8	57.6	49.6	49.6

TABEL D-5

Gamma Intensity Via Radiacs During Recovery Phase

Sequence of Recovery	Date	Time	At RAMS Station No. 1	2	3	4	5	6	7	8	9	10
Pre-Recovery	17 Oct 1960 (D + 9)	0805	31.6	103	105	30.0	23.3	40.0	40.0	53.3	35.0	35.0
Terrance and Pavements		1105	21.8	16.7	92.1	20.1	15.1	26.8	26.8	36.8	25.1	26.8
Roofs 570, 571, 572		1610	16.9	15.2	102	15.2	16.9	22.0	18.6	30.4	30.4	28.8
Morning Survey	18 Oct 1960 (D + 10)	0730	19.3	15.8	102	17.6	17.6	24.6	21.0	31.6	28.1	29.8
Roof Bldg. 573		1130	17.7	17.7	95.4	15.9	15.9	19.4	19.4	30.0	21.2	19.4
All but Lawn Recovered		1625	16.1	17.9	51.9	26.8	30.4	23.2	19.2	28.6	17.9	17.9
Morning Survey	19 Oct 1960 (D + 11)	0705	16.5	16.5	51.5	23.9	46.0	18.4	16.5	25.8	18.4	18.4
All Areas Recovered	20 Oct 1960 (D + 12)	1305	2.8	11.8	31.6	3.0	3.0	6.7	6.1	7.9	5.1	6.3
Flower Beds - Bldg 571		1510										

Sequence of Recovery	Date	Time	11	12	13	14	15	16	17	18	19	20
Pre-Recovery	17 Oct 1960 (D + 9)	0805	26.6	28.3	38.3	43.3	51.6	56.6	41.6	46.6	43.3	40.0
Terrace and Pavements		1105	16.7	16.7	33.4	30.1	33.4	46.9	33.4	43.5	33.4	33.4
Roofs 570, 571, 572		1610	16.9	18.6	25.4	27.1	25.4	37.3	27.1	30.4	30.4	30.4
Morning Survey	18 Oct 1960 (D + 10)	0730	19.3	21.0	28.1	28.1	28.1	42.0	28.1	35.2	33.4	31.6
Roof Bldg. 573		1130	17.7	15.9	27.7	26.4	22.9	38.9	30.0	31.8	31.8	35.3
All but Lawns Recovered		1625	16.1	12.5	17.9	21.4	23.2	35.8	23.2	30.4	26.8	26.8
Morning Survey	19 Oct 1960 (D + 11)	0705	11.0	11.0	18.4	22.0	18.4	36.8	23.9	27.6	25.8	23.9
All Areas Recovered	20 Oct 1960 (D + 12)	1305	4.5	4.5	8.3	5.9	6.3	7.9	5.5	4.9	4.3	6.5
Flower Beds - Bldg. 571					3.3	2.3	2.3	-	-	-	2.5	3.5

TABLE D-6

Gamma Intensity via Radiacs at Roof Height During Recovery Phase

Sequence of Recovery	Date	Time	Above RAMS Station No.										
			6R	7R	8R	9R	10R	13R	14R	15R	16R	17R	18R
Pre-Recovery	17 Oct 1960 (D + 9)	0805	49.9	53.2	56.6	51.6	46.6	53.2	59.9	68.2	58.3	53.2	49.9
Terrace and Pavements		1105	35.2	40.2	45.1	41.9	35.2	41.9	45.1	48.6	55.2	50.2	38.6
Roofs 570, 571, 572		1610	16.9	18.6	27.1	40.6	37.3	23.7	23.7	27.1	33.9	30.4	30.4
Morning Survey	18 Oct 1960 (D + 10)	0730	21.0	22.8	29.8	43.9	38.6	29.8	26.3	29.8	35.2	33.4	31.6
Roof Bldg. 573		1130	17.7	19.4	24.7	17.7	15.9	22.9	22.9	25.4	35.3	30.0	30.0
All but Lawns Recovered		1625	17.9	17.9	25.0	19.2	16.1	19.2	19.2	23.2	32.2	26.8	23.2
Morning Survey	19 Oct 1960 (D + 11)	0705	20.2	23.9	27.6	22.1	22.1	16.5	18.4	20.2	31.3	25.8	23.9
All Areas Recovered	20 Oct 1960 (D + 12)	1305	8.5	8.1	9.3	7.3	8.3	8.9	7.1	7.1	7.5	6.1	5.7
Flower Beds - Bldg. 571		1510	-	-	-	-	-	4.3	3.5	3.7	-	-	-

APPENDIX E

CONTRIBUTION FACTOR CALCULATIONS

To avoid complex column headings in Tables E-1 through E-5, the columns are numbered according to the following key:

1 A, sector area (ft^2) - see Appendix B.

2 d_a, apparent distance between reference location and centroid of contributing sector (ft) - see Appendix B.

3 cf, unshielded contribution factor = A/d_a^2

4 τ, mass thickness of shielding material between reference location, station 19, and centroid of contributing sector (lb_m/ft^2) - see Appendix G.

5 s, shielding reduction factor (Fig. 3.25) - see Appendix F.

6 cf_s, shielded contribution factor = cf x s.

7 Σ cf_s, subtotal and total contribution factors.

TABLE E.1

Contribution Factors - Paved Areas - Station 19

		1 A App. B	2 d_a App. B	3 cf ①/②^2	4 r App. C	5 s Fig. 3.25	6 cf_s ③ x ⑤	7 Σ cf_s Σ ⑥
Hamilton	H-1	3420	184	.1010	10^{3+}	0	0	
	2	611	190	.0169	19	.75	.0127	
	3	1767	180	.0545	0	1.0	.0545	
	4	2240	188	.0634	28_2	.65	.0412	
	5	2020	216	.0433	10^2	.13	.0056	
	6	2850	265	.0406	10^2	.13	.0053	
	7	320	301	.0035	10^2	.13	.0005	
								.1198
10th St.	T-1	416	155	.0173	0	1.0	.0173	
	2	1025	133	.0580	0	1.0	.0580	
	3	1216	98	.1265	0	1.0	.1265	
	4	1025	63	.2582	0	1.0	.2582	
	5	992	32	.9675	0	1.0	.9675	
	6	1057	-	11.2160	0	1.0	11.2160	
	7	1025	33	.9406	0	1.0	.9406	
	8	1025	65	.2430	0	1.0	.2430	
	9	704	92	.0832	0	1.0	.0832	
	10	1025	119	.0724	0	1.0	.0724	
	11	863	149	.0389	0	1.0	.0389	
	12	286	170	.0099	0	1.0	.0099	
	13	198	174	.0065	0	1.0	.0065	
	14	1025	172	.0347	0	1.0	.0347	
	15	1025	180	.0316	19	.75	.0237	
	16	1182	196	.0308	25	.68	.0209	
	17	96	202	.0024	31	.61	.0015	
								14.1188
Plaza	P-1	2210	166	.0802	125	.0685	.0055	
	2	2100	121	.1434	28	.65	.0932	
	3	2100	105	.1905	6	.916	.1745	
	4	2100	131	.1225	125	.0685	.0084	
	5	1170	169	.0410	125	.0685	.0028	
	6	660	204	.0159	125	.0685	.0011	
	7	900	185	.0263	125	.0685	.0018	
	8	1740	158	.0698	41	.504	.0352	
	9	1800	137	.0960	0	1.0	.0960	
	10	900	137	.0480	1.0	.98	.0470	
	11	1800	150	.0800	125	.0685	.0055	
	12	840	174	.0278	125	.0685	.0019	
	13	3160	210	.0716	125	.0685	.0049	
	14	3160	176	.1021	0	1.0	.1021	
	15	1424	162	.0539	41	.504	.0272	
	16	2590	239	.0453	38	.535	.0244	
	17	588	208	.0136	0	1.0	.0136	
	18	578	270	.0079	125	.0685	.0005	
								.6456
Parking Stps.	D-1	650	54	.2230	0	1.0	.2230	
	2	650	30	.7220	0	1.0	.7220	
	3	380	119	.0269	0	1.0	.0269	
	4	1950	149	.0878	41	.504	.0443	
	5	1045	127	.0648	125	.0685	.0044	
	6	1025	192	.1211	75	.236	.0286	
	7	702	52	.2699	0	1.0	.2699	
	8	674	77	.1139	0	1.0	.1139	
	9	448	136	.0276	125	.0685	.0019	
				17.3535				1.4349 15.3191

TABLE E.2

Contribution Factors - Roofs and Land Areas - Station 19

		1 A App. B	2 d_h App. B	3 cf ①/②^2	4 τ App. C	5 s Fig. 3.25	6 cf_s ③ x ⑤	7 Σ cf_s Σ ⑥
Bldg. 570	A	884	132	.0506	134	.0545	.0028	
	B	910	101	.0885	100	.128	.0113	
	C	910	74	.1630	73	.247	.0403	
								.0544
Bldg. 571	A	832	63	.205	68	.280	.0574	
	B	910	86	.122	96	.142	.0173	
	C	960	117	.070	119	.0795	.0056	
								.0803
Bldg. 572	A	936	121	.064	71	.260	.0166	
	B	884	90	.106	56	.356	.0377	
	C	884	66	.194	44	.475	.0922	
								.1465
Bldg. 573	A'	1008	75	.162	54	.382	.0619	
	A"	1023	100	.097	67	.284	.0275	
	B	1770	138	.090	82	.200	.0180	
	C	2030	192	.054	125	.0685	.0037	
								.1111
				1.4660				.3923
Terrace	T-1	1250	156	.0514	27	.67	.0344	
	2	870	147	.0403	27	.67	.0270	
	3	3190	125	.204	27	.67	.1367	
	4	1760	109	.148	0	1.0	.1480	
	5	2550	109	.215	0	1.0	.2150	
	6	3070	131	.179	58	.35	.0627	
	7	3120	172	.106	38	.54	.0572	
	8	3070	221	.063	44	.475	.0299	
	9	2450	269	.034	58	.35	.0119	
								.7228
East Land	E-1	2400	253	.0375	44	.475	.0178	
	2	540	172	.0183	3	.95	.0174	
	3	220	179	.0069	8	.89	.0061	
	4	3390	229	.0647	0	1.0	.0647	
	5	3390	230	.0641	0	1.0	.0641	
	6	640	203	.0155	103+	0	0	
	7	1600	230	.0303	22	.71	.0215	
	8	1240	264	.0178	10	.86	.0153	
	9	1390	234	.0254	28	.62	.0157	
	10	2130	256	.0325	35	.56	.0182	
								.2408
				1.3430				.9636

TABLE E.3

Contribution Factors - Sidewalks - Station 19

		1 A App. B	2 d_a App. B	3 cf ①/②^2	4 τ App. C	5 s Fig. 3.25	6 cf_a ③ x ⑤	7 Σ cf_a Σ ⑥
Bldg. 570	1	87	151	.0038	63	.312	.0012	
	2A	54	165	.0020	10^2	.13	.0003	
	2B	72	132	.0041	10^2	.13	.0005	
	2C	75	112	.0060	81	.206	.0012	
	2D	72	94	.0082	81	.206	.0017	
	2E	57	78	.0094	63	.312	.0029	
	3	104	92	.0123	63	.312	.0038	
	4	87	61	.0234	0	1.0	.0234	
	5A	48	47	.0217	10^3+	0	0	
	5B	81	75	.0144	10^3+	0	0	
	5C	84	105	.0076	10^3+	0	0	
	5D	93	132	.0053	10^3+	0	0	
	6	112	57	.0345	10^3+	0	0	
	7	113	87	.0150	103+	0	0	
								.0350
Bldg. 571	1	81	37	.0592	0	1.0	.0592	
	2A	78	76	.0135	63	.312	.0042	
	2B	84	50	.0336	81	.206	.0069	
	2C	87	111	.0071	81	.206	.0014	
	2D	63	133	.0035	10^2	.13	.0005	
	3	18	124	.0012	10^2	.13	.0002	
	4	90	136	.0049	63	.312	.0015	
	5A	63	122	.0042	0	1.0	.0042	
	5B	84	94	.0045	0	1.0	.0045	
	5C	78	67	.0174	0	1.0	.0174	
	5D	78	48	.0392	0	1.0	.0392	
	6	112	107	.0098	0	1.0	.0098	
	7	113	77	.0191	0	1.0	.0191	
								.1681
Bldg. 572	1	96	140	.0049	10^3+	0	0	
	2A	60	126	.0038	0	1.0	.0038	
	2B	81	100	.0081	0	1.0	.0081	

								.0350
Bldg. 571	1	81	37	.0592	0	1.0	.0592	
	2A	78	76	.0135	63	.312	.0042	
	2B	84	50	.0336	81	.206	.0069	
	2C	87	111	.0071	81	.206	.0014	
	2D	63	133	.0035	10^2	.13	.0005	
	3	18	124	.0012	10^2	.13	.0002	
	4	90	136	.0049	63	.312	.0015	
	5A	63	122	.0042	0	1.0	.0042	
	5B	84	94	.0045	0	1.0	.0045	
	5C	78	67	.0174	0	1.0	.0174	
	5D	78	48	.0392	0	1.0	.0392	
	6	112	107	.0098	0	1.0	.0098	
	7	113	77	.0191	0	1.0	.0191	
								.1681
Bldg. 572	1	96	140	.0049	10^3+	0	0	
	2A	60	126	.0038	0	1.0	.0038	
	2B	81	100	.0081	0	1.0	.0081	
	2C	84	71	.0167	0	1.0	.0167	
	2D	75	51	.0288	0	1.0	.0288	
	3	81	113	.0063	0	1.0	.0063	
	4	81	83	.0118	0	1.0	.0118	
	5A	162	136	.0088	0	1.0	.0088	
	5B	120	113	.0094	0	1.0	.0094	
	5C	120	93	.0139	0	1.0	.0139	
	5D	120	74	.0219	0	1.0	.0219	
	5E	120	55	.0395	0	1.0	.0395	
	5F	114	37	.0884	0	1.0	.0884	
	6	416	74	.0760	0	1.0	.0760	
	7A	168	80	.0263	19	.75	.0197	
	7B	160	90	.0198	25	.68	.0135	
	7C	160	103	.0151	28	.65	.0098	
	7D	160	118	.0115	33	.59	.0068	
	7E	160	134	.0089	38	.535	.0048	
	8	203	154	.0086	40	510	.0044	
								.3924
Bldg. 573	1	108	64	.0264	0	1.0	.0264	
	2A	63	54	.0216	0	1.0	.0216	
	2B	66	71	.0131	0	1.0	.0131	
	2C	66	90	.0082	0	1.0	.0082	
	2D	48	100	.0048	0	1.0	.0048	
	3	140	108	.0120	13	.83	.0099	
	4	140	148	.0064	19	.75	.0048	
	5A	90	22	.1859	0	1.0	.1859	
	5B	120	35	.0980	0	1.0	.0980	
	5C	120	52	.0444	0	1.0	.0444	
	5D	120	71	.0238	0	1.0	.0238	
	5E	120	91	.0145	0	1.0	.0145	
	5F	180	116	.0134	0	1.0	.0134	
	5G	162	143	.0079	0	1.0	.0079	
	6A	45	157	.0018	19	.75	.0014	
	6B	66	171	.0023	19	.75	.0017	
	6C	66	193	.0018	19	.75	.0014	
	6D	63	214	.0014	19	.75	.0011	
	7	81	227	.0016	63	.312	.0005	
	8A	240	214	.0052	10^3+	0	0	
	8B	240	182	.0069	10^3+	0	0	
	8C	240	165	.0088	10^3+	0	0	
	8D	240	140	.0123	10^3+	0	0	
	8E	240	116	.0178	19	.75	.0134	
	8F	240	96	.0261	19	.75	.0196	
	8G	144	84	.0204	4	.94	.0192	
	8H	152	79	.0244	0	1.0	.0244	
	9	212	62	.0552	0	1.0	.0552	
								.6146
				1.4848				1.2102

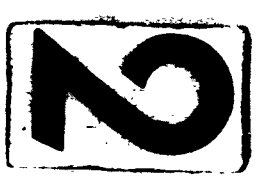

TABLE E.4

Contribution Factors - Planter Beds - Station 19

		1	2	3	4	5	6	7
		A	d_s	cf	τ	s	cf_s	Σ cf_s
		App. B	App. B	①/②^2	App. C	Fig. 3.25	③ x ⑤	Σ ⑥
Bldg. 570	0-1	70	132	.0040	10^3+	0	0	
	2	70	106	.0062	10^3+	0	0	
	3	70	77	.0180	10^3+	0	0	
	4	40	57	.0123	10^3+	0	0	
	5	39	62	.0101	0	1.0	.0101	
	6	24	77	.0040	10^2	.13	.0005	
	7	36	93	.0042	10^2	.13	.0006	
	8	38	111	.0031	125	.0685	.0002	
	9	21	148	.0010	10^3+	0	0	
	10	65	149	.0030	10^3+	0	0	
								.0114
Bldg. 571	1-1	62	50	.0248	0	1.0	.0248	
	2	65	69	.0137	0	1.0	.0137	
	3	68	91	.0082	0	1.0	.0082	
	4	42	121	.0028	0	1.0	.0028	
	5	26	134	.0014	10^3+	0	0	
	6	17	133	.0010	10^3+	0	0	
	7	29	110	.0024	10^3+	0	0	
	8	29	89	.0037	10^3+	0	0	
	9	26	74	.0047	63	.312	.0015	
								.0510
Bldg. 572	2-1	39	138	.0020	25	.62	.0012	
	2	34	126	.0021	0	1.0	.0021	
	3	54	101	.0053	0	1.0	.0053	
	4	56	73	.0105	0	1.0	.0105	
	5	48	53	.0171	0	1.0	.0171	
	6	60	77	.0101	19	.75	.0076	
	7	54	94	.0061	28	.65	.0040	
	8	54	114	.0042	33	.59	.0025	
	9	34	134	.0019	38	.535	.0010	
								.0513
Bldg. 573	3-1	46	64	.0113	0	1.0	.0113	
	2	50	63	.0126	0	1.0	.0126	
	3	51	91	.0062	0	1.0	.0062	
	4	32	102	.0031	0	1.0	.0031	
	5	45	154	.0019	19	.75	.0014	
	6	119	172	.0040	19	.75	.0030	
	7	119	205	.0028	19	.75	.0021	
	8	62	224	.0012	63	.312	.0004	
	9	82	214	.0018	10^3+	0	0	
	10	85	183	.0025	10^3+	0	0	
	11	85	110	.0070	19	.75	.0056	
	12	83	87	.0110	19	.75	.0083	
								.0540
				.2573				.1677

TABLE E.5

Contribution Factors - Lawns - Station 19

		1	2	3	4	5	6	7
		A	d_a	cf	r	s	cf_s	Σ cf_s
		App. B	App. B	①/②^2	App. C	Fig. 3.25	③ x ⑤	Σ ⑥
Bldg. 570	LO-1	760	146	.0357	11	.85	.0303	
	2	760	107	.0664	10^{3+}	0	0	
	3	513	70	.1050	10^{3+}	0	0	
	4	703	39	.4620	19	.75	.3465	
	5	608	58	.1807	0	1.0	.1807	
	6	703	85	.0974	8	.89	.0867	
	7	854	110	.0706	10^2	.13	.0092	
	8	624	165	.0230	10^2	.13	.0030	
	9	734	162	.0280	68	.28	.0078	
								.6642
Bldg. 571	L1-1	513	20	1.281	0	1.0	1.281	
	2	475	39	.326	0	1.0	.326	
	3	513	61	.138	0	1.0	.138	
	4	532	91	.064	0	1.0	.064	
								1.809
Bldg. 572	L2-1	528	160	.0206	8	.89	.0183	
	2	429	148	.0196	14	.81	.0159	
	3	527	149e	.0237	0	1.0	.0237	
	4	260	124	.0169	0	1.0	.0169	
	5	364	97	.0387	0	1.0	.0387	
	6	351	68	.0775	0	1.0	.0775	
	7	325	45	.1604	0	1.0	.1604	
								.6514
Bldg. 573	L3-1	250	71	.0497	0	1.0	.0497	
	2	500	48	.2170	0	1.0	.2170	
	3	390	34	.3380	0	1.0	.3380	
	4	390	57	.1200	0	1.0	.1200	
	5	390	84	.0554	0	1.0	.0554	
	6	558	128	.0341	19	.75	.0256	
				4.0494				.8057
								3.9303

APPENDIX F

DETERMINATION OF AN APPROPRIATE SHIELDING CURVE

In Section 3.4.1 of Chapter 3 it was explained why the shielding curves used in Complex II for wood and concrete were considered to be no longer suitable. They were constructed from a bare minimum of pertinent information - all that was then available. And, they were later found not to agree satisfactorily with the special shielding measurements made in connection with Complex III.

At the close of the Complex III experiment, Lee and Rinnert of USNRDL conducted a series of shielding measurements within the target complex area. The basic data consisted of dose rate readings taken at station 19. The radiation source, a Ba^{140}-La^{140} capsule, was moved to specific locations so as to cover the range of possible shielding thicknesses existing in the complex. For a given distance between source and detector, the ratio of a shielded reading (from within the complex) to an unshielded reading (from the instrument calibration range) provided an estimate of s, the shielding (reduction) factor. By computing the corresponding mass thicknesses according to the method described in Appendix G, it was possible to obtain the s versus τ plot shown in Fig. F.1.

Superimposed on this plot are three shielding curves. The lower curve, shown as a dashed line, is the Complex II curve for wood, which appeared earlier in Fig. 3.25. The equation of this straight line on a semi-log plot may be expressed as

$$s = I/I_o = e^{-c\tau} \qquad \text{(F-1)}$$

where I_o = the incident intensity from a collimated source
I = the emergent intensity
c = the mass absorption coefficient
$c\tau$ = the number of mean free paths

Although quite scattered, the plotted points of Fig. F.1 indicate a trend which lies to the right of the dashed curve representing equation F-1. Since it was desired to refine the contribution calculations

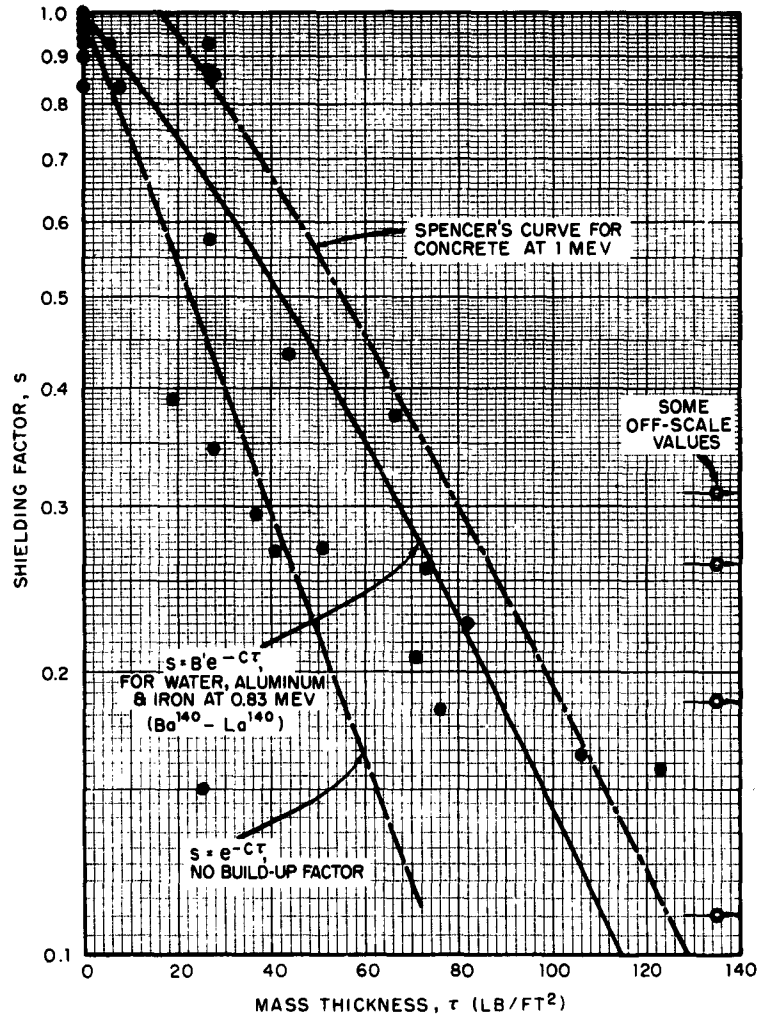

Fig. F.1 Comparison of Shielding Effects Estimates and Measurements

for Complex III, a curve which more nearly fit the s and τ data was required. The obvious approach was to correct Eq. F-1 for the effects of multiple scattering by introducing a build-up factor B. That is, the equation for simple shielding should read

$$s = B\, e^{-c\tau} \qquad \text{(F-2)}$$

Unfortunately B is not a constant. It varies with the density of the shielding material, the energy of the source and according to the number of mean free paths (mfp) indicated by the exponent $c\tau$. A complete array of building up factors are available from the work of Goldstein and Wilkins.[12] Their tabulations include B values for aluminum, water and iron - three substances having mass absorption coefficients representative of building materials. By using these values it was possible to plot a family of curves relating B-1* to photon energy E_p for four separate multiples of mfp as shown in Fig. F.2.

Cross plots from these curves at a constant energy of 0.83 Mev (the approximate mean photon energy for Ba^{140}-La^{140}) were then constructed to obtain the relationship between build-up factor and the product $c\tau$. Figure F.3 gives the results as three curves; one for water, one for aluminum and one for iron. Note that the curves are extrapolated for all values of $c\tau < 1$.

It must be pointed out that the concept of build-up factor assumes both source and detector are immersed in a 4π homogeneous medium. The physical arrangement of interest here concerns a semi-infinite medium. This means that B values from Fig. F.3 must be converted to a 2π geometry consistent with an above ground source-detector system in air.

The simplest equation for build-up factor in an infinite medium assumes B = 1 + b, when b depends upon energy and mfp. If B' equals the build-up factor in a semi-infinite medium, it may be expressed as 1 + kb, where k is a constant. Then

$$B' = 1 + k\,(B-1) \qquad \text{(F-3)}$$

*Since the term B-1 consistently appears in nearly all the equations of this development, plotting it (instead of B) against $c\tau$ was more expedient.

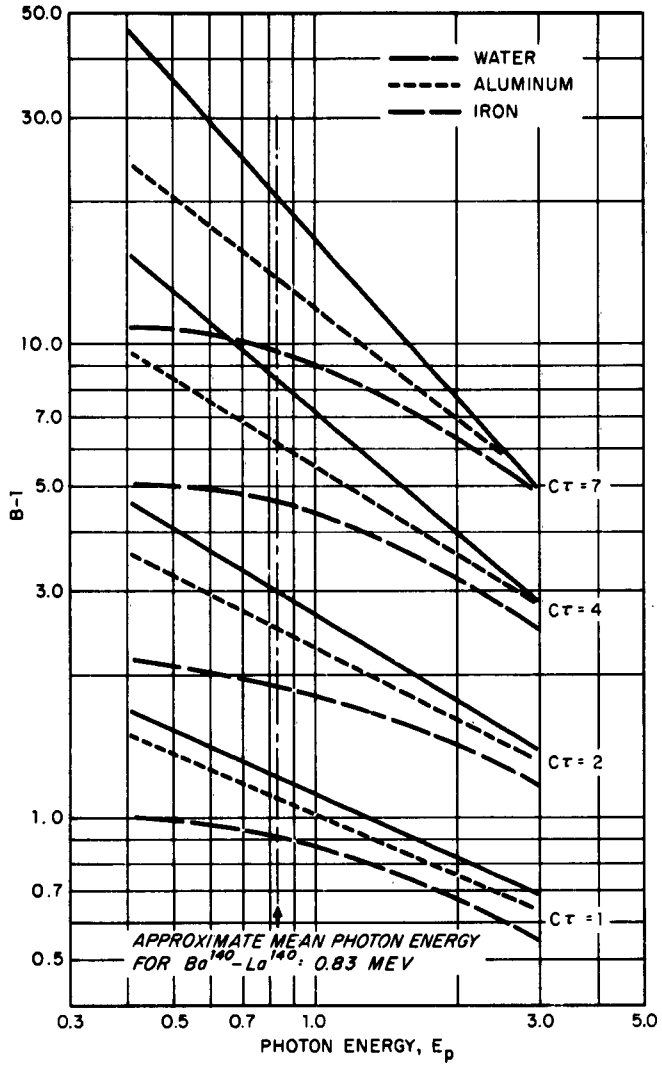

Fig. F.2 Build-up Factor as a Function of Energy for Various Multiples of MFP, $c\tau$

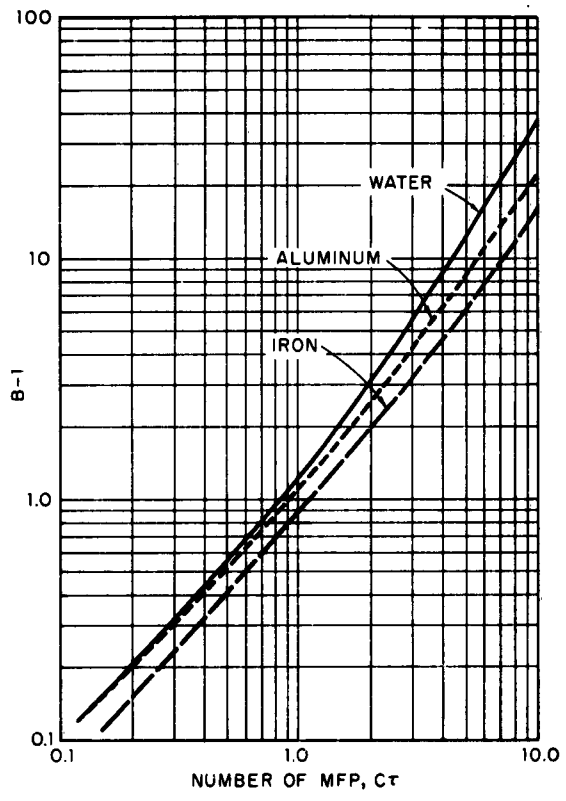

Fig. F.3 Build-up Factor as a Function of MFP Multiples for a Constant Photon Energy of 0.83 Mev

The constant k appearing in the above equation may be estimated from the experimental intensities that Lee and Rinnert measured at various distances in air from an unshielded Ba^{140}-La^{140} source. The measured intensities I_m are represented mathematically as

$$I_m = I_u B' (e^{-c\tau}/d^2) \qquad (F\text{-}4)$$

where d is the distance between source and detector and I_u is the source intensity at unit distance. Rewriting Eq. F-4 becomes

$$I_u B' = I_m d^2 e^{c\tau} = Y \qquad (F\text{-}5)$$

Using the above mentioned data, it was possible to solve the equation for Y over a range of source-to-detector distances. The stepwise solution is given in Table F.1. A plot of the resultant Y values against corresponding $c\tau$ values is shown in Fig. F.4. The equation of the least squares fit of a straight line to this plot is

$$Y = 827 + 627\ c\tau \qquad (F\text{-}6)$$

where $827 = Y_o$, the Y intercept, at a $c\tau$ value of zero. Under this condition B' is unity, since d is so small that any build-up due to scattering is negligible. Therefore, from Eq. F-5, $I_u = Y_o$ (at $c\tau = 0$). Eliminating Y between Eqs. F-5 and F-6 and dividing through by $Y_o = 827$

$$\frac{Y}{Y_o} = \frac{Y}{I_u} = B' = 1 + 0.757\ c\tau \qquad (F\text{-}7)$$

Setting this equal to Eq. F-3

$$k\ (B\text{-}1) = 0.757\ c\tau$$

or

$$k = 0.757\ c\tau/(B\text{-}1) \qquad (F\text{-}8)$$

At this point it may not be clear why it is necessary to find k and solve Eq. F-3 for B' when Eq. F-7 already offers a direct solution. The latter expression was derived from data restricted to $c\tau$ values equal to or less than 1.0. In this region the curve of B' versus $c\tau$ is

TABLE F.1

Calculation of Y From Unshielded Measurements of Gamma Intensities

1	2	3	4	5	6
d* (ft) Observed	d^2 (10^3 ft^2) (1)^2	c_T** (1)/367	e^{c_T} $e^{(3)}$	I_m* (mr/hr) Observed	Y (r/hr) (2) x (4) x (5)
40	1.6	0.109	1.115	513	940
50	2.5	0.136	1.146	314	900
60	3.6	0.164	1.178	212	900
70	4.9	0.191	1.210	157	930
80	6.4	0.218	1.244	117	930
100	10.4	0.272	1.312	79	1080
120	14.4	0.327	1.387	53	1060
140	19.6	0.382	1.465	38	1090
160	25.6	0.431	1.547	28	1110
180	32.4	0.491	1.634	21	1110
200	40.0	0.545	1.725	17	1170
230	52.9	0.627	1.870	12	1190
260	67.6	0.708	2.03	9.3	1280
300	90.0	0.818	2.27	6.5	1330

* Basic data collected by Lee and Rinnert.

**c_T, the number of mfp's is based on an air mass absorption coefficient of 0.341 ft^2/lb and an air density of 0.080 lb/ft^3.

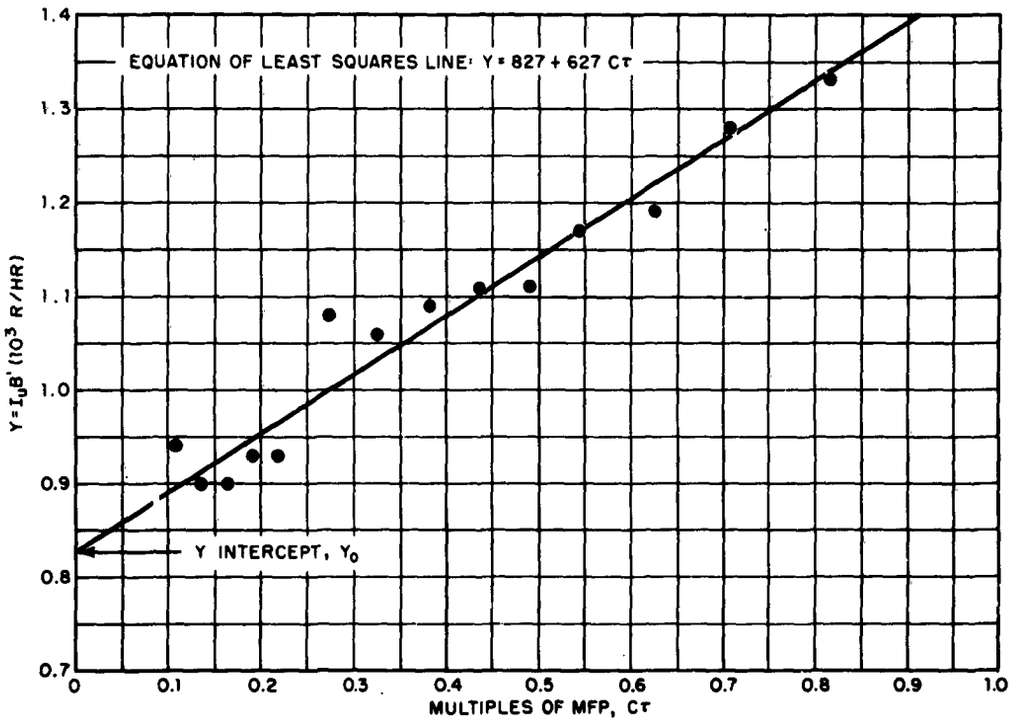

Fig. F.4 Determination of Y Intercept, $Y_o = I_u$, in Eq. F-6

a relatively straight line. Since B' is known to be a function of density as embodied in the product $c\tau$, it is unlikely that the curve would continue as a straight line. Therefore Eq. F-7 is not suitable as a general expression of B', and Eq. F-3 is preferred.

From Eq. F-8 it was possible to estimate an average value of k. This together with the build-up factors available let Eq. F-3 give B' values for a number of materials - water, aluminum and iron in particular. Reference 12 does not include build-up factors for air. Therefore, the solution to Eq. F-8 must rely upon the substitution of B values computed for water, a substance having a relatively low Z number. Taking B values from the upper curve in Fig. F.3 over the range $0 < c\tau < 1$, Eq. F-8 gives an average value of k equal to 0.67. Thus Eq. F-3 becomes

$$B' = 1 + 0.67\ (B-1) \qquad \text{(F-9)}$$

or

$$B' = 0.67\ B + 0.33$$

Columns 1 through 4 of Table F.2 present a solution to Eq. F-9 for four arbitrary values of $c\tau$. The curves of Fig. F.3 were used again for obtaining necessary B values as input data.

The remaining columns of Table F.2 represent a solution to the shielding equation

$$s = B'\ e^{-c\tau} \qquad \text{(F-10)}$$

where B' has been substituted for B in Eq. F-2. By dividing the $c\tau$ values by the respective mass absorption coefficient c given in the table, the mass thicknesses shown in column 5 were obtained. Columns 6 and 7 complete the solution.

A graph of the resultant s values (in column 7) versus the τ values (in column 5) is shown in Fig. F.1 by the solid line. This curve appears to provide a better fit to the data points than the dashed curve described by Eq. F-1. The effect of introducing the build-up factor into Eq. F-1 is obvious from the relative position of the two curves.

The uppermost curve appearing in Fig. F.1 is that derived by Spencer[13]* for concrete and 1 Mev gamma energy. It is based on a far more sophisticated approach** than the approximate method just described in this

* See Fig. 22.1, page 17 of Reference 10.

**Spencer used the moments method, and assumed an infinite water medium and a plane perpendicular source.

TABLE F.2

Calculations of B' and s for Arbitrary Values of c_T and τ

1	2	3	4	5	6	7
c_T No. of mfp	B Fig. F.3	.67 B .67 (2)	B' (3) + 0.33	τ (1)/c	e^{-c_T} $e^{-(1)}$	s (4) x (6)
			Water (c = 0.0380 ft^2/lb)			
1	2.24	1.50	1.83	26.3	.368	.674
2	4.05	2.72	3.05	52.6	.135	.412
3	6.50	4.36	4.69	78.9	.0497	.233
4	9.50	6.37	6.70	105.2	.0182	.122
			Aluminum (c = 0.0330 ft^2/lb)			
1	2.12	1.42	1.75	30.3	.368	.644
2	3.50	2.35	2.68	60.6	.135	.361
3	5.25	3.52	3.85	90.9	.0497	.191
4	7.30	4.80	5.13	121.2	.0182	.093
			Iron (c = 0.0323 ft^2/lb)			
1	1.89	1.27	1.60	31.0	.368	.589
2	2.98	2.00	2.33	62.0	.135	.314
3	4.18	2.80	3.13	93.0	0.487	.155
4	5.50	3.69	4.02	124.0	.0182	.073

appendix. Nevertheless, the curves are nearly parallel over their entire length. This relatively constant displacement is probably caused by terrain and geometry factors and differences in source configuration. The agreement in slope and form, however, is interesting in view of the totally divorced avenues of approach employed in the curves' derivations. Because of this agreement and the reasonable proximity of data points, it may be concluded that the water-aluminum-iron curve is suited for its intended use. In addition, this same curve may be assumed to represent other materials having a relatively low Z number such as concrete, earth, glass, wood, copper, etc.

It should be pointed out that the solid curve presented previously in Fig. 3.25 is not the same as its counterpart in Fig. F.1. The former curve is the result of an earlier derivation based on an average photon energy of 0.7 Mev. The more correct value of 0.83 Mev was determined later. However, this earlier curve was used in the contribution factor calculations. Fortunately the two curves do not differ significantly, except for large values of mass thickness. For instance, at τ values in excess of 100 lb/ft^2, s values differ by 10 % or more. This might account, to some degree, for the size of the errors (e_p) in the predicted fractional contributions (f_p) reported in Section 3.4. These errors, it will be recalled, were attributed largely to the shielding factors.

APPENDIX G

SYSTEMATIC CALCULATIONS FOR MASS THICKNESS

It is evident from Appendix E that meaningful contribution factor calculations must include a correction to account for the inherent shielding properties of the buildings within the target complex. The approach used to make these shielding corrections was first to find the effective mass thickness of all the intervening shields between a particular contributing source and some arbitrary receiving location. Then, from Fig. 3.25 the corresponding shielding reduction factor was determined.

Before presenting the detailed and systematic solution to the above problem, it should be clear what is meant by the concept of mass thickness. For the purposes of this report, the apparent mass thickness, τ, of a given material is simply the product of its density, ρ, and the thickness, t; where t is measured normal to the surface. Since the density for a given material is a constant, mass thickness τ is always proportional to linear thickness t. Keeping consistent units in the above product, τ will be in pounds (mass) per unit area (lbs/ft^2).

Mass thickness is a convenient quantity for two reasons, namely:

(1) The weights of structural materials in lb/ft^2 are available in architectural handbooks.*

(2) A plot of shielding protection factors versus mass thickness for any number of common construction materials (wood, earth, concrete, aluminum, copper and steel) results in essentially one curve at each energy level.

The various building elements (roofs, floors, walls, and partitions) constituting shielding in the target complex are randomly oriented with respect to some arbitrary receiving point. Consider a simple

*See E. W. Cannon's Building Materials Commonly used in Existing Urban Buildings in the United States, (8 Jan 1958, PROJECT CIVIL, Institute of Engineering Research, University of California) for typical mass thickness values.

shielding situation created by the free standing wall shown in Fig. G.1. For this and subsequent examples the following definitions and relationships apply:

τ = minimum mass thickness
τ_e = effective mass thickness
t = minimum thickness of shielding material
t_a = any slant thickness in a horizontal plane
t_e = effective thickness (a true slant thickness)
Δh = height differential between contributing source and receiver
d_a = horizontal distance between source and receiver
l = that line (normal to a wall) acting as the leg of a horizontally oriented right triangle having d_a as a hypotenuse.

From Fig. G.1 it is apparent that the line-of-sight radiation path between a contributing source and the receiver will be oriented obliquely with a given shielding element. As a result, the incident radiation must traverse the building elements over an effective thickness, t_e, which exceeds the minimum thickness, t. Therefore, the effective mass thickness, which is proportional to t_e, will usually exceed the handbook value.

By definition $\tau = \rho t$, where density ρ may be considered a constant of proportionality. Thus $\tau_e = \rho\ t_e$. Eliminating ρ between these two expressions gives

$$\tau_e = \tau \frac{t_e}{t} \qquad \text{(G-1)}$$

In essence, then, determination of a true or <u>effective</u> mass thickness requires finding the <u>effective</u> thickness t_e <u>along the line-of-sight</u> radiation path. A systematic method for obtaining t_e (and, hence, τ_e) for a number of shielding situations is demonstrated in the following figures and tables.

For horizontally oriented shields, such as roofs (as found in the target complex) and floors, the situation is as pictured in Fig. G.2. From the right triangles involved it is evident that

$$t_e = t \csc \alpha \qquad \text{(G-2)}$$

In the case of vertically oriented shields it is necessary to differentiate between walls and partitions as follows:

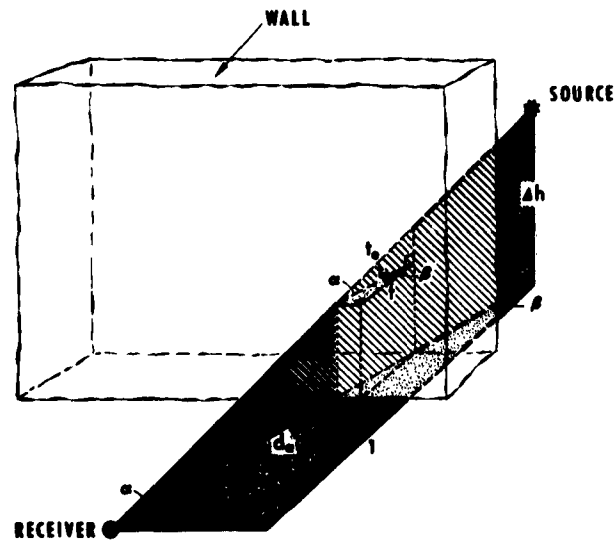

Fig. G.1 Example of Simple Shielding in the Oblique Direction

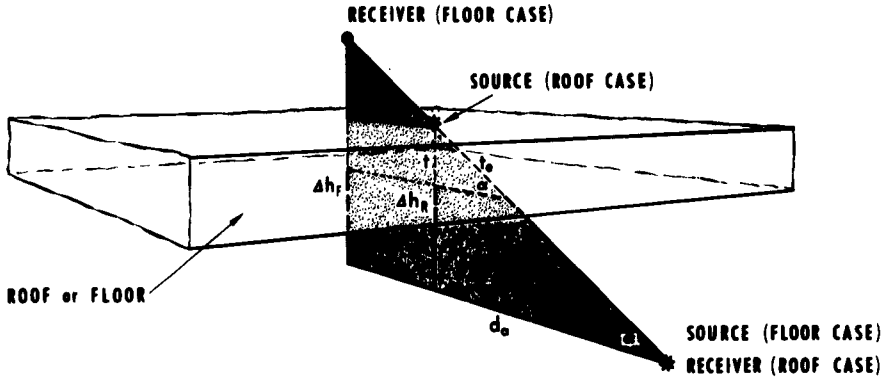

Fig. G.2 Horizontally Oriented Shielding Elements

Exterior wall - the building element, other than a roof or floor, between the source and receiver that acts as a shield.

Interior wall - any shielding element between the source and receiver that is parallel to the relevant exterior wall.

Partition - a vertical shielding surface between the source and receiver that is positioned at 90° with an exterior wall.

The distinction is clearly shown in Fig. G.3. Here the element labeled wall could be either interior or exterior.

From the right triangles of Fig. G.3 appropriate expressions may be derived for the effective thickness t_e.

For walls:

$$t_a = t \sec \beta$$

and $$t_e = t_a \sec \alpha$$

thus $$t_e = t \sec \beta \sec \alpha \qquad \text{(G-3)}$$

For partitions:

$$t_a = t \csc \beta$$

and $$t_e = t_a \sec \alpha$$

thus $$t_e = t \csc \beta \sec \alpha \qquad \text{(G-4)}$$

By substituting Eq. G-2, G-3 or G-4 for t_e into Eq. G-1, we will find the relationships between the minimum mass thickness and the effective mass thickness for three basic shielding situations.

Roof and Floor:

$$\tau_e = \tau \csc \beta \qquad \text{(G-5)}$$

Wall:

$$\tau_e = \tau \sec \beta \sec \alpha \qquad \text{(G-6)}$$

Partition:

$$\tau_e = \tau \csc \beta \sec \alpha \qquad \text{(G-7)}$$

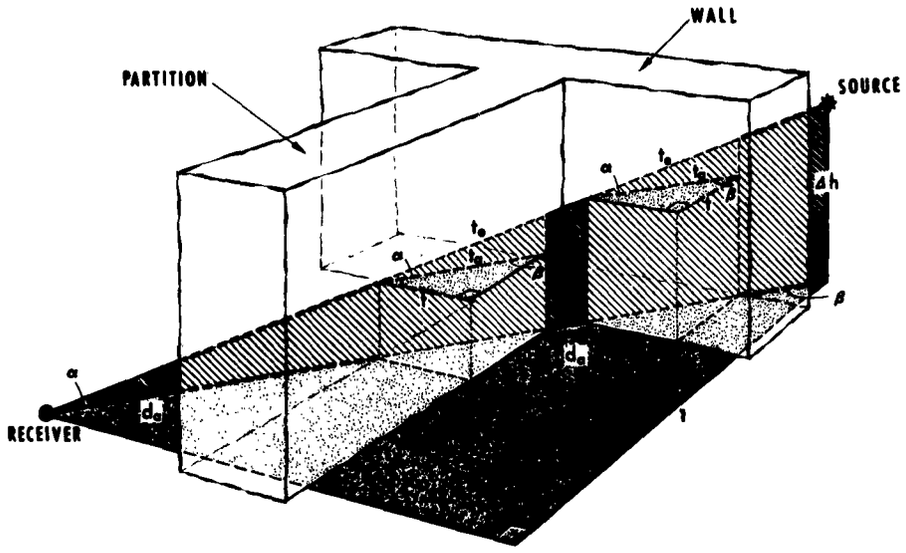

Fig. G.3 Vertically Oriented Shielding Elements

The following example demonstrates the computational steps required. It is desired to find the effective mass thicknesses between roof sections A, B, and C of Bldg. 570 as the source and Station 19 as the receiver. From the layouts and elevation data given in Appendix B the following table may be constructed.

Source Location	Δh (ft)	d_a (ft)	l (ft)
Bldg. 570 - Roof A	6.6	132	53
Bldg. 570 - Roof B	6.6	101	53
Bldg. 570 - Roof C	6.6	74	53

From the right triangles bounded by Δh, d_a and l (refer to Fig. G.1, G.2 and G.3) the required trigonometric functions of angles α and β are determined. These are tabled below.

Source Location	csc α	sec α	sec β	csc β
Bldg. 570 - Roof A	20.00	1.00	2.49	1.09
Bldg. 570 - Roof B	15.34	1.00	1.41	1.17
Bldg. 570 - Roof C	11.27	1.00	1.40	1.43

Required minimum mass thickness values taken from the Cannon Report give:

$$\tau\,(\text{roof}) = 6.1 \text{ lbs/ft}^2$$
$$\tau\,(\text{wall}) = 3.3 \text{ lbs/ft}^2$$
$$\tau\,(\text{partn}) = 3.7 \text{ lbs/ft}^2$$

Using Eqs. G-5, G-6, and G-7 and the values in the above table, the following effective mass thickness values result:

Source Location	τ_e (roof)	τ_e (wall)	τ_e (partn)	τ_e (total)
Bldg. 570 Roof A	122 lbs/ft^2	8.0 lbs/ft^2	4.0 lbs/ft^2	134 lbs/ft^2
Bldg. 570 Roof B	94 lbs/ft^2	6.0 lbs/ft^2	-	100 lbs/ft^2
Bldg. 570 Roof C	68.3 lbs/ft^2	4.7 lbs/ft^2	-	73 lbs/ft^2

These are identical to those shown in column 4 of Table E.2 in the contribution factor calculations. It is now simply a matter of reading the corresponding shielding factors for each of the three roof segments from the curve in Fig. 3.32 or, more correctly, Fig. F.1.

OCD Dist.

INITIAL DISTRIBUTION

Copies

NAVY

2	Chief, Bureau of Ships (Code 210L)
2	Chief, Bureau of Ships (Code 320)
1	Chief, Bureau of Medicine and Surgery
1	Chief, Bureau of Naval Weapons (Code RRRE-5)
1	Chief, Bureau of Yards and Docks (Code 42.330)
1	Chief, Bureau of Supplies and Accounts (Code L12)
1	Chief of Naval Operations (OP-07T10)
1	Chief of Naval Research (Code 104)
1	CO-Dir., U.S. Naval Civil Engineering Lab.
1	CO-Dir., U.S. Naval Civil Engineering Lab. (Cdr. Christensen)
1	Office of the Surgeon General (LtCol. C.R. Lewis)
1	Hq., Medical R&D Command (Widenkaph)

ARMY

1	Coordinator, Marine Corps Landing Force Dev. Activities.
1	U.S. Army Material Office (Schmidt)
1	Army Nuclear Defense Laboratory (Maloney)
3	Army Library, Civil Defense Unit
1	Assistant Secretary of the Army (R&D)
1	Hq., Medical Div. USAREUR (Col. F.H. Whitley)

AIR FORCE

1	Air Force Office of Civil Engineering (Bohannon)

OTHER DOD ACTIVITIES

60	Office of Civil Defense (Dir. for Research)
1	Office of Emergency Planning (Coker)
20	Defense Documentation Center
1	U.S. Dept. of Agriculture (Todd)
1	U.S. Dept. of Commerce, Water & Sewage

AEC ACTIVITIES AND OTHERS

1	Advance Research Inc. (Fernald)
1	American Institute for Research
1	Cornell University (McGinnis)
1	Civil Defense Training Program (McConnell)
1	Curtiss-Wright Incorporated (Wheeler)
1	Engineering Science Inc. (Ludwig)
1	General Dynamics Corp. (Bell)
1	Georgia Institute of Technology (Bellinger)
1	Hudson Institute (Kahn)
1	IIT Research Foundation (Sevin)
1	Ionics Inc. (McRae)
1	Isotopes Incorporated (Kulp)
1	National Academy of Sciences (Park)
1	Oak Ridge National Laboratory (Parker)
1	PARM Project
1	Research Triangle Institute (Parsons)
1	Stanford Research Institute (Miller)
1	Technical Operations Inc. (Clarke)
1	University of Florida (Furman)
1	University of Georgia
1	United Research Services (Kaplan)
1	U.S. Public Health Service (Abercrombie)
1	U.S. Public Health Service, DHEW (Parrino)
1	U.S. Public Health Service, DHEW (McCallum)
1	U.S. Public Health Service, DHEW (Burke)
1	U.S. Geological Survey (Dr. Leopold)

USNRDL

50	Technical Information Division

DISTRIBUTION DATE: 16 March 1964

Naval Radiological Defense Laboratory
USNRDL-TR-700
RADIOLOGICAL RECOVERY OF LAND TARGET COMPONENTS - COMPLEX III by W.L. Owen and J.D. Sartor 20 November 1963 173 p. tables illus. 13 refs. UNCLASSIFIED

The radiological recovery of essential facilities within a fallout area is a complex task. It involves the scheduling, application and control of a variety of tools and skills for recovery. Execution of a recovery operation must be swift and efficient to avoid the over-exposure (over)

1. Radioactive fallout.
2. Nuclear explosion damage.
3. Radiological contamination.
4. Countermeasures.
5. Recovery.

I. Owen, W.L.
II. Sartor, J.D.
III. Title.

UNCLASSIFIED

Naval Radiological Defense Laboratory
USNRDL-TR-700
RADIOLCGICAL RECOVERY OF LAND TARGET COMPONENTS - COMPLEX III by W.L. Owen and J.D. Sartor 20 November 1963 173 p. tables illus. 13 refs. UNCLASSIFIED

The radiological recovery of essential facilities within a fallout area is a complex task. It involves the scheduling, application and control of a variety of tools and skills for recovery. Execution of a recovery operation must be swift and efficient to avoid the over-exposure (over)

1. Radioactive fallout.
2. Nuclear explosion damage.
3. Radiological contamination.
4. Countermeasures.
5. Recovery.

I. Owen, W.L.
II. Sartor, J.D.
III. Title.

UNCLASSIFIED

of work crews to the radiation hazard. Thus, safe and effective performance will depend upon the advance formulation of a detailed radiological recovery plan.

A special recovery planning procedure has been under development for several years. In its present form the procedural concept has proved quite feasible, as demonstrated by the results of the Complex II experiment. However, a number of critical planning variables and related factors have required closer inspection and measurement. For this reason the Complex III experiment was instituted.

As a result of this experiment, the fallout reduction effects of wind erosion and recovery effort were determined. The list of reclamation coefficients (needed to compute reclamation crew dosage) was extended, and the behavior of these coefficients as a function of method and effort was studied. The method of predicting the radiation contributions of various target components to a common location of interest was made more reliable. Correction factors were found for adjusting recovery time and effort estimates. Together, these findings will permit further refinement of the recovery planning procedure. UNCLASSIFIED

of work crews to the radiation hazard. Thus, safe and effective performance will depend upon the advance formulation of a detailed radiological recovery plan.

A special recovery planning procedure has been under development for several years. In its present form the procedural concept has proved quite feasible, as demonstrated by the results of the Complex II experiment. However, a number of critical planning variables and related factors have required closer inspection and measurement. For this reason the Complex III experiment was instituted.

As a result of this experiment, the fallout reduction effects of wind erosion and recovery effort were determined. The list of reclamation coefficients (needed to compute reclamation crew dosage) was extended, and the behavior of these coefficients as a function of method and effort was studied. The method of predicting the radiation contributions of various target components to a common location of interest was made more reliable. Correction factors were found for adjusting recovery time and effort estimates. Together, these findings will permit further refinement of the recovery planning procedure. UNCLASSIFIED